EVALUATING THE EFFECT OF STONE BUNDS EROSION CONTROL ON VEGETATION TREND IN SOUTH-WEST BURKINA FASO - A FINE SCALE REMOTE SENSING PERSPECTIVE IN THE IOBA PROVINCE

By

Yaw Mensah Asare

(B.Sc. Geodetic Eng., M.Sc. Geomatic Eng.)

A thesis submitted to the Department of Civil Engineering, College of Engineering, Kwame Nkrumah University of Science and Technology, Kumasi in partial fulfilment of the requirement for the degree of

DOCTOR OF PHILOSOPHY

in

Climate Change and Land Use

November 2019

DECLARATION

I hereby declare that this submission is my own work and that, to the best of my knowledge and belief, it contains no material previously published or written by another person nor material which to a substantial extent has been accepted for the award of any other degree or diploma at Kwame Nkrumah University of Science and Technology, Kumasi or any other educational institution, except where due acknowledgment is made in the thesis.

Yaw Mensah Asare (PG 7281016) …… …….
……

Signature Date

Student Name & ID

Certified by:

…… …….

Prof. Eric K. Forkuo
…… Signature Date

Supervisor(s) Name

Certified by:

Dr. Michael Thiel
…… …….
Supervisor(s) Name Signature Date

Certified by:

Prof. Sampson Oduro-Kwarteng
…… …… …….

Head of Department's Name Signature Date

DEDICATION

I dedicate this work to my parents Mr. Mike Kwasi Addai and Anna Nketia.

ABSTRACT

Soil erosion by water has become a worldwide issue due to its environmental and socioeconomic impact in the light of rising concerns over climate change. To minimize the impact of soil erosion by water in West Africa, several erosion control measures have been adopted and are being practiced. The type of erosion control measure practiced depends on the climatic zone in which the area falls. In South-West Burkina Faso where this study was undertaken, rainfall is relatively high compared to the other areas within the country. As a result, the use of stone bunds/lines is the most commonly practiced erosion control measure. But after the implementation of these erosion controls, very little has been done on evaluating the impact of these erosion controls on vegetation (crops and natural vegetation) improvement using remote sensing data. This is because until recently, organized erosion control measures more especially using stone bunds over thousands of hectares of both agriculture and non-agriculture lands was rare. This study, therefore, investigated the effect of stone bunds erosion control measure on vegetation trend using remote sensing data. A time series analysis of NDVI data from 2004 to 2017 was conducted to find: (i) the trend of vegetation in the whole study area and (ii) the trend of vegetation in areas with stone bunds erosion control and areas without. Subsequently, a comparison using the ANOVA test was done between the trends of NDVI in these two areas. Also, a seasonal analysis of the crop heights of cotton and millet was conducted using photographs from UAV. Lastly, a pixel-wise trend was conducted for climate variables (rainfall and temperature) and a correlation analysis was also performed between NDVI and climate variable time series. The results showed that, the NDVI trend of the whole study area is significantly increasing at a rate of 3.7×10^{-4} ΔNDVI/month at 95% confidence interval (CI). Similarly, areas with stone bunds erosion control and areas without stone bunds erosion control had significant increasing trends ranging from 3.14×10^{-4} to 3.95×10^{-4} ΔNDVI/month and 3.83×10^{-4} to 3.91×10^{-4} ΔNDVI/month respectively. In comparing the NDVI trends of the two areas, the result from the ANOVA test showed that there is no significant difference between the NDVI trends of areas with stone bunds erosion control and areas without stone bunds erosion control (p-value = 0.319). Although, the mean NDVI trends for the whole area gave a positive trend, the results of the pixel-wise analysis showed that, positive, stable and negative NDVI trends were widespread in the study area with a range of -0.001 to a maximum of 0.002 ΔNDVI/month. Only 10.6% of the NDVI trends was statistically significant at 95% CI. In comparing the crop heights in areas with stone bunds erosion control and areas without, at 95% CI, the t-test revealed that there is no significant difference between the means of the crop heights of cotton (p-value = 0.389) and millet (p-value = 0.884) in these two areas. For trends of climate variables, rainfall and temperature had a positive increase in the monthly trend of 0.12mm/month and 0.01°C/month respectively. In terms of the correlation between NDVI and climate variables, there was a positive correlation between NDVI and rainfall (Kendall τ of 0.513), whiles a negative correlation (τ = -0.322) was observed between NDVI and temperature. The results from this study will help future studies of evaluation of erosion control measures in West Africa. By combining data from other satellites such as the Sentinel, this will go a long way to help to bridge the problem of data availability for vegetation time series analysis.

TABLE OF CONTENTS

LIST OF TABLES

LIST OF FIGURES

LIST OF ABBREVIATIONS

4K – 4000 pixels

5S – Simulation of the Satellite Signal in the Solar Spectrum

6S – Second Simulation of the Satellite Signal in the Solar Spectrum

AEJ – African Easterly Jet

AIC – Akaike's Information Criterion

AOT – Aerosol Optical Thickness

ARIMA – Auto-regressive Integrated Moving Average

AVHRR – Advanced Very High Resolution Radiometer

AWLHM – Adaptive Window Linear Histogram Matching

CFmask – Function of mask in C programming language

CI – Confidence Interval

CO_2 – Carbon Dioxide

DEM – Digital Elevation Model

DJI – Da-Jiang Innovations

DSM – Digital Surface Model

DTM – Digital Terrain Model

ECA – Erosion Controlled Areas

EKF – Energy and Climate Fund

EROS – Earth Resources Observation and Science

ESPA – EROS' Science Processing Architecture

ETM+ – Enhanced Thematic Mapper plus EUROSEM

– European Soil Erosion Model

EXIF – Exchangeable Image File Format

Fmask – Function of Mask

FOV – Field of View

GCPs – Ground Control Points

GIS – Geographic Information System

GLASOD – Global Assessment of Soil Degradation

GNSPI – Geostatistical Neighbourhood Similar Pixel Interpolator GNSS – Global Navigation Satellite System

GPCP – Global Precipitation Climatology Project

GPP – Gross Primary Productivity

GPS – Global Position Systems

GS – Ground Station

IAEA – International Atomic Energy Agency

IDL – Interactive Data Language

IMU – Inertial Measurement Unit

ITCZ – Inter Tropical Convergence Zone

LAI – Leaf Area Index

LaSRC – Landsat 8 Surface Reflectance Code

LEDAPS – Landsat Ecosystem Disturbance Adaptive Processing System

LGAC – Landsat Global Archive Consolidation

LLHM – Localised Linear Histogram Matching

MA – Moving Average

MAE – Mean Absolute Error

MCSs – Mesoscale Convective Systems

MODIS – Moderate Resolution Imaging Spectro-radiometer

NASA – National Aeronautics and Space Agency

NDSI – Normalized Difference Soil Index nDSM

– Normalized Digital Surface Model

NDVI – Normalized Difference Vegetation Index

NECA – Non-Erosion Controlled Areas

NGOs – Non-Governmental Organizations

NIR – Near Infra-Red

NNE-SSW – North-North-East – South-South –West

NOAA – National Oceanic and Atmospheric Administration

OLI – Operational land imager

PABSO – Programme d'Aménagement de Bas-Fonds dans le Sud-Ouest

PCPs – Potential Cloud Pixels

QA – Quality Assurance

RMSE – Root Mean Square Error

RUSLE – Revised Universal Soil Loss Equation

SLC – Scan Line Corrector

SPOT – Satellite Pour l'Observation de la Terre

SR – Surface Reflectance

SWAT – Soil and Water Assessment Tool

SWIR – Short wave Infra-Red

TEJ – Tropical Easterly Jet

TM – Thematic Mapper

TOA - Top of Atmosphere

TRMM – Tropical Rainfall Measuring Mission

UAV – Un-manned Aerial Vehicle

UHD - Ultra-High-Definition

USGS – United States Geological Survey

USLE – Universal Soil Loss Equation

UTM – Universal Transverse Mercator

WAM – West African monsoon

WASCAL – West African Science Service Centre on Climate Change and Adapted Land-use

WAWJ – West African Westerly Jet

WRS – Worldwide Reference System

ACKNOWLEDGEMENT

"He who have labored and are heavy laden should come to me and I will give you rest". I thank God almighty for giving me life, grace, strength and wisdom to complete this work successfully.

I am grateful to the German Federal Ministry of Education and Research (BMBF) for providing financial assistance for this study through the West African Science Service Center for Climate Change and Adapted Land Use (WASCAL).

My profound gratitude goes to my supervisors, Prof. Eric Kwabena Forkuo and Dr. Michael Thiel for their guidance, suggestion, criticism and encouragement. Your brilliant ideas significantly shaped this work in the right direction. I am grateful for your effort.

My sincere thanks go to Dr. Gerald Forkuor for his priceless encouragement, guidance, comments and suggestions to make this study better. I really appreciate your effort, Senior. I also thank those who helped me in proof-reading this thesis, especially, Emmanuel Adu Afari and Henrietta Adokoma.

I will like to thank my colleagues at the Department of Geomatic Engineering, KNUST for their support and encouragement throughout the period of my study. I also thank the staff and students of the Department of Remote Sensing, University of Wuerzburg, Germany for their warm reception and assistance during my stay in Germany. I would also like to appreciate the staff of Energy and Climate Fund (EKF) project, Diebougou, Burkina Faso, for their help and assistance during my field data collection. I will like to thank Dr. Martin Baumgart (project manager) and Mr. Novant Poda for the logistical support and care during my stay in Diebougou. Am also grateful to Mr. Ladjie Toure, Mr. Mamadou Niang, Mrs Some and the others. Also, to the staff of WASCAL competence center, Ouagadougou, am grateful for your help.

Lastly, I want to thank my family and friends for their support, encouragement and prayers throughout this journey. I know their prayers guided and protected me in my numerous travels. I am grateful to my wife, Adjowa for her love and support.

CHAPTER 1: INTRODUCTION

1.1 Background

Since the 1980s, soil erosion by water has become a worldwide issue owing to its impacts on the environment and socio-economics activities (UNEP, 1986; UNFCC, 1997; IPCC, 2000). Especially, accelerated erosion, which is caused by anthropogenic activities (Foth, 1990; Blinkov, Kostadinov and Marinov, 2013). Global Assessment of Soil Degradation (GLASOD) study has reported that about 15% of the earth's ice-free land surface is affected by various kinds of land degradation, with 55% of it attributed to accelerated soil erosion (Bridges and Oldeman, 1999). Also, more than 80% of agricultural fields world-wide experience moderate to severe erosion whiles 10% suffers slight to moderate erosion (Bouma and Batjes, 2000; Li and Fang, 2016). Prolonged soil erosion in certain areas around the world have reached a stage of irreversibility (Blinkov, Kostadinov and Marinov, 2013). Considering the slow rate of soil formation, any soil loss of more than 1 t/ha/yr may be regarded as irreversible within a time span of 50 to 100 years (Gobin *et al.*, 2004a; Blinkov, Kostadinov and Marinov, 2013). Currently, the effects of erosion on sustainable agriculture and ecosystem services have become alarmed in the era of growing concerns over climate change and food security (Cilek *et al.*, 2015; Posthumus *et al.*, 2015).

Climate change influence on soil erosion has mainly been associated with rainfall (high intensity of rainfall will result in high erosivity), plant biomass (plant maturity) and crop management practices (adaptation measure) (O'Neal *et al.*, 2005; Nearing, Pruski and O'Neal, 2004). The changes in rainfall distribution, amount and intensity have a direct impact on soil erosion (Li and Fang, 2016). The rate of water induced soil erosion is likely to rise as a result of the effects of climate change and land use if no measures are put in place to control it. This is because, it is estimated that rainfall will increase in Africa and other areas around the globe (IPCC, 2001; Mooij *et al.*, 2005; Nyeko-Ogiramoi, Willems and Ngirane-Katashaya, 2013; Paroissien *et al.*, 2015). On the contrary, rainfall impacts on soil erosion are sometimes positive. Prolonged rainfall period may result in the increase in plant growth, thereby minimizing runoffs and erosion (Nearing, Pruski and O'Neal, 2004). With the potential of increase in the rate of soil erosion due to climate change and land use, modelling future erosion rate is an important way of measuring the vulnerability of agriculture and the natural environment (Mullan, 2013). The accurate prediction of the extent of impact caused by climate change and a balance of the

consequences of other different factors still remain uncertain (Li and Fang, 2016). However, with the use of soil erosion models, researchers have made future projections.

Soil erosion models (empirical or event-based) which have the capacity for estimating, assessing and predicting risk of soil erosion have been developed, tried, tested and used all over the world (Morgan *et al.*, 1998; Cilek *et al.*, 2015; Fernández and Vega, 2016). Although each model has its own strength and weakness, researchers are relentless in improving these models. Soil erosion models such as, the Universal Soil Loss Equation (USLE) (Wischmeier and Smith, 1978), the Revised Universal Soil Loss Equation (RUSLE) (Renard *et al.*, 1991), the European Soil Erosion Model (EUROSEM) (Morgan *et al.*, 1998), the Soil and Water Assessment Tool (SWAT) (Arnold *et al.*, 1998), SHETRAN (Ewen, Parkin and O'Connell, 2000) and many others have existed over the years and have been applied in research. The current practice is the integration of remotely sensed data (such as Land use/cover data and DEM) and Geographic Information System (GIS) data into erosion models (Kefi *et al.*, 2009; Farhan, Zregat and Farhan, 2013; Carvalho *et al.*, 2014; Lu *et al.*, 2004; Chen and Du, 2014; Tang *et al.*, 2014; Ganasri and Ramesh, 2016; Rawat, Mishra and Bhattacharyya, 2016; Parveen and Kumar, 2012).

The development and implementation of organized soil erosion controls started from the 20th century and its 'golden period' was the period of 1945 to 1990 (Dotterweich, 2013a). Countries such as Russia in the 19th century started researching into the design and application of soil conservation measures to reduce soil lose in cultivated fields (Golosov and Belyaev, 2013). Currently, there are wide spread of erosion control measures all over the world but few of them are reported in research works (Zhao *et al.*, 2013; Blinkov, Kostadinov and Marinov, 2013; Dotterweich, 2013b; Golosov and Belyaev, 2013).

To minimize the impact of water induced soil erosion in Africa, several erosion control measures (example, agroforestry, stone bunds, earth bunds, stone storage dam, mulching, terracing, cover cropping, afforestation, etc) have been adopted and is being practice (Vanlauwe *et al.*, 2014; Zougmoré, Jalloh and Tioro, 2014; Maisharou *et al.*, 2015; Chirwa and Mahamane, 2017). The type of erosion control measure practiced depends on the climatic zone in which the area falls. In semi-arid areas of West Africa, specifically, South-West Burkina Faso where this study was undertaken, rainfall is relatively high compared to the other areas within the country. As a result, the use of stone bunds/lines is the most practiced erosion control measure (Nyamekye *et al.*, 2018). Stone bunds though an indigenous practice by farmers in Africa (Zougmoré, Jalloh and Tioro, 2014) has been adopted and improved by researchers. The

implementation of organized stone bunds erosion control measure begun in the early 1980's in Africa, especially in Northern Ethiopia (Tigray Highlands) and West African Sahel (Gebremichael *et al.*, 2005; Reij, Tappan and Belemvire, 2005). This was as a response to the series of drought years, which had devastating consequences on the entire region in the 1970's (Reij, Tappan and Belemvire, 2005). Due to its effectiveness in reducing soil erosion (Zougmoré, Jalloh and Tioro, 2014; Taye *et al.*, 2015), government and non-governmental organizations (NGOs) are assisting (technical and logistical support) its implementation in many areas within the region (Zougmoré, Jalloh and Tioro, 2014).

The effectiveness of an erosion control measure is mostly associated with the improvement of vegetation cover, increase in crop yield and reduction of top soil removal (Gobin *et al.*, 2004b; Zhao *et al.*, 2013; Ibrahim *et al.*, 2015; Gomiero, 2016). On agricultural lands, many research in Africa (Vancampenhout *et al.*, 2006; Adimassu *et al.*, 2014) have shown positive relationship between erosion control with stone bunds and crop/plant growth. This is because, the stone bunds help to minimize soil and soil nutrients transport and also increase soil water through infiltration (Sawadogo, 2011; Zougmoré, Jalloh and Tioro, 2014; Subhatu *et al.*, 2017; Mekuriaw *et al.*, 2018). Gebremichael *et al.* (2005) showed that the implementation of stone bunds in the Tigray region of Ethiopia reduced the annual soil loss by 68%. In terms of crop yield, Nyssen *et al.* (2007) reported an average increase in grain yield of about 53% from 3 to 21 years after the implementation of stone bunds in the highlands of Northern Ethiopian. In a similar study conducted at Saria Agricultural Research Station in Burkina Faso, Zougmoré *et al.* (2004) also reported a significant increase in yield in all crop types under stone bunds erosion control measure. In a natural environment where erosion controls have been implemented as an intervention to stop or minimize land degradation due to soil erosion, it is expected that the vegetation cover will gradually improve naturally or be accelerated by afforestation (Li *et al.*, 2011). The fast improvement of vegetation cover on an erosion controlled land will in turn help to minimize the rate of erosion drastically.

The use of remote sensing techniques for capturing data is unarguably the most efficient and effective way and widely used mode of assessment and analysis of degraded lands or changes in land productivity (Yengoh *et al.*, 2014; Ibrahim *et al.*, 2015; Hird *et al.*, 2017; Nash *et al.*, 2017a). It involves the assessment of historic and future (projections) trends in land degradation or productivity. The use of vegetation indices from remote sensing data in extracting physical and biophysical properties of vegetation have been developed over the years (Tucker, 1979; Liu and Huete, 1995). The underlying assumption of the development and use of these indices

is that, some arithmetic combination of the spectral bands of remote sensing data can reveal biophysical and biochemical variables. Such variables include, canopy chlorophyll content, photosynthetic capacity, leaf area index (LAI) and distribution, gross primary productivity (GPP), water content in leaves, deficiencies in minerals and sign of pest and disease attacks (Chen and Cihlar, 1996; Blackburn, 1998; Boegh *et al.*, 2002; Jensen and Im, 2007).

The development of systems to monitor vegetation phenology of large fields using the Normalized Difference Vegetation Index (NDVI) (Rouse Jr *et al.*, 1974; Tucker, 1979) started more than 45 years ago. It was an important milestone in the development of automatic methods for analyzing plant growth and biomass (Myneni *et al.*, 1997) because it is by far the most widely used vegetation index (Higginbottom and Symeonakis, 2014; Yengoh *et al.*, 2014). The NDVI is a spectral ratio index based on the red and infrared bands (Rouse Jr *et al.*, 1974; Tucker, 1979). It measures vegetation greenness and has proved to be positively correlated with vegetation productivity (Nash *et al.*, 2017b). The capability to measure chlorophyll status from remote sensing data allowed plant health to be measured in large fields (Perez-sanz, Navarro and Egea-cortines, 2018). It has also been used to estimate crop yields, plant growth and performance (photosynthetic activities), vegetation cover and rangeland carrying capacities among others (Amri *et al.*, 2011; Li *et al.*, 2015; Lausch *et al.*, 2016; Liu, Wimberly and Dwomoh, 2017; Nash *et al.*, 2017b). The use of NDVI to identify the period of photosynthetic activities can be interpreted to show the period of growing season. This is because, the period of maximum NDVI corresponds to time of highest photosynthesis. The NDVI with seasonality shows photosynthetic activity during the growing season; and the rate of change in NDVI may be associated with the speed of rise or decline of photosynthesis (Yengoh *et al.*, 2014).

1.2 Problem Statement

Although there have been many research work on the implementation of water induced soil erosion controls all over the world (Wortley, Hero and Howes, 2013; Dang *et al.*, 2014; Mekonnen *et al.*, 2015), very little has been done on evaluating the impact of these erosion controls on vegetation (crops and natural vegetation) growth using remote sensing data in West

Africa. This is because until recently, organized erosion control measures more especially using stone bunds over thousands of hectares of both agriculture and non-agriculture lands were rare (Zougmoré, Jalloh and Tioro, 2014). The reason being that, agriculture in West Africa is done on a subsistence level (Bayala *et al.*, 2012). As a result, the implementation of erosion control measure such as stone bunds are also practiced on a per farm basis (small scale) and by farmers who can afford the cost involved in the implementation.

Consequently, evaluating the impact of stone bunds erosion control on vegetation phenology using remote sensing data was virtually impossible due to the small scale and the fragmented nature of its implementation. Currently, the few studies conducted on the evaluation of stone bunds erosion control on soil and soil nutrients transport and vegetation improvement were done on an on-site basis (Nyssen *et al.*, 2007; Adimassu *et al.*, 2014) and hardly apply remote sensing technology. These studies have alluded that implementation of stone bunds erosion control substantially helped to minimize soil and soil nutrient transport (Gebremichael *et al.*, 2005; Adimassu *et al.*, 2014) and had a positive impact on crop yields and the regeneration of woody and herbaceous vegetation (Zougmoré *et al.*, 2004; Vancampenhout *et al.*, 2006; Sawadogo, 2011).

In the quest to rehabilitate degraded lands by minimizing the effect of soil erosion, stone bunds erosion controls are now widespread and are being implemented on a larger scale in Burkina Faso through the efforts of successive governments and non-governmental organizations (NGOs) (Sawadogo, 2011; Zougmoré, Jalloh and Tioro, 2014). For instance, projects such as PABSO (project to develop the South-western lowlands) and EKF (Energy and climate Fund) aimed at combating land degradation in South-west region of Burkina Faso through the implementation of stone bunds erosion control and other sustainable land management approaches.

Consequently, the use of remotely sensed data, more especially medium to high resolution data such as Landsat in evaluating and monitoring post implementation of stone bunds erosion control on vegetation growth is vital in assessing the recovery of degrading lands.

1.3 Objectives of Study

The overall goal of this research is to analyze the effect of stone bunds erosion control measure on vegetation trend using a fine scale remote sensing approach in the Ioba Province of Burkina Faso.

Concurrent with the overall objective, the specific objectives are to;

i. To analyze NDVI time series for vegetation trend in the Ioba province from 2004 to 2017.

ii. To investigate if areas with stone bunds erosion control measure have a similar NDVI trend and if these trends are different from areas without stone bunds erosion control measure.

iii. To compare the short-term changes in crop height between areas with stone bunds erosion control measure and areas without using photographs from Un-manned Aerial Vehicle (UAV).

iv. To analyze the trend of climate variables (rainfall and temperature) and determine their relationship with NDVI trends from 2004 to 2017.

1.4 Research Questions

i. What is the overall trend of vegetation in the Ioba province?

ii. Do areas under stone bunds erosion control show the same vegetation trend as areas without? iii. Are there differences in the crop height in areas with stone bunds erosion controls and areas without? iv. What are the trends of climate variables (rainfall and temperature) and their relationship with NDVI trends?

1.5 Justification for the Study

Accelerated soil erosion has become a major issue of concern in the era of climate change due to its effect on food security. To mitigate the impact of soil erosion, several soil erosion methods have been introduced in West Africa and are being practiced, most especially in heavily affected areas. Burkina Faso is one of the countries in West Africa which is heavily affected by soil erosion (Nyamekye *et al.*, 2018). As a result, local farmers, governments and NGOs are all assisting to minimize the impact of soil erosion. Several projects dating back from 1970s to date have tried to combat soil erosion and rehabilitate degraded lands (Nyamekye *et al.*, 2018).

Most of these projects only seek to implement these erosion control measures without doing a post implementation evaluation on the impact of the erosion control measure on vegetation improvement. In the natural environment, once the vegetation cover improves, it will in turn serve as a measure to control soil erosion. Also, on agricultural lands, once soil erosion is prevented, it is likely that crops will grow well, and yield will also improve. In view of these,

vegetation cover improvement can be used to assess if an erosion control measure is yielding the required results.

This research work will inform decision makers the level of vegetation improvement that has been achieved by the implementation of stone bunds as an erosion control measure in the Ioba province of South-west Burkina Faso.

With the devastation nature of soil erosion by water on the environment and its consequences on vegetation growth on both agricultural lands and the natural environment, it is worth researching into issues of soil erosion control especially its impact on vegetation improvement.

1.6 Outline of Thesis

The subsequent chapters of this thesis comprise of chapters 2 through to chapter 8. Chapter 2 outlines a review of pertinent issues and research in relation to the subject of this research. Issues of soil erosion in West Africa, Landsat data and its issues, vegetation indexes with special emphasis on NDVI and UAV technology. The focus is on the use of the abovementioned technology and datasets for vegetation phenology analysis. Chapter 3 highlights the study area, its geographic location, biophysical and socio-economic characteristics. Chapter 4 describes the data (satellite and ancillary) and the pre-processing done to make the data suitable for use. In chapter 5, the methodology employed to achieve the set objectives was laid out. Chapter 6 presents the results obtained from the methodology and the discussion of the results is presented in chapter 7. Conclusions and recommendations for future studies are outlined in chapter 8.

CHAPTER 2: LITERATURE REVIEW

2.1 Introduction

This chapter presents some terminologies used in this research and a review of some concepts in remote sensing and soil erosion. It has been organized into eight sections. Section 2.2 provides some definitions and explanations of some terminologies used in soil erosion control evaluation and remote sensing. Sections 2.2 to 2.5 deal with soil erosion, its control measures and how climate change is impacting on it. Section 2.6 focuses on data and data issues with regards to Landsat sensors. Sections 2.7, 2.8 and 2.9 describe the use of satellite data in

vegetation trend analysis and NDVI applications. The last section, 2.10 highlights Un-manned Aerial Vehicle (UAV) application in vegetation monitoring and mapping.

2.2 Definitions

i. Soil Erosion

Soil erosion is the wearing away of the earth's surface by the force of wind and water, and consists of soil particle dislodgement, entrainment, transport, and deposition. Soil erosion by water is the constant process of water detaching and transporting soil particles downslope to the lowest point in a basin, be it an ocean or closed basin (MaCool and Williams, 2008). Soil erosion by wind involves the transport of soil particles by suspension, surface creep, or saltation over distances ranging from a few centimeters to hundreds of kilometers (Bullock, 2005).

ii. Soil Erosion Control Measure

Erosion control measure is the practice of preventing or controlling the extent of erosion. In the case of water erosion, by reducing the flow velocity of runoff water. Increasing the infiltration capacity, land cover and surface roughness of the soil. The most widely practiced erosion control measures include: conservation agriculture (including reduced tillage and notill farming, suitable crop rotations, mulching, cover crops), strip farming, contour farming, the installation of vegetative buffers and strips, and terracing (Vogel, Deumlich and Kaupenjohann, 2016).

iii. Stone Bunds/Lines

A stone bund/line may be defined as an embankment of stones, rocks or lateritic duricrust built along the contour across a sloping land to reduce or stop the velocity of overland flow, and consequently to reduce soil erosion (Morgan, 1995).

iv. Vegetation Phenology

It is the timing of periodic developmental stages in the life cycle of plant such as bud burst, crown growth, flowering, and senescence, that are closely related to the seasonal variation in climate trends. It is an essential and critical component of environmental science, and

influences biodiversity, species interactions, their ecological functioning, and their effects on fluxes of water, energy, and biogeochemical elements at various scales (Kimball, 2014).

v. Optical Satellite Image

These are satellite images captured in the visible bands, near infrared and short-wave infrared portions of the electromagnetic spectrum. Because optical images are obtained from the visible bands and infrared bands, they are only captured in the day time. Also, bad weather (e.g. cloudy weather) is a big hinderance to optical images and they render them almost useless. The most popular optical satellite image is the Landsat data.

vi. Un-manned Aerial Vehicle (UAV)

Un-manned Aerial Vehicle also known as drones are a class of aircrafts that can fly without an on-board presence of pilots. Unmanned aircraft systems consist of the aircraft component, sensor payloads and a ground control station. They can be controlled by onboard electronic equipment or via control equipment from the ground (Narayanan and Ibe, 2015). Its sensors (e.g. camera and infrared device) make it a useful tool for capturing aerial images for remote sensing applications.

2.3 Soil Erosion by Water, Mechanisms and Processes

Soil erosion by water starts when raindrops hit exposed soil with an explosive effect, launching soil particles into the air (Pimentel *et al.*, 1995). The process involves particle detachment, entrainment, transport and deposition (Choi *et al.*, 2005; MaCool and Williams, 2008) and their effect may be on-site where soil detachment and transport occurs or off-site, where eroded soil particles are deposited (Posthumus *et al.*, 2015). Deposition mostly takes place in a low lying area (Boix-fayos, Vente and Albaladejo, 2009). The detachment processes occur when soil particles are separated from the soil matrix at the surface due to the impact of raindrop and runoffs (Zhang *et al.*, 2003; Fu *et al.*, 2011). The detached particles are transported mostly by the runoffs and the splash from the raindrops. The deposition detached soil particles occurs when sediment load of eroded particles exceeds its corresponding transport capacity (Choi *et*

al., 2005). The factors that influence the transportation and deposition of the sediments by runoff include; sediment size distribution, coarseness, slope of the terrain, vegetation and stone covers (Kiani-harchegani, Sadeghi and Asadi, 2018).

The sources of energy needed to undergo the erosion process is obtained from the raindrops and the onward surface flow of water (Young and Wiersma, 1973; Nearing *et al.*, 2017). The relative importance of the fundamental processes of soil erosion depends on whether the processes are occurring on inter-rill or rill areas and in the levels of the controlling variables. Understanding the soil erosion process is necessary in the design of assessment criteria and the development of an appropriate soil erosion control measure (Choi *et al.*, 2005).

2.4 Soil and Water Conservation Practices in Burkina Faso

Soil and water conservation methods practiced worldwide to control water induced soil erosion may be classified into two main groups; the barrier method and the cover method (Young, 1989). In the barrier method, techniques such as terraces, bunds and stone wall, grass strips and hedgerows are used as fences to obstruct the washing away of sediments and soil nutrients by runoffs. The cover method involves the use of plants, crop residue and other types of waste to prevent raindrops from striking the surface of the soil and minimizing the flow velocity of runoffs. Although the two methods can be complementary, the barrier methods are costly and needs a lot of time to construct. As a result, the cover method is mostly practiced at the local level (Bobe, 2004).

In Burkina Faso, soil erosion is one of the major hinderance to sustainable agriculture and socio-economic development (Nyamekye *et al.*, 2018). As a result, from time in memorial, local farmers have adopted some soil and water conservation practices. But the type of conservation method practiced in an area depends on the agro-climate zone in which the area falls. In areas with very low rainfall such as northern Burkina Faso, the zai and half-moon which involves the concentration of rainfall and soil organic matter in smaller pits and moonlike dugouts respectively are the main water conservation method used (Zougmoré, Jalloh and Tioro, 2014). However, in the central and southern Burkina, the intensity of rainfall is much higher causing high surface runoff, therefore, the use of stone bunds or walls and grass strips are common (Nyamekye *et al.*, 2018).

Most of the current soil and water conservation methods being implemented by the government and NGOs in Burkina Faso are knowledge from indigenous practice that has been refined by

scientist and researchers (Sawadogo, 2011). Since combating soil erosion is a national affair, technical and logistical supports are given to local farmers for large scale implementation (Zougmoré, Jalloh and Tioro, 2014).

2.5 Soil Erosion Control using Stone Bunds

The use of stone bunds as a mechanism to combat soil erosion is an indigenous practice by farmers in Africa (Zougmoré, Jalloh and Tioro, 2014) especially, where land degradation due to water induced soil erosion is severe. Due to its effectiveness in reducing soil erosion, governments and NGOs are assisting in the large-scale implementation of the technique after series a of studies on the parameters (for example, gradient, spacing, number of stone lines per bund, etc.) (Zougmoré, 2003) used in the technique and support (technical and logistical) for the collection and transportation of the stones (Zougmoré, Jalloh and Tioro, 2014).

The construction of stone bunds along contours is an efficient method to harvest rain water and minimize run-off (Zougmoré *et al.*, 2004). Contour stone bunds are erosion control structures built with quarry rock, stones or lateritic duricrust (Figure 2-1) in a series of two or more. The stones are arranged in lines to follow the contour of the terrain. Before the stones are laid, a linear trench with a depth of about 10–15 cm is dug. Normally, they are built to a height of about 20-30 cm high and a spacing of about 20-50 m apart depending on the slope of the terrain (Zougmoré, Jalloh and Tioro, 2014). Nonetheless, the height can go higher depending on the volume of overland flow.

Figure 2-1: Stone bund constructed with lateritic duricrust on cropland in Manzour (a) and Dibogh (b) in the Ioba province of Burkina Faso. Images captured on 29th May, 2017 during field visit.

The on-site impact of stone bunds on soil erosion can be grouped into short, medium and long term effects based on the period the bunds will become effective to mitigate soil erosion (Morgan, 1995). In the short term, some researchers have highlighted the reduction of slope length and the creation of retaining walls to check runoff and sediment. There is also a reduction in the rate of overland flow and erosivity. These effects of the stone bunds appear immediately after construction (Gebremichael *et al.*, 2005). The medium and long-term effects, include the reduction in hillslope gradient by progressive terrace formation, the growing of vegetation cover on the bunds themselves and the change in land management (Nyssen *et al.*, 2007). The off-site effects of stone bunds result in an enhanced hydrological conditions of the area and decline in sediment accumulation in rivers and dams (Nigussie *et al.*, 2005).

The successes of stone bunds have been recorded by several research (Zougmoré, Jalloh and Tioro, 2014; Taye *et al.*, 2015), especially in Ethiopia where a lot of research work have been conducted on the post implementation of stone bunds (Vancampenhout *et al.*, 2006; Nyssen *et al.*, 2007; Wolka, Moges and Yimer, 2011). For instance, in the works of Gebremichael et al. (2005) the construction of stone bunds in the Tigray region reduced the annual soil loss by 68%. In terms of crop yield, a study conducted by Nyssen et al. (2007) outlined an average increase in yield of about 53% between the space of 3 to 21 years after implementation. In a similar study, Vancampenhout et al. (2006) also reported a significant increase in yield for all crop types. On-farm studies has alluded to the effectiveness of stone bunds in the increase of soil moisture and reduction in soil erosion and downhill sediment transport (Zougmoré, Jalloh and Tioro, 2014). The technique is mainly effective for the reduction of run-off and enhancing water infiltration (Zougmoré *et al.*, 2004).

2.6 Climate Change Impact on Soil Erosion

Climate change impacts resulting from changes in precipitation and temperature (Li and Fang, 2016) has impacted soil erosion since the 1940s (Leopold, 1951; Langbein and Schumm, 1958). Extreme conditions of rainfall and temperature due to climate change have mostly affected soil erosion due to the removal of natural vegetation for the purposes of agriculture and other activities. Also, the use of land management practices unsuitable for the land in use (Bullock, 2005). Rainfall is regarded as the primary causative agent of soil erosion and directly influence soil particles and sediment detachment and transport by runoff (Li and Fang, 2016). Numerous research on climate change impact on erosion have proposed that the rise in rainfall intensity and distribution will exposed the vulnerability of many lands to erosion if nothing is done to protect these lands (Pruski and Nearing, 2002a; Kundzewicz *et al.*, 2007).

Soil erosion rates may change as a result of changes in rainfall patterns for various reasons, but the most direct effect is the increase in the erosivity rate of rainwater (Williams *et al.*, 1996; Pruski and Nearing, 2002a; Nearing *et al.*, 2005). The responds of soil erosion are on both the total amount of rainfall and the variation in rainfall intensity. Nevertheless, the main driver of soil erosion seems to be the intensity and energy but not the rainfall amount alone (Nearing *et al.*, 2005). Studies have shown a predicted increase in soil erosion rate of about 1.7% for every 1% in a statistical rise in total rainfall amount and intensity (Pruski and Nearing, 2002b).

Another pathway of influence of soil erosion by climate change relates to temperature and carbon dioxide (CO_2) driven fluctuations in plant biomass. A system where climate change

affects plant biomass, and where biomass variations influence runoff and soil erosion in a complex manner (Williams *et al.*, 1996; Pruski and Nearing, 2002a).

The amount of CO_2 in the atmosphere has a direct impact on the rate of biomass produced by various plants through direct CO_2 fertilization effects (Stockle *et al.*, 1992). Such biomass variations affect tree crown and ground residue, which affect erosion rates. The rise in CO_2 can also improve stomatal resistance, suppress transpiration, and result in a more moisture soils, favorable to higher erosion due to runoff (Schulze, 2000). Temperature may also influence evapo-transpiration rates, which affect soil moisture, and in turn may impact the level of infiltration and runoff rates (Pruski and Nearing, 2002a)

Again, changes in land use and agricultural practice to adapt to the current climatic regime can result in an indirect effect of climate change on soil erosion (Williams *et al.*, 1996). Adjustments in the dates of crop sowing and harvesting and the use of crops which can adapt to the climate and entire changes in the land use are possible, all of which can potentially change the rates and trends of soil erosion (Nearing *et al.*, 2005). Soil erosion is therefore likely to be influenced badly under future climate variability in several studies across the world most especially in tropical regions such as West Africa (Paroissien *et al.*, 2015). This will in turn threaten the food security in the sub-region.

2.7 Data and Data Issue

2.7.1 Landsat Data

The Landsat mission conceived in the 1960s has seen seven successful satellite launches contributing to an unprecedented 47-year records of Earth Observations that captured global land surface conditions and dynamics (Williams, Goward and Arvidson, 2006; Loveland and Dwyer, 2012). It has demonstrated its value by providing consistent moderate spatial and temporal resolution and multispectral images which is accessible to the public free of charge since January 2008 (Woodcock *et al.*, 2008; Fraser *et al.*, 2014; Birtwistle *et al.*, 2016). Due to its moderate resolution, accurate radiometric calibration, and high geometric precision, the Landsat sensors have become the leader in satellite data for land surface classification, monitoring and change analysis (Wulder *et al.*, 2008; Bhandari, Kumar and Singh, 2012) in many application areas such as agriculture (Leslie, Serbina and Miller, 2017; Hamuda *et al.*, 2018), soil (Aksoy, Özsoy, and Dirim 2009; Azabdaftari and Sunar 2016; Nawar *et al.*, 2014), water (Laili *et al.*, 2015; Hellweger *et al.*, 2004), forestry (White *et al.*, 2017; Onojeghuo and

Onojeghuo, 2015) and settlements (Hu *et al.*, 2016; Esch *et al.*, 2009; Bhatti and Tripathi, 2014).

Its numerous sensors over the years and its overlapping operational periods (Figure 2-2) have guaranteed consistency and continuity of capturing land surface. Due to the periodic enhancements in the data, it has increased the usefulness of the data for scientific and commercial applications (Loveland and Dwyer, 2012). It has also resulted in a reduced temporal resolution (from 16 to 8 days) when two sensors are combined in some instance (She *et al.*, 2015).

The Landsat Global Archive Consolidation (LGAC) initiative managed by the United States Geological Survey (USGS) Earth Resources Observation and Science (EROS) Centre has about four million Landsat images around the globe since 1972, with about 400 scenes added daily (Loveland and Dwyer, 2012; Wulder *et al.*, 2016).

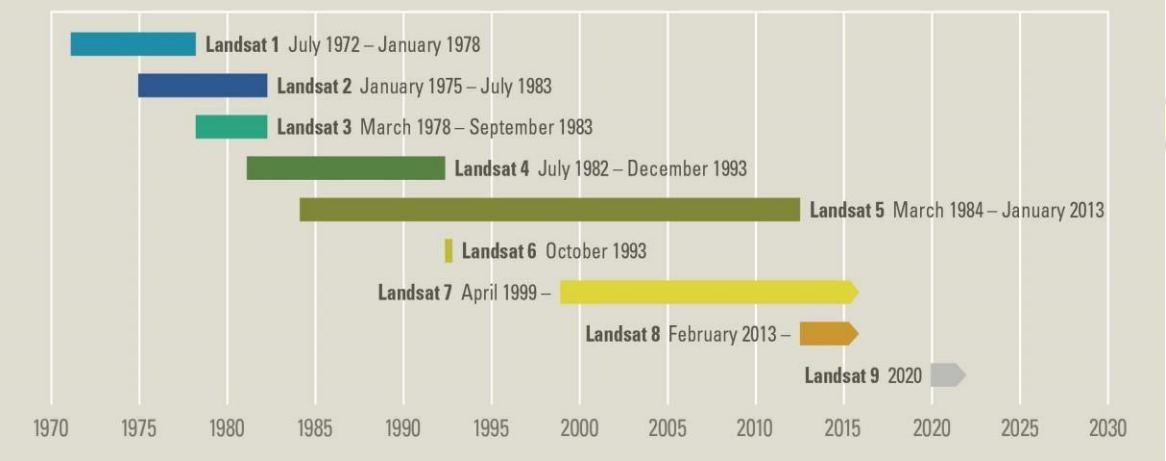

Figure 2-2: Landsat satellite series operational periods (source: Forkuor et al. 2017)

Due to the changes in the USGS-NASA (National Aeronautics and Space Agency) Landsat data policy in late 2008, the U.S. Department of the Interior announced that all Landsat data would be "web-enable", meaning that a standard Landsat product would be made available from the USGS archives via electronic distribution at no cost to the end user. Implicit in this announcement was sustainment of the longstanding policy of non-discriminatory access to the archive. Achieving this revolutionary change in Landsat data policy required a transformation in the product generation and distribution systems (Loveland and Dwyer, 2012).

2.7.2 Landsat Data Issues

Although the Landsat mission has long-term plans for periodic and systematic data capture (Williams, Goward and Arvidson, 2006) and enhanced and free availability to Landsat images through global archive consolidation efforts (Woodcock *et al.*, 2008; Roy, Ju, Kline, *et al.*, 2010; Loveland and Dwyer, 2012), the Landsat image availability for many areas is less than required (Roy, Ju, Mbow, *et al.*, 2010). Landsat data just like any other optical image is challenged with clouds and cloud shadows (Wijedasa *et al.*, 2012; Pouliot and Latifovic, 2018), especially in tropical regions. Again, haze and image artefacts resulting from sensor malfunctioning (Zhang, Li and Travis, 2007; USGS, 2013) have reduced the usability of many Landsat scenes. In persistent cloudy regions such as West Africa, the available images are insufficient for time series analysis, both within and between years (Gómez, White and Wulder, 2016). In the case of sensor artifacts, the Landsat 7 Enhanced Thematic Mapper plus (ETM+) instrument is the worse among all the Landsat mission since May 2003 (Storey *et al.*, 2005). Figure 2-3 shows the resulting data arising from the sensor artifact of Landsat 7 ETM+.

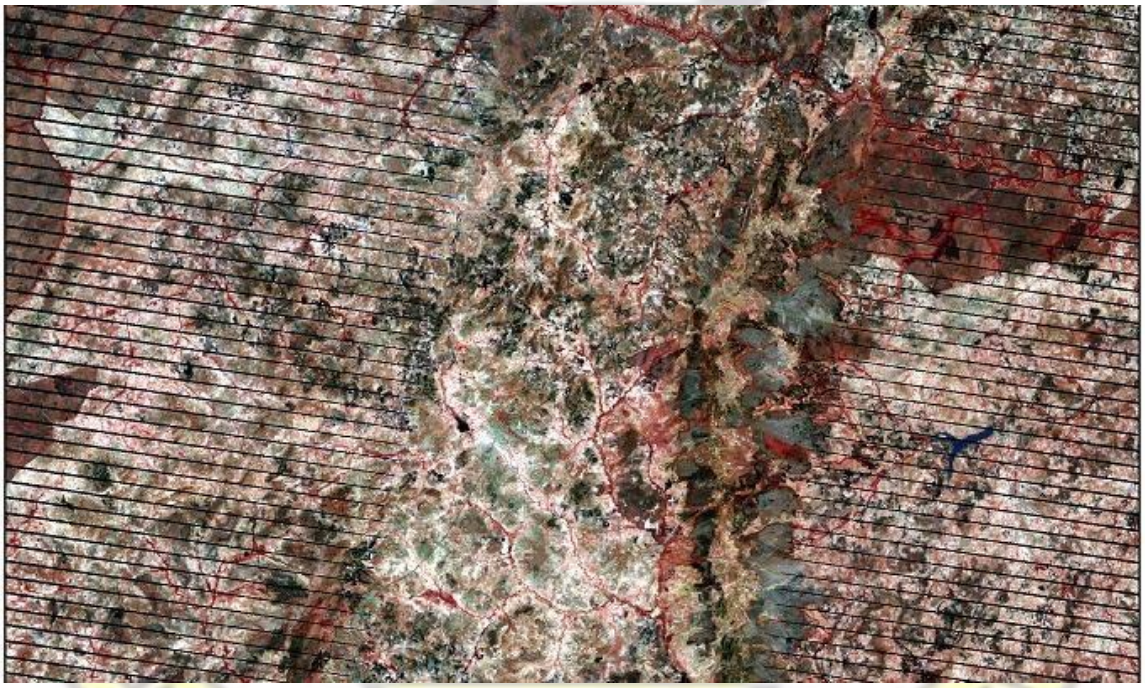

Figure 2-3: A section of Landsat 7 ETM+ SLC-off image; image date: 19/01/2010, path/row 196/052, band combination 4-3-2)

2.8 Satellite Data in Vegetation Phenology Studies

The use of satellite data to study vegetation phenology trends have significantly improved our knowledge on seasonal and yearly variations in vegetation (Fensholt *et al.*, 2009), especially in the era of climate change (Richardson *et al.*, 2013; Tang *et al.*, 2015; Qiang *et al.*, 2016). In vegetation phenology studies, the use of time series approach is fast gaining grounds than the

bi-temporal approach of comparing two images in time (Singh, 1989; Coppin *et al.*, 2004). This is because in the time series approach, data is captured for the whole growing period so changes directly associated to seasonality could be parted from the other changes (Coppin *et al.*, 2004). Numerous research on regional and global scale of vegetation trends (Herrmann, Anyamba and Tucker, 2005; Forkel *et al.*, 2013; Liu *et al.*, 2015; Tian *et al.*, 2016; Zhang *et al.*, 2017; Lamchin *et al.*, 2018) have been done and have identified that vegetation phenology is driven by rainfall and temperature interactions (Hickler *et al.*, 2005; Verbesselt, Hyndman, Newnham, *et al.*, 2010). The use of satellite data to monitor vegetation phenology over a wide area started more than four decades ago (Rouse Jr *et al.*, 1974; Tucker, 1979). Currently, there is a wide utilization of satellite data in vegetation phenology studies.

Satellite data like the Advanced Very High Resolution Radiometer (AVHRR), Satellite Pour l'Observation de la Terre (SPOT) VEGETATION and the Moderate Resolution Imaging Spectro-radiometer (MODIS) are the most frequently used data in vegetation trend studies to due to their high temporal resolution and large scene coverage (Xie, Sha and Yu, 2008; Higginbottom and Symeonakis, 2014; Eckert *et al.*, 2015; Leroux *et al.*, 2017). But its coarse resolutions (250 m to 8 km) (Hostert *et al.*, 2015) cannot detect and monitor small-scale change categories of land cover and ecosystems (Coppin *et al.*, 2004; Rao *et al.*, 2015). Especially those from agriculture activities (Schroeder *et al.*, 2011; Begue *et al.*, 2014) and as such it is useful for regional and global scale application (Ju and Masek, 2016). Since trends in greenness are very important at the local level (Zhu *et al.*, 2017), the use of medium to high resolution data is vital in this quest (White *et al.*, 2017).

2.9 Applications of NDVI

The use of the ratio of red and near-infrared bands to study vegetation started in the late 1960s (Yengoh *et al.*, 2014). Tucker (1979) was the first to use it for determining total dry matter accumulation, first from hand-held instruments and later from National Oceanic and Atmospheric Administration (NOAA) AVHRR satellite data. He demonstrated that the growing season integral of frequent NDVI measurements represented the summation of photosynthetic potential as total dry matter accumulation (Yengoh *et al.*, 2014). Currently, NDVI has been used in a lot of studies around the globe (Higginbottom and Symeonakis, 2014; Xie, Sha and Yu, 2008; Cao *et al.*, 2018; Meroni *et al.*, 2019) for vegetation monitoring and mapping. The use of NDVI data has blossomed into many fields of natural resources

investigation such as land use/cover dynamics, drought, desertification, soil erosion, vegetation fires, biodiversity monitoring and conservation, and soil organic carbon (Yengoh *et al.*, 2014).

2.10 Un-manned Area vehicle (UAV) Application in Vegetation Mapping/Monitoring The potential for environmental remote sensing using small UAV has been highlighted since the last 30 years (Hardin *et al.*, 2018). The last decade has seen a rising expansions and improvement in UAV technology, together with the improvement of the sensing devices installed on them have provided brilliant avenue for remotely sensed applications (Pajares, 2015). A UAV system is mainly made up of sensor payload for data capture, automatic piloting for control of the entire craft, Global positioning System (GPS) for navigation, Inertial Measurement Unit (IMU) for attitude measurement, data link for signal transfer and ground station for mission planning and information interaction (Hackney and Clayton, 2015).

The UAV has been extensively applied for monitoring vegetation and environmental parameters aiming at optimization. Due to its high to ultrahigh spatial resolution imagery which can be obtained in real time, it is used for precision agriculture and environmental and ecosystems studies at a fine scale (Candiago *et al.*, 2015; Gago *et al.*, 2015; Lu and He, 2018).

The UAV has been used in numerous research such as agriculture, urban vegetation mapping and ecosystems monitoring (Zhong *et al.*, 2018). In the field of agriculture, it can be used to identify the signs of diseases and pest infestation, crop growth and maturity. For example, in the works of Herwitz et al. (2004), they highlighted the worthiness of UAVs to notice irrigation and fertilization anomalies and crop maturity in crop field. Similarly, Candiago et al. (2015) reported some experiences related to the analysis of cultivations (vineyards and tomatoes) with Tetra-cam multispectral data. In the area of ecosystem studies, Lu & He (2018) used it for species classification in a heterogenous grassland ecosystems. They concluded that, the advantages of the UAV being, flying at relatively low altitudes, better image resolution and cost effective, a very high temporal resolution, it will be the preferred choice in such studies.

CHAPTER 3: STUDY AREA

3.1 Introduction

This chapter describes the area where this study was conducted. It is divided into two main sub-sections. The first sub-section highlights the geographical location of the study area in Burkina Faso. The second sub-section elaborate on the biophysical characteristics (land cover/use, topography, geology and soils, climate and the socio-economic characteristics) of the study area.

3.2 Geographical Location

The Study was conducted in the Ioba province of Burkina Faso in West Africa. It is located between latitude 011° 20' 47" and 010° 42' 20" N and longitude 003° 26' 05" and 002° 37' 28" W with a total land mass of about 2,648 km^2. Hydrologically, the study area falls within the Black Volta basin which stretches from Mali (Western neighbour) through to Ghana (southern neighbor). The Ioba together with Bougouriba, Poni and Noumbiel are the four provinces in the South-West Region of Burkina Faso. The Ioba province, which is the north-most province in the South-West Region, sits on the north-western border of Ghana along the Black Volta River (Mouhoun) (Figure 3-1a). The province is further divided into 6 communes (Dano, Dissihn, Ouessa, Oronkua, Guéguéré and Koper) with Dano as its administrative capital. The names of the communes represent the major towns in the province. There are several rural settlements scattered within the farming areas in each commune.

Four basins with implemented stone bunds erosion controlled systems on both agricultural lands and natural vegetation were selected for vegetation improvement analysis. The basins, Batiara, Badiere, Namere and Dibogh, located in the Dano, Gueguere, Dissinh and Koper communes (Figure 3-1c) have a size of 4634.82 ha, 8211.32 ha, 8214.36 ha and 4634.07 ha respectively. The non-erosion controlled areas, which describe areas without stone bunds erosion controlled systems, were selected from four different sites based on field campaigns and with the help of google earth images. The areas are, Bankandi, Biengane, Bisserke and Wizini.

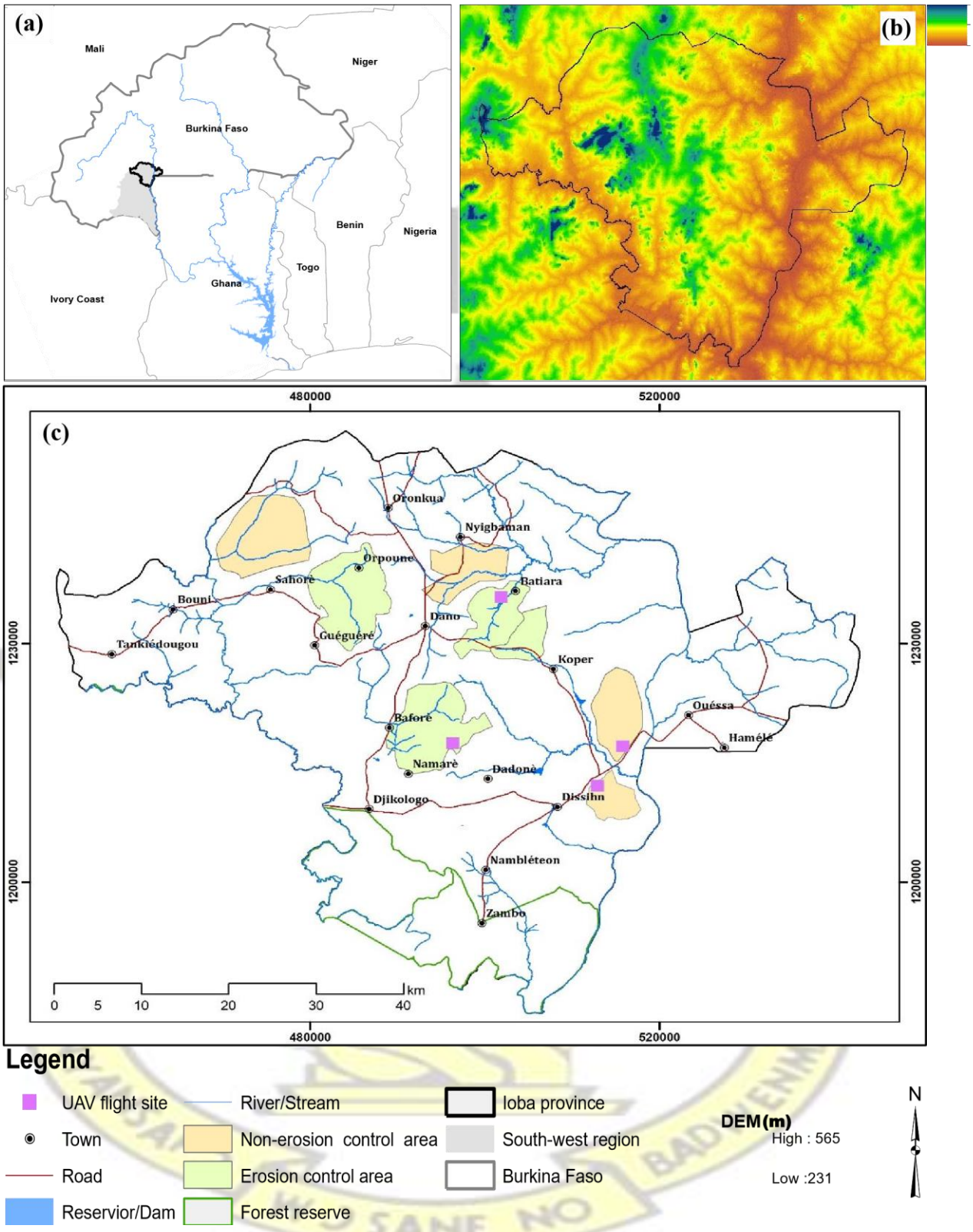

Figure 3-1: Map of study area; (a) location of the study area within West Africa, (b) DEM of the study area, (c) location of test sites within the study area.

3.3 Biophysical Characteristics

3.3.1 Land Cover/Use

The study area falls within the Sudanian savanna climatic zone and as such the natural vegetation is made up of forest, savanna woodland, arboraceous or scrubby savanna and abundant perennial grasses. The dominant woody species includes *Gardenia sp, Combretum micranthum, Parkia biglobosa* (African locust bean), *Vitellaria paradoxa* (Shea tree), *Bombax costatum, Berlinia grandifotia* (Zoungrana *et al.*, 2015). The major land use in the area is agriculture (crop production). The main staple crops cultivated are millet (*Pennisetum glaucum*), sorghum (*Sorghum bicolor*), maize (*Zea mays*) and cowpeas (*Vigna unguiculata*). About 80% of the area cultivated are occupied by these staple crops (Ouattara, 2007). Cotton (*Gossypium hirsutum*) is the most important cash crop cultivated (Hipt *et al.*, 2017). Most farmers cultivate cotton because of its lucrative nature alongside food crops. The type of farming practice in the area is parkland agroforestry (Nikiema, 2005). This is whereby useful indigenous tree species are left on crop lands to become part of the farmland. The establishment of a parklands system relies on indigenous agricultural practices which involves the clearing of natural vegetation for cultivation, but woody species and tree crops which have economic value are left on the land to be part of the crop fields (Nikiema, 2005). Parkland trees are trees/tree crops which have economic value. They are used for food (cooking oil, fruits), medicine, firewood, shelter, tools and forage. Example include, *Vitellaria paradoxa, Parkia biglobosa and Lannea microcarpa*.

In the study area, crop cultivation depends more on increase in farm size than increase in yield and this has resulted to the fast conversion of the other land cover/use types (example forest and savanna grassland) to agriculture (Ouattara, 2007). Because rainfall in the Sudanian has a short period (May to October) followed by dry season (November to April), there are several irrigation dams purposely for dry season cultivation. The crops under irrigation are mostly vegetables (tomatoes, onion, cabbage, pepper etc). Crop cultivation is subsistence with farmers using hand hoe as the tillage tool (Callo-Concha, Gaiser and Ewert, 2012). As a form of residue management, farmers after harvesting use stems of sorghum/millet to cover the soil. The main soil and water conservation practice is the use of stone bunds (Zougmoré, Jalloh and Tioro, 2014). The study area has several networks of rivers but most of them are seasonal (flows when there are rains and dries up in the dry season). The most prominent rivers are the Bougouriba and the Black Volta rivers. The southern part of the study area is home to the Bontioli National Park which is the biggest protected area in the province.

3.3.2 Topography

Topographically, the Ioba province is relatively flat with some slight undulating areas with concave and convex slopes. The elevation is between 230 m and 566 m above msl (mean sea level) (Figure 3-1b). In Dano, the relief is characterized by the Ioba mountains, the fragments of an ancient eroded Birimian mountain range oriented in the North-north east to South-south west (NNE-SSW) direction (Schmengler, 2010). From the field campaign, it was observed that the hilltops are characterized by lateritic residuum (duricrust). Also, there are few inland valleys where water discharges forming a seasonal or permanent river/stream. These valleys are mostly suitable for growing rice during the rainy season and vegetables during the dry season.

3.3.3 Geology and Soils

The geological formation lies predominantly on a Paleoproterozoic granitoid made up of Birimian rocks (Callo-Concha, Gaiser and Ewert, 2012). Granites dominate the Birimian rocks. Magmatic rocks such as dolerites (gabbro) and andesites can also be found in the area. Evidence of strong physical and chemical weathering can be found. This is evident in the presence of metamorphic rocks like quartzite and its mineralized forms such as pyrite and quartzolite (Schmengler, 2010).

The soil in the study area are mostly lixisols made up of sandy loams of more than 70% being sand. This is as a result of the parental material (granitic rock) and the impact of erosion and leaching of clay particles. Because of its low organic matter content, they have high rate of water infiltration and low water retention capacity in the top layers making it susceptible to erosion and compaction (Callo-Concha, Gaiser and Ewert, 2012; Forkuor, 2014). A study conducted by Schmengler (2010) in Dano which involved an integrated scale-dependent method to evaluate on-site and off-site impacts of soil erosion at hillsides and catchment scales concluded that, the average soil loss rates of less than 5 t ha^{-1} yr^{-1} and maximum erosion rates of more than 50 t ha^{-1} yr^{-1} can be achieved in erosion hotspots. Other minority soil types in the area include, leptosols, fluvisols, Rhodic cambisols and luvisols. Rhodic cambisols have clay to silty clay texture. Due to their high cation exchange capacity, richness of bases and good soil fertility, they are favorable for agriculture. Leptosols which have clay loam to loam texture, have very shallow topsoil and limited water holding capacity (Schmengler, 2010). Soils in cultivated areas have poor organic matter content. Consequently, farmers use organic and inorganic fertilizers in other to obtain an appreciable yield (IUSS, 2006). Secondly, the use of soil and water conservation structures is being practiced to minimize erosion of the little nutrients left.

Lateritic residuum (duricrust, loose gravels and pisolithic soils) are also common in the area. Loose lateritic gravels and pisoliths are widespread and have formed lags on truncated and preexisting preserved relict surfaces (Arhin, Zango and Ruerrger, 2015). The duricrust are mostly found on hill top, hill sides and sometimes in valleys. Butt and Bristow (2013) reported that, the duricrusts in the study area are mainly ferricretes, that is, Iron-oxide cemented sediments.

Because of scarcity of land, some farmers are forced to plant between these lateritic duricrusts.

3.3.4 Climate

Climate patterns in West Africa are as a result of the movement of the Inter Tropical Convergence Zone (ITCZ) (Landsberg, 1972). The ITCZ is manifested by the convergence of the north-eastern winds originating from the Sahara desert and the flow of the south-west monsoon from the Atlantic (Nicholson, 2013). The classical definition of the ITCZ is the convergence of the trade winds of the two hemispheres (Nicholson, 2009). This zone is characterized by low pressure, rising motion, clouds and precipitation (Nicholson, 2009). The northward migration of the ITCZ during northern spring and summer is linked to the start of the monsoon system over West Africa (Sultan and Janicot, 2000).

The most prominent feature of the West African climate system is the West African monsoon (WAM). It occurs during the boreal summer due to the differential warming over the land surface and the ocean (Roudier *et al.*, 2011). It contributes to majority of the yearly rainfall and is therefore importance for people who rely on rainfed agriculture for sustainable economy in West African (Fink, Vincent and Ermert, 2006; Omotosho and Abiodun, 2007; Weldeab, Schneider and Andersen, 2007; Akinsanola and Ogunjobi, 2015; Klein *et al.*, 2015). Several precipitation systems associated to the WAM have been identified to cause rainfall over West Africa in the period of summer monsoon. These are made up of organized mesoscale convective systems (MCSs), monsoon rains, and unorganized local thunderstorms or showers and others (Fink, Vincent and Ermert, 2006).

In the Sudanian savanna, the climate is characterized by high temperature and a uni-modal (single peak) rainfall pattern. The rainfall period is mostly between May and October followed by a long period (November to April) of dry season (Figure 3-2). In the dry season, the harmattan winds carry dust-laden air masses made up of very high concentration of aerosol from the Sahara, reaching its peak in January (Schmengler, 2010).

3.3.4.1 Rainfall

In the Ioba province, the high variability of onset of rains, has bedeviled local farmers with the problem to decide when to grow their crops (Laux, Kunstmann and Bardossy, 2008). Depending on the year, it may be at the beginning, mid or end of May. The first scattered rainfalls in April are still considered as dry season rains (referred to as the "Mango rain") and this signifies the end of the dry season (Schmengler, 2010). In the rainy season, rainfall is characterized by heavy down pours which sometimes last for few minutes. The average annual rainfall from 2000 to 2017 is about 988mm with 2016 being the year of highest rainfall (about 1166mm) and a value of about 715mm was recorded as the lowest which occurred in 2005. Rainfall peaks are mostly observed in the month of August (Figure 3-2) with a maximum value of about 300mm (from 2000 to 2017 station data). Studies by Omotosho (2008) and Nicholson (2013) have shown declining rainfall totals in WA in the past few decades and this has been associated with the seasonal cycle and a westward travelling intra-seasonal scale atmospheric circulation pattern in the monsoon layer (Sultan and Janicot, 2000).

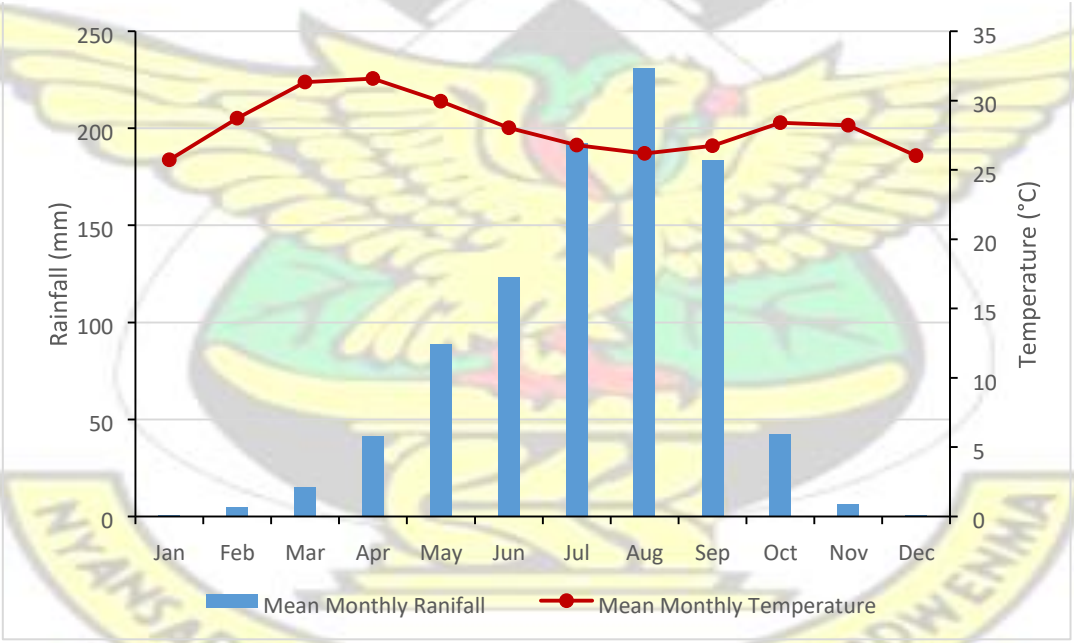

Figure 3-2: Average Monthly Rainfall and Temperature in Ioba Province from 2000 to 2017 (data obtained from Burkina Faso Meteorological agency through WASCAL for climate station in Dano)

3.3.4.2 Temperature

In Burkina Faso, there is a significant difference in temperature as you move from south to north. The Sudanian savanna zone experiences a relatively low temperature compared to the other climatic zones. During the dry season, day-time temperatures are very high and mostly

peaks in the month of March/April (Figure 3-2) with average value of 37.7 °C from 2000 to 2017. In the rainy season, lowest day-time temperatures (average of about 30.8 °C) are recorded in the months of July, August and September. Temperatures are mostly low (values as low as 12.1 °C can sometimes be recorded) at night-time in the months of December and January and these low temperatures are as a result of the harmattan winds. The average annual temperature in the study area is about 28.1 °C. Studies conducted by Ouédraogo (2004) and Sandwidi (2007) show an increase in average temperature of about 1 °C between 1960 and 1990 over West Africa.

3.3.5 Socio-Economic Characteristics

3.3.5.1 Demography

Burkina Faso is one of the countries in West Africa with the highest population growth (rate of about 3%). In the Ioba province, data from the National Institute of Statistics and Demography of Burkina Faso shows an increase in population of about 10% from 1985 to 2006. Despite this increase, population density in the province is less than 100 people per km^2 (Forkuor, 2014). The province has a very high population of rural dwellers (about 90%). Out of this, women and young people (below 18 years) form the majority. The growing population in the rural areas has caused an expansion in agriculture. This has gradually intensified leading to a decrease in land fallow periods and cultivation of marginal lands which have negatively affected soil fertility (Callo-Concha, Gaiser and Ewert, 2012; Yira and Diekkrüger, 2016). Since 1990, an average of 2% of savanna in the study area is converted annually to agricultural land leading to the destruction of natural vegetation and encroachment on reserved forest (Yira and Diekkrüger, 2016).

3.3.5.2 Livelihood and Income

The rural population are mostly smallholder, subsistence farmers (cropping and livestock rearing), with poor technology and low investments (Callo-Concha, Gaiser and Ewert, 2012). Crop cultivation is mostly rainfed and occurs from May to October. Nonetheless, there are very few irrigated areas, which are mostly used for vegetable production. The major limitations for crop cultivation are lack of farming inputs (for example, fertilizers and pesticides) and labor, and poor soil and water conservation management (Kassam *et al.*, 2009). Although access to credit is a major problem in the area, the few farmers who get them use it to cultivate cash crops

(specifically, cotton). The proceeds from the cash crops are used for household expenditure and for buying farm inputs for the up-coming farming season. The people need to make a long-time savings in other to buy bicycles and motorbikes for commuting.

In the study area, few people are engaged in off-farm activities. Trading activities and provision of services mostly occur in the major towns. In the rural areas, women are engaged in processing and sale of local beer, shea butter, fruits and firewood gathering. The men engage in animal rearing such as cattle, goat, sheet, pig and poultry to support their expenditure. During market days, the trade in agricultural products such as cereals, vegetables and livestock is organized mostly by peasant producers and intermediaries (Callo-Concha, Gaiser and Ewert, 2012).

Aside agriculture, another source of income engaged mostly by the youth is illegal small-scale mining. Although it started in some few years, its lucrative nature cannot be under estimated compared to the income the people generated from agriculture. Consequently, the local people are ready to sell or rent their arable lands to these miners (most of them migrated from other parts of the country and neighboring Ghana) for lump sum without considering the destructive nature of the mining activities.

Non-availability of agricultural lands has led to the outmigration of the youth to cities. The few youthful population remaining also engage in seasonal outmigration (Callo-Concha, Gaiser and Ewert, 2012). During the dry season, they migrate to the southern part of neighboring Ghana in search for jobs such as laborers on cocoa plantations, small scale mining concessions and menial jobs in the cities. Those who find lucrative jobs become permanent migrants and on a regular basis send remittances to their family back home.

CHAPTER 4: DATA AND DATA PRE-PROCESSING

4.1 Introduction

In this chapter, the data used in this study and the pre-processing that were carried out prior to the analysis have been outlined and explained. From the objectives of the research, two main

data sets were involved. The first section (4.1) describes the Landsat data (NDVI) used in the study. It also highlighted on the source and the steps undertaken in the online processing of Landsat images into NDVI data. Section 4.2 introduces the aerial photos obtained from the UAV survey conducted on a regular basis from the start of crop cultivation until harvesting. The last section (4.3) explains the ancillary data used in the study. They include reference data collected through field visits and climate (rainfall and temperature) data acquired from stakeholder institutions.

4.2 Landsat Data

Landsat data were used for analyzing the vegetation trend for the whole province and subsequently for areas with stone bunds erosion control and non-erosion controlled area. The study area is located within 196/052 (path/row) with the Worldwide Reference System (WRS).

All available Landsat data from 2004 to 2017 with cloud cover less than 30% were considered for further processing into NDVI data. Images from Landsat 8 Operational land imager (OLI), Landsat 7 ETM+ and Landsat 5 Thematic Mapper (TM) sensors were selected from the USGS database through the earthexplorer platform (http://earthexplorer.usgs.gov/). Due to the scarcity of Landsat data in the region as a result of persistent cloud cover especially during the rainy seasons, a total of 109 images out of 168 (one image was selected from each month) for the study period were suitable. Out of the 109 images, 21 images were TM images, 51 were ETM+ SLC-off images and 37 were OLI images. Although, the data with more than 30% of cloud cover were rejected, some of the months did not have data at all in the USGS database (Table 4-1). In all, data for 59 months were either non-available in most cases or full of clouds and therefore cannot be used. Figure 4-1 shows the distribution of missing data within the period of study. The 109 selected Landsat scenes were then processed using the USGS Earth Resources Observation and Science (EROS) Center's Science Processing Architecture (ESPA) on-demand interface (https://espa.cr.usgs.gov/). On the ESPA platform, the processing of TM and ETM+ data into surface reflectance (SR) were done using the Landsat Ecosystem Disturbance Adaptive Processing System (LEDAPS) (USGS, 2017) and the OLI data with the Landsat 8 Surface Reflectance Code (LaSRC) algorithms (Vermote *et al.*, 2016). Further processing of SR data into spectral indices (NDVI in this case) was also done on the ESPA platform. The ESPA processing system also generates the pixel quality assurance (QA). The QA band contains the pixel condition such as clouds, cloud shadows and snow in Landsat data based on the spectral and spatial information. The QA band is generated using the CFmask, C

code based on the Function of Mask (Fmask) algorithm proposed by Zhu and Woodcock (2012) and Zhu, Wang, and Woodcock (2015). In the case of this study, the QA band had only clouds and cloud shadows without snow. The QA bands were used to mask-out the NDVI pixels with clouds and cloud shadows. The NDVI images together with the pixel QA band (Figure 4-2) and the Metadata file were then downloaded for analysis.

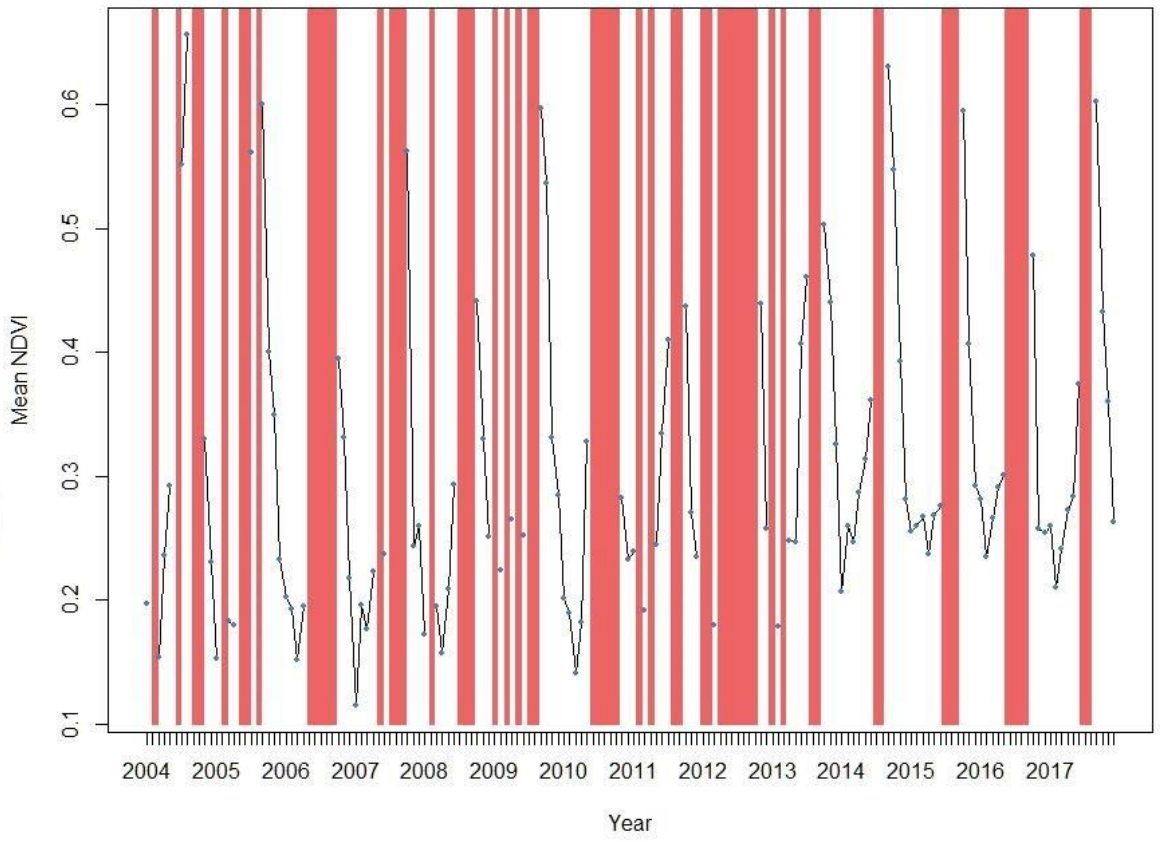

Figure 4-1: Distribution of Missing data within the period under study (the blue dots are the available data points and the red strips represent missing data)

Table 4-1: Landsat NDVI time series data obtained from the USGS database (path/row, 192/052)

YEAR	JAN	FEB	MAR	APR	MAY	JUN	JUL	AUG	SEP	OCT	NOV	DEC
2004												
2005												
2006												

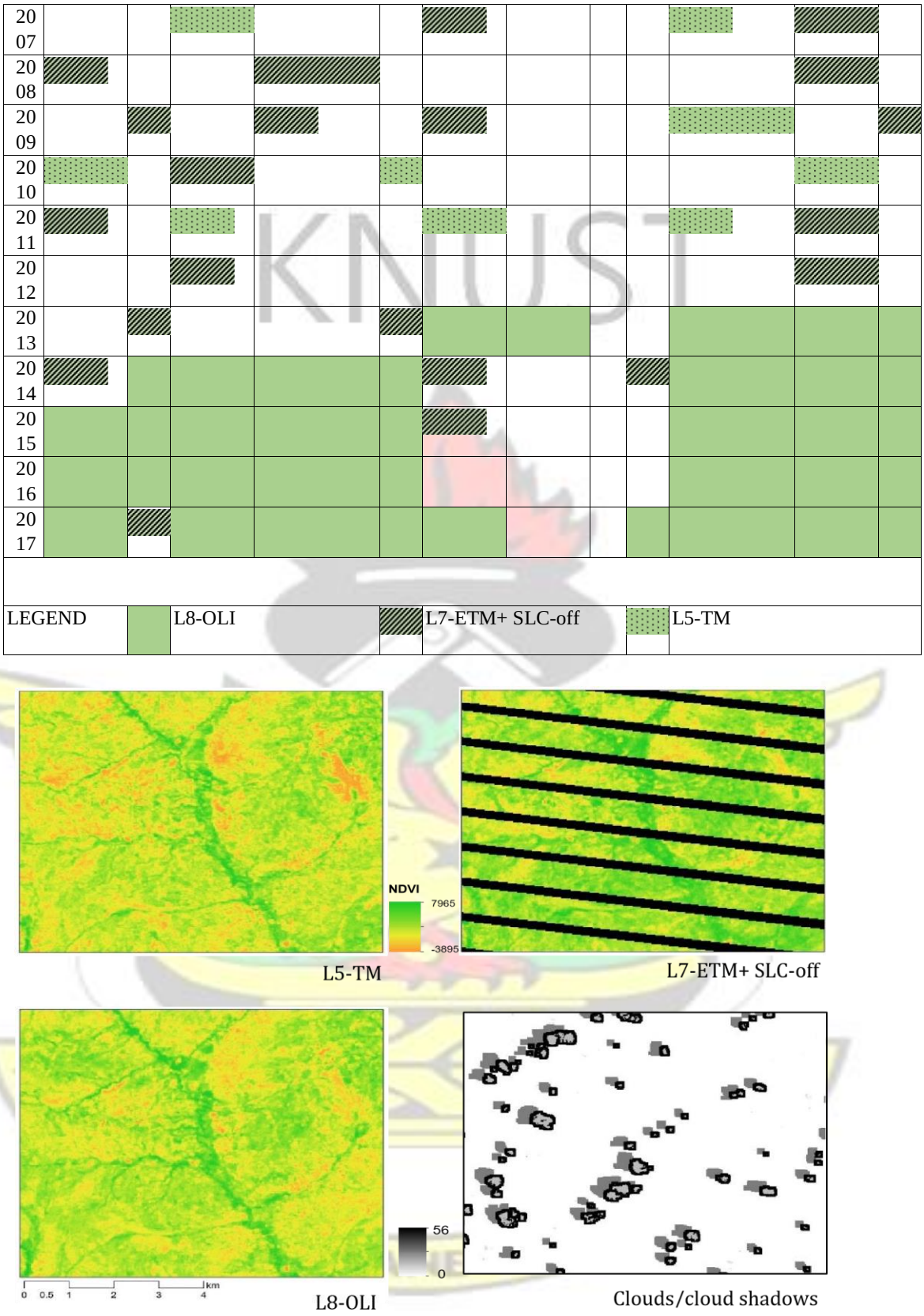

Figure 4-2: Sample of Landsat data from each sensor downloaded from the ESPA platform after processing. (Data acquired on: L5-TM: 29-10-2011; L7-ETM+ SLC-off: 28-10-2008; L8-OLI: 29-10-2017, note: NDVI values are multiplied by 10,000)

4.2.1 The LEDAPS and LaSRC Algorithms

The LEDAPS and LaSRC atmospheric correction algorithms hosted on the ESPA platform aid in rapid processing of large quantities of Landsat level-1 data into SR products. It was initially used to generate a SR record of over 2000 Landsat images over North America (Masek *et al.*, 2006) and has subsequently been extended globally through NASA/USGS Global Land Survey (GLS) program (Feng *et al.*, 2012). Several studies (Masek *et al.*, 2006; Feng *et al.*, 2012; Ju *et al.*, 2012; Maiersperger *et al.*, 2013; Vermote *et al.*, 2016) have examined the performance of the LEDAPS and the LaSRC systems, compared them to many reference data and have found it useful for processing of Landsat top of atmosphere (TOA) reflectance to SR data. The LEDAPS SR algorithm described in Masek et al. (2006) uses the Second Simulation of the Satellite Signal in the Solar Spectrum (6S) radiative transfer code to calculate the transmission, intrinsic reflectance, and spherical albedo for relevant atmospheric constituents (Vermote *et al.*, 1997). It then computes the SR by accounting for the effects of atmospheric scattering and absorption on the TOA reflectance. In general, the LEDAPS correction scheme is applied to reflective bands to adjust for the effects of molecular scattering and absorption of atmospheric constituents including gases, ozone, water vapor, and aerosols, as well as for Rayleigh scattering (Vermote *et al.*, 1997; Feng *et al.*, 2012; Maiersperger *et al.*, 2013). The 6S is an enhanced form of the Simulation of the Satellite Signal in the Solar Spectrum (5S) developed by the Laboratoire d'Optique Atmospherique.

The processing involves, first and foremost the conversion of Landsat 5 or 7 Level-1 data to TOA reflectance and brightness temperature using published calibration coefficients. Then the 6S radiative transfer model is used to derive lookup tables for application of the correction (Maiersperger *et al.*, 2013). The LEDAPS depends heavily on independent auxiliary data sources for air pressure, air temperature, ozone, and topography, and also uses a scenedependent dense dark vegetation (DDV) approach (Kaufman *et al.*, 1997) for aerosol retrieval. A fixed continental aerosol model is used for estimating the aerosol optical thickness (AOT) parameter, which in turn is used for final correction.

The LaSRC algorithm proposed by Vermote et al. (2016) has a similar approach like the LEDAPS but the LaSRC takes advantage of some of the new spectral bands (e.g., the cirrus band and the new blue band) that are less subject to atmospheric absorption, as well as using better ancillary datasets (Vermote *et al.*, 2016). The LaSRC is based on a rigorous radiative transfer model, the Vectorial (V) version of the 6S code known as the 6SV. The method adopted

for atmospheric correction relies on the inversion of the relatively simple equation in the Lambertian case with no adjacency effects, that accounts for a simplified coupling of the absorption by atmospheric gases and scattering by molecules and aerosols (Vermote *et al.*, 1997). This approach has been applied to MODIS data since the year 2000 to produce daily and 8-day SR products.

4.2.2 Function of Mask (Fmask) Algorithm

The Fmask algorithm, which was first proposed by Zhu and Woodcock (2012) and later improved and expanded by Zhu et al. (2015), is an object-based cloud, cloud shadows, and snow detection algorithm for Landsat images. The input data are TOA reflectance for the reflective bands and brightness temperature (BT) for the thermal bands.

The first stage of the Fmask algorithm uses rules based on cloud physical properties (which involves the combination of several spectral tests such as NDVI and NDSI) to identify the Potential Cloud Pixels (PCPs) and clear-sky pixels. This test is one of the fundamental tests in cloud identification. The clear-sky pixels are then used to compute cloud probability separately for water (by combining temperature and brightness probabilities) and land (by combining temperature and variability probabilities). This separation is done because there can be variations in the temperature distributions as well as the range of reflectance of water and land in time and space (Zhu and Woodcock, 2012). The temperature probability is very effective because clouds are typically colder than the subjacent land surface (Frantz *et al.*, 2018).

The next stage, which involves detection of potential cloud shadows, is done by applying the flood-fill transformation (Soille, Vogt and Colombo, 2003) to the near infra-red (NIR) band. This is achieved because the diffusive radiation in the shadows will be relatively smaller at longer wavelengths (for example NIR and SWIR bands), making the shadowed pixels darker than their surroundings (Luo, Trishchenko and Khlopenkov, 2008). This darkening effect of cloud shadows is most obvious in the NIR band (Zhu and Woodcock, 2012).

In the final stage, the cloud and cloud shadows are marched by predicting the possible cloud shadow location based on the geometric relationship between a cloud and its shadow. By using the satellite's view angle, the solar zenith angle and the solar azimuth angle, the projected direction of the cloud shadow can be calculated. With the idea that clouds and their shadows have similar shape, the cloud object is then matched with the potential shadow. In the case of

cloud and cloud shadow detection in Landsat 8 images, Zhu et al., (2015) added the cirrus band to facilitate better detection of thin cirrus clouds.

The Fmask algorithm as tested by Zhu and Woodcock (2012) gave a cloud overall accuracy of 96.41%, cloud producer's accuracy of 92.1%, and cloud user's accuracy of 89.4%. Based on the accuracies achieved by the Fmask algorithm, some researchers (Foga *et al.*, 2017; Frantz *et al.*, 2018) have rated the algorithm as one of the best so far.

4.2.3 NDVI Data

The NDVI data used in the study were processed on the ESPA processing platform. They were generated at 30m spatial resolution on a Universal Transverse Mercator (UTM) in a Geo TIFF file format. The NDVI was calculated as the ratio of the difference between the near-infrared band (NIR) and the red band (R) and the sum of these two bands (equation 4-1) in the traditional fashion (Rouse Jr *et al.*, 1974; Tucker, 1979).

$$NDVI = \frac{(NIR-Red)}{(NIR+Red)} \quad (4\text{-}1)$$

Where NIR is reflectance in the near-infrared band and Red is reflectance in the visible red band. The NDVI values ranges from −1 to +1 with positive values corresponding to vegetation. The higher the value, the greater the chlorophyll content (greenness) of the vegetation.

4.2.4 Gap-filling of Landsat 7 SLC-off Images

In May 2003, a small mirror in the optical path of the Landsat 7 Enhanced Thematic Mapper plus (ETM+) instrument known as the Scan Line Corrector (SLC) failed permanently (Zhang, Li and Travis, 2007; USGS, 2013). The failure of the SLC whose function was to compensate for the forward motion of the satellite during data acquisition has resulted in images with wedge-shaped gaps that range from a single pixel near the centre of the image to about 14 pixels along the east and west edges (Maxwell, 2004; Maxwell, Schmidt and Storey, 2007). On average, each scene has lost about 22% of the image's data. Nonetheless, the remaining spectral information exhibits the same radiometric and geometric qualities as images taken before the failure (Storey *et al.*, 2005). This type of ETM+ images is known as SLC-off images. In searching for the available Landsat images, the choice of OLI and TM for a particular month always supersedes the choice of ETM+ SLC-off image (since OLI and TM does not have the

above defect) unless they are hindered by excessive cloud cover. In that instance then the ETM+ SLC-off image was chosen. As reported by USGS (2013), for local scale applications (e.g. mapping or event monitoring) the effect of the data gaps may have substantial influence on the results. Due to this and the fact that the ETM+ SLC will be combined with OLI and TM there was the need to fill the gaps in the ETM+ SLC-off images.

After the failure of the SLC, many algorithms have been proposed to fill the gaps in the SLCoff image. The first among such methods were the Localised Linear Histogram Matching (LLHM) and the Adaptive Window Linear Histogram Matching (AWLHM) developed by a joint USGS/NASA (National Aeronautics and Space Administration) research team (Scaramuzza, Micijevic and Chander, 2004). Subsequently, other methods (Zhang, Li and Travis, 2007; Pringle, Schmidt and Muir, 2009; Mariethoz, Renard and Straubhaar, 2010; Chen *et al.*, 2011; Zhu, Liu and Chen, 2012; Zeng, Shen and Zhang, 2013; Zhang, Li and Civco, 2014) have been developed and have proved superior to the premiere methods. In all these approaches, one thing is common. They use auxiliary data from previously or currently acquired Landsat image (SLC-on or SLC-off images from Landsat 7 or TM images from Landsat 5) to fill the missing data (gaps).

In this study, the gap-filling algorithm, Geostatistical Neighbourhood Similar Pixel Interpolator (GNSPI) proposed by Zhu, Liu and Chen (2012) was used. The GNSPI combines deterministic interpolation and geostatistical principles. The technique uses physical or empirical models to first detrend the data in the target image (the image whose gaps is to be filled) and subsequently uses ordinary Kriging to predict the residual. The algorithm involves a six step process; data de-trending using empirical or physical models (steps 1 & 2); estimation of the semi-variogram of the residuals arising from the de-trending model (step 3); prediction of the residuals of the locations without observation from ordinary kriging (steps 4 & 5); and the final prediction of locations without observation is obtained by adding back the trend (step 6). Although the GNSPI has similar accuracies compared to other methods when using a temporarily close input images (images used to fill the gaps in the target image), the strength of the GNSPI is visible when using temporarily further input images. The GNSPI is therefore a better choice in cloudy areas because of the difficulty in obtaining a temporarily close input image. The choice of this method was due to the heavy cloud cover especially during the rainy season in the study area. A comparative studies conducted by Yin et al. (2017) and Romero-sanchez et al. (2015) rated the GNSPI very high over several others. The algorithm is written in the Interactive Data Language (IDL) and was run in ENVI 5.3 + IDL 8.5. The following parameters were set because they gave optimum results after a lot of trials; sample size of 20, the maximum window

size of 12, the estimated number of classes was 5, the number of images in the time series excluding the input image was 1, the range of minimum and maximum DN values of the image was [0, 1], and the block size was 500.

All the Landsat 7 NDVI images used in the study were SLC-off images and so needed to be gap-filled. Figure 4-3 shows the flow of the algorithm processes to arrive at the final results. The input images were selected as close as possible to the target images where necessary. The TM, ETM+ SLC-on and ETM+ SLC-off images were used as input images. The use of SLCoff images is possible because the location of the scan gaps are different for each SLC-off scene (Storey *et al.*, 2005). The algorithm requires a minimum of one input image but a second or a third input images (known as a time series image) would be required if the input images are ETM+ SLC-off images. This is because a single ETM+ SLC-off images may not be able to completely fill all the gaps in the target image. The Portions of the target image with data (no gaps) were not altered in the gap filling process. The output gap-filled images were visually assessed to check if there were some gaps still left on them. The results show that all the gaps were completely filled, and the image looks spatially continuous with no anomalies or artefacts on them. A sample of the ETM+ SLC-off (target image) and the gap-filled images are show in Figure 4-4.

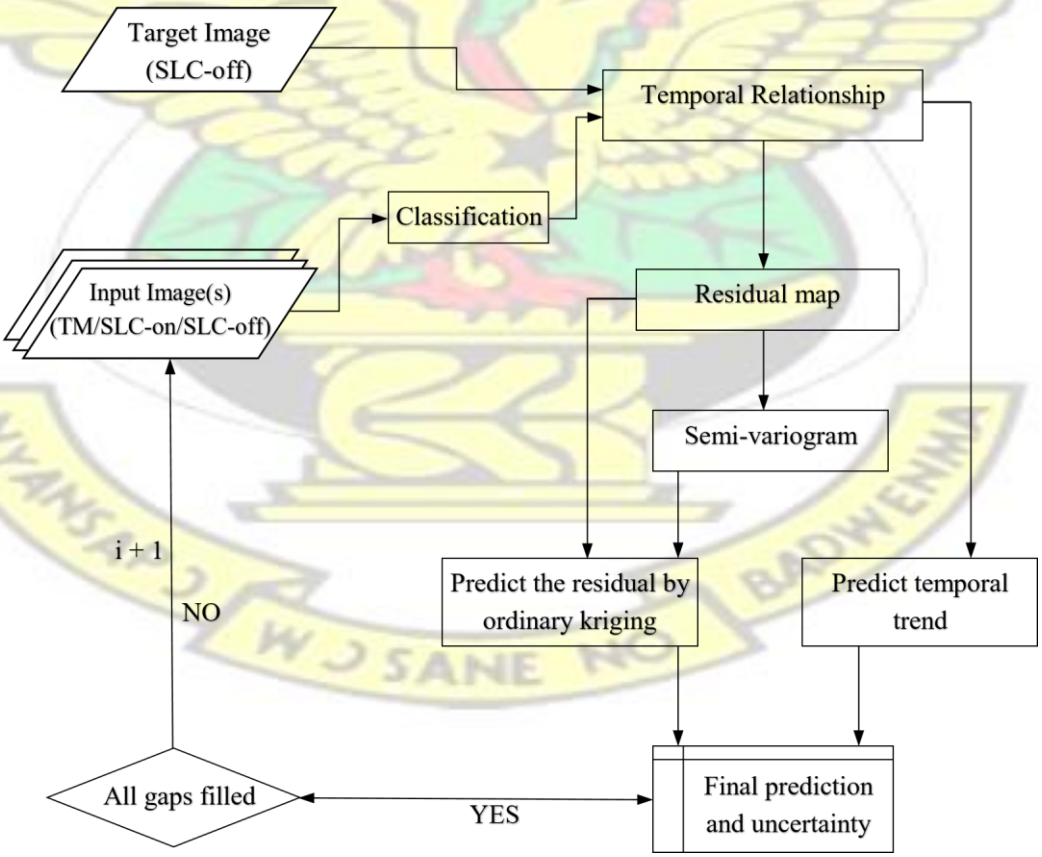

Figure 4-3: Flow chart of GNSPI algorithm (Adapted from Zhu et al., 2012)

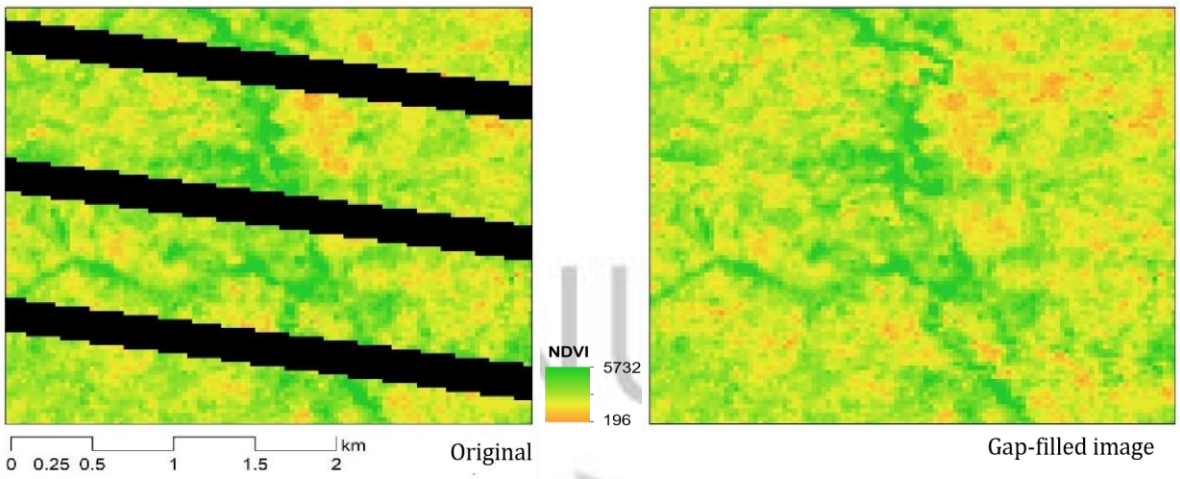

Figure 4-4: Comparison of Landsat ETM+ SLC-off image with a corresponding gap-filled image (date acquired: 07/02/2017, NDVI values is by a factor of 10,000, black strips show areas of no data)

4.2.5 Image Subset

Since the study area (Ioba province) covers a small portion of the Landsat scene (path/row 196/052), there was the need to subset the study area from the Landsat scenes. The subset process was done in R software by writing a loop command to subset all the images using the study area shape (Figure 3-1) as the subset feature. This process was used because all the images did not have the same extent and as a result it was difficult to stack all the images together and perform a subset on the stack. Both the NDVI images and the pixel QA images (clouds and cloud shadows) were undertaken through the subset process.

4.2.6 Cloud Masking

Landsat image availability for land use/cover studies in West Africa has been a big challenge due to excessive clouds and cloud shadows especially in rainy season. Since the period of the study spans all seasons (rainy and dry), there were some amount of clouds in some of the images especially images from the rainy season. The presence of clouds in satellite images can sometimes cause high saturation of pixels (Scaramuzza, Micijevic and Chander, 2004). Therefore, the was the need to remove the cloud and their shadows pixels. The detection of clouds and their shadows using the CFmask algorithm on the ESPA platform made it easier and quicker to deal with them. The clouds and cloud shadows image (Figure 4-2) was used to mask out the clouds and shadows. This task was also executed in R software.

4.3 Aerial Photograph

In other to estimate the crop heights of both erosion controlled and non-erosion controlled sites, an UVA was used to capture aerial photos of the sites. Two sites each of erosion controlled and non-erosion controlled were selected and flown. The initial planning was to capture photos every two weeks beginning from the start of the planting season (mostly in June) till the time the crops attain their highest growth (mostly in September). But this was not achieved because of unfavorable weather conditions and logistical challenges. Table 4-2 shows the site information and the dates of the flights. The first images were captured on the 1st of June 2018 when farmers were still preparing their land for cultivation. This was necessary to obtain the digital terrain model (DTM) which will serve as the basis for estimation of crop height from subsequent digital surface model (DSM) when the crops are growing. In most cases, the flight was taken between 10am and 3pm to minimize shadows from trees. A minimum of 200 and a maximum of 235 photos were captured on each site. Figure 4-5 shows samples of aerial photos used in the study.

Table 4-2: UAV flight site information and corresponding dates of flight. The EC and NEC in site ID stands for erosion controlled and non-erosion controlled.

Site ID	**Location**	**Size (Ha)**	**Date of flight**						
			1st	**2nd**	**3rd**	**4th**	**5th**	**6th**	**7th**
DS-ECA001	Tambiri	25.44	01-06-2018	22-06-2018	05-07-2018	26-07-2018	16-08-2018	06-09-2018	28-09-2018
DS-ECA002	Dadme	24.80							
DS-NECA001	Dissinh	25.37							
DS-NECA002	Kpomane	24.61							

(a)   (b)

Figure 4-5: Samples of UAV photos used for crop height estimation at Tambiri ECA; (a) captured during land preparation (01-06-2018), (b) captured during the final stages of crop growth (28-09-2018), pixel size = 2.2cm

4.3.1 UAV Flight Planning

The Da-Jiang Innovations' (DJI) Phantom 4 pro UAV together with the GL300F controller connected to an iPad pro (model A1674) for display were used to capture the aerial photographs. The Phantom 4 pro is a rotor-wing UAV with four rotors (quadcopter) and has on-board a Global Navigation Satellite System (GNSS) receiver for positioning. Its weight is 1.338g (without the propellers and battery) with a maximum flight time of 30 minutes. It has a 20 megapixel camera that produces an RGB image with an ultra-high-definition (UHD) 4000 pixels (4K) resolution and a field of view (FOV) of 84° (DJI, 2016).

The flight planning was done using the DJI Ground Station (GS) pro v1.0 application. The DJI GS pro software was chosen because it offers a simple flight planning and allows the aircraft to automatically control the planned mission. It automatically generates efficient flight paths (grids) after defining the required area to be captured and setting the camera parameters. Once the mission is started, the aircraft will follow the grids throughout (DJI, 2017). Secondly, it is a free software but only compatible with iPad product line. The following flight parameters were used for all the sites; altitude, 80m; front overlap, 70%; side overlap, 55%; shutter interval, 3 seconds. Parameters such as the speed of the UAV and the resolution of the photos (pixel size) were calculated automatically from the distance and time intervals and the altitude respectively. Therefore, a speed of 8m/s (meters per second) and a resolution of 2.2cm per pixel were realized. Several factors were considered before the selection of the above parameters

with the most paramount being the prohibition of UAV flights of more than 100m above ground. Although, Burkina Faso does not have a UAV/drone Law, this was adhered to because of international best practices. Also, the trade-off between the parameters and the battery life was considered. A drone flight permit (No. 2017-00508) was obtained from Burkina Faso's Ministry of Security prior to its usage.

4.4 Climate Data

Rainfall and temperature data were obtained from the Burkina Faso meteorological agency through West African Science Service Centre on Climate Change and Adapted Land-use (WASCAL). The data comprised daily readings obtained from the climate station in Dano (Latitude 11.15°N and Longitude 3.0667°W) from 2004 to 2017. A quality assessment done on the rainfall data revealed some missing data. Although the missing data were very few (less than 5%), there was the need to fill the data gaps. The two most widely used satellite rainfall data (the Tropical Rainfall Measuring Mission (TRMM) and the Global Precipitation Climatology Project (GPCP)) were tested for filling the missing values in the station data obtained from the meteorological agency of Burkina Faso. The analysis was executed in R software. Although both datasets gave similar results (Table 4-3), the TRMM was chosen over the GPCP because it had a better resolution (5km as against 111km of GPCP).

Table 4-3: Statistics of gap-filling of missing values in the station data obtained from the Meteorological agency of Burkina Faso. TRMM_Fill and GPCP_Fill represents the station data filled with TRMM and GPCP respectively.

Data	Mean	SD	Correlation (Kendall's tau)	T-test
Station	2.65	8.37		
TRMM	2.73	6.13		
GPCP	2.85	6.14		
TRMM_Fill	2.56	8.17		
GPCP_Fill	2.57	8.18		
Station Vs TRMM			0.35	-0.18
Station Vs GPCP			0.34	-0.30
Station Vs TRMM_Fill			1	0
Station Vs GPCP_Fill			1	0

4.5 Ancillary Data

4.5.1 Shapefiles

Polygon shapefiles defining areas with stone bunds erosion control were obtained from the Climate change adaptation project (EKF project) under the Ministry of Agriculture of Burkina Faso. The project, which aimed among other things at the restoration of 20,000 hectares of degraded land through the construction of physical structures such as stone bunds, rock dams/dikes and the treatment of gully erosion. The polygons cover four basins located within four communes in the Ioba province in the south-west region of Burkina Faso (see section 3.0). Several shapefiles such as the study area polygon, Dams and reservoir polygons and other artificial and natural features shapefiles were also obtained from the project database.

4.5.2 Field Mapping and Verification

Firstly, field visits were made to verify the erosion control area polygons obtained from the EKF project and identify the types of land cover in each polygon. With the help of Google

Earth engine and a handheld GPS device, navigations were made around the boundaries of the polygons and through them to ascertain whether the area has stone bunds erosion control measure implemented.

Secondly, non-erosion controlled polygons were marked by overlaying the erosion controlled polygons and the study area polygon on Google Earth engine. The high-resolution nature of the images on Google Earth necessitated the process because the stone bunds could be clearly seen on the images. After defining the non-erosion controlled areas, the same process of field verification conducted on erosion controlled areas were employed to ascertain if the boundaries marked do not have stone bund erosion control.

4.5.3 UAV Site Information and Validation Data Capture

A data sheet was designed to record the UAV site information and validation data capture (Appendix A). The form was made up of four sections (A, B, C and D). Section 'A' is on the general information about the site such as site ID, locality, date and time of the flight and central GPS coordinate of the site. Also, one photograph each was taken facing the north, east, south and west. Section 'B' deals with the terrain characteristics. This include, the slope, evidence of erosion and presence of duricrust. Section 'C' is on land use/cover information and measurements. For each cultivated field, records of crop type, age of crop at the time of the flight, crop height, planting distance and density per metre square was taken. Also, information on type of fertilizer used was recorded. Section 'D' deals with the UAV flight information such as flight grid type, flight height, Scene overlap and camera angle.

The terrain characteristics were necessary to ensure that erosion controlled and non-erosion controlled sites had similar features so that there will be no biases in comparing the crop growth from these two sites. The crop height measurements were necessary because it will be used to validate the crop heights extracted from the DSM generated from the aerial photographs. Millet and cotton were considered and measured because they were the dominant crops in the study sites. At each site, measurements were done on at least two different farms for each crop type. The measurements were taken by randomly defining a one metre square grid and finding the average of the heights of the crops within the square grid. On each farm, four of such square grids were laid. The GPS coordinates of each measured grid was recorded. This was necessary to identify the exact farm visited since the UAV flight covered a wider area with similar farms but different planting times.

CHAPTER 5: METHODOLOGY

5.1 Introduction

This chapter explains the detailed processes used in this study to achieve the set objectives. Three levels of analysis (made up of two spatial scales) were done. The first spatial scale which is in two-fold includes, a detailed analysis of NDVI trend of the whole Ioba province. Secondly, sites within the province representing stone bunds erosion-controlled areas (ECA) and nonstone bunds erosion-controlled areas (NECA) were also analyzed and compared. The second spatial scale which involved a continuous monitoring of crop growth at finer scale using UAV was done on two selected sites each of ECA and NECA for comparison. Lastly, because vegetation growth is influenced by climate, an analysis of the trend of climate variables (rainfall and temperature) and their relationship to the NDVI trend was conducted to ascertain if the change or otherwise of climate variable have impacted the vegetation growth over the period. The above-mentioned processes run through sections 5.2 to 5.4. A schematic diagram of the scale of analysis is presented in Figure 5-1.

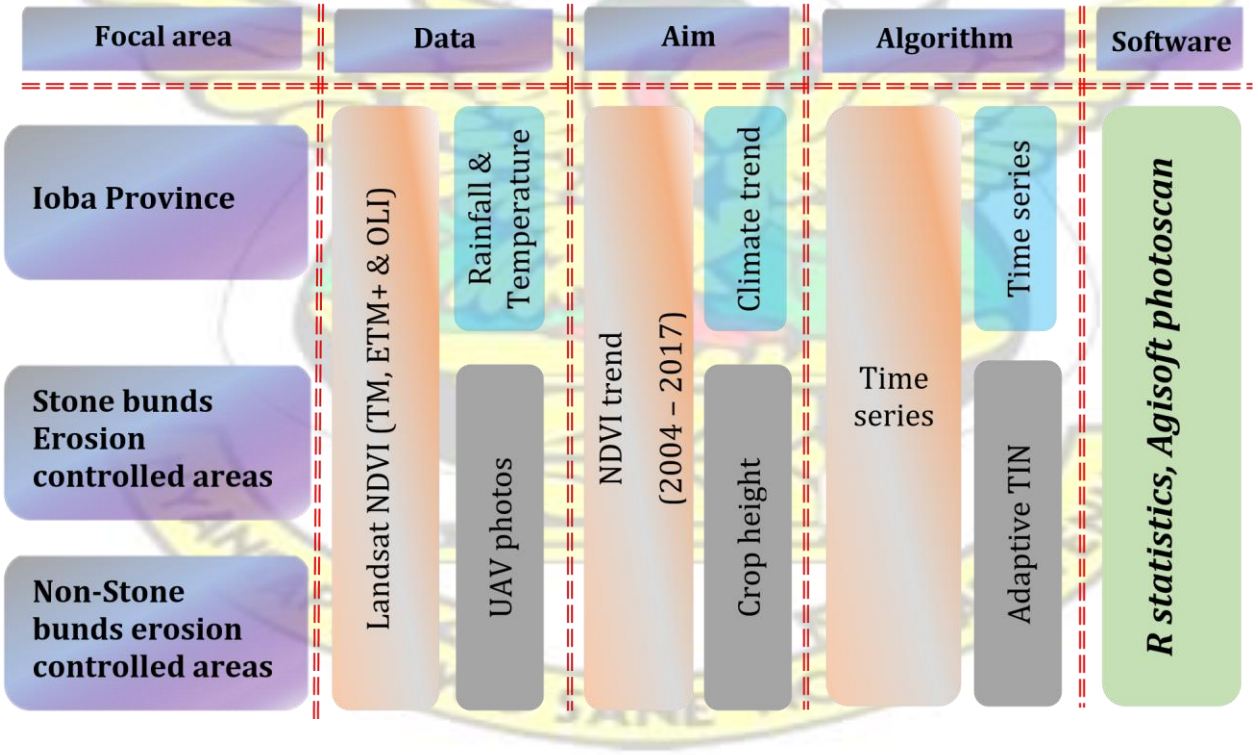

Figure 5-1 Overview of the different scale of analysis performed in the study

5.2 NDVI Time Series Analysis

The main purpose of time series analysis is to read about the past observations of an event and then collect them carefully to develop a suitable model which describes the essential structure of the event (Jain and Mallick, 2017). The derived model can then be used to forecast future trends of the event (Fernández-Manso, Quintano and Fernández-Manso, 2011).

The NDVI time series is univariate, meaning it is composed of one attribute that is observed over time. This implies that, for an NDVI observations, o_1, o_2, o_3, …o_n, there is a corresponding time steps of t_1, t_2, t_3, …t_n. An NDVI time series over a long period usually consists of three components, a long term directional trend, seasonal (systematic movements) and additional irregular (unsystematic) component depicting short term fluctuations (Kuenzer, Dech and Wagner, 2015). In remote sensing time series analysis for land surface dynamics, each of these three components can be used separately or together depending on the research focus (Verbesselt, Hyndman, Zeileis, *et al.*, 2010).

The NDVI time series datasets used for the study were captured by three different Landsat sensors (Landsat 5, 7 & 8). The study area just like many other tropical regions of the earth is Landsat data scarce. The existence of clouds most especially during the growing seasons is a big challenge to optical satellite images. The scarcity of Landsat images was a big hindrance to the time span of this research. Out of 168 Landsat images required to cover from 2004 to 2017 (one image per month), only 109 images were found credible for the study. The remaining 59 images were in most cases not available in the USGS database or were simply un-usable because of excessive cloud cover. In a time series, missing values may result in serious problems in subsequent processes and analysis because most time series algorithms rely on complete datasets (Moritz *et al.*, 2015). With about 35% of the data time-steps missing at random, it was very difficult to get a robust and widely accepted time series tool for analysis since most time series tools require a regular time step (Moritz *et al.*, 2015). Therefore, the missing values needed to be filled in order to obtain a regular time series. This process in statistics is referred to as imputation.

Two types of NDVI time series analysis were conducted in this study. First, all the NDVI values for each pixel in the Ioba province were aggregated to a mean NDVI value representing the whole area. Secondly, the Ioba province, ECA and NECA were undertaken through a per pixel based NDVI time series analysis for smaller scale assessment.

All pixels representing water bodies (dams and rivers) and settlements were masked out of the stack image before the analysis. Figure 5-2 shows the flow chart of the method used in the NDVI time series analysis.

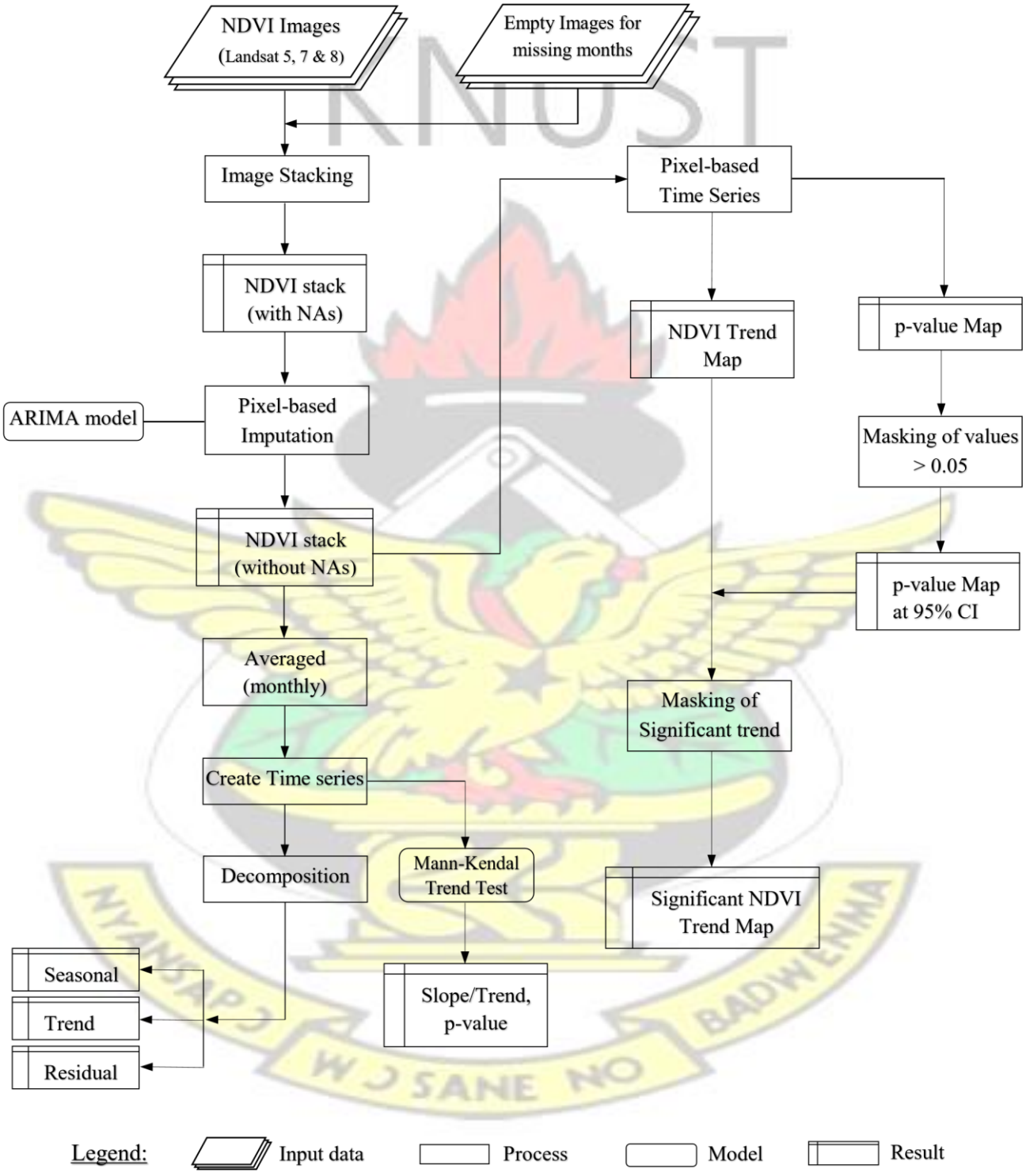

Figure 5-2: Flow chart of the method used in the NDVI time series analysis

The idea of this analysis was to be able to obtain a pixel-wise trend of NDVI between the period of study. The analysis processes which is shown in Figure 5-2 involved first, finding the NDVI trend for all pixels within the study area and finally extracting the areas of significant trend using a 95% confidence interval (CI).

5.2.1 Imputation of NDVI Time Series Data

Missing data is a common problem in data capture more especially in situations whereby the data collection device (for example satellite sensors) is greatly influenced by weather and some environmental factorss. In the use of satellite images, particularly optical images (Landsat, ASTER, Sentinel 2, etc.), missing data mostly arises due to sensor failure and extensive cloud cover. In the case of a sensor failure, the data may not be captured at all but in the case of cloud cover, the data captured cannot be used. These missing data points results in irregular time series of satellite data. Since remote sensing time series contains the temporal and the spatial characteristics of land surface features, the filling of missing data (imputation) requires a more robust algorithm in order not to disturb the series' statistical properties (Yozgatligil *et al.*, 2013). But most standard imputation techniques cannot be applied directly because they rely on inter-attribute correlations (multivariate time series) to estimate values for the missing data. For a univariate time series like the one used in this study, the imputation algorithm needs to employ time dependencies (Moritz *et al.*, 2015). A pixel-based imputation was therefore done using the auto-regressive integrated moving average (ARIMA) model and Kalman filter in R statistics software. This approach was adapted from Moritz et al. (2015) but was modified to suite the raster dataset. The imputation process begun by first creating empty raster layers of the same size and shape as the study area to fill each of the missing time steps. A total of 59 empty raster layers were created. The distribution of the empty raster can be seen in Figure 4-1.

5.2.2 ARIMA Model and Kalman Filter for NDVI Time Series Imputation

The imputation procedure was executed in a three-step process. The first step involved the fitting of an ARIMA model using the function 'auto.arima' under the 'forecast' library in R statistics. The function 'auto.arima' was preferred to the native 'arima' function because the 'auto.arima' function automatically searches the probable model found in the provided order constraints and returns the best ARIMA model (in-sample fit) based on the penalized likelihood

such as the Akaike's Information Criterion (AIC) (Hyndman and Khandakar, 2008). Before this process, the raw NDVI time series data stack was converted to a time series object of class 'ts' from the 'tseries' package. Missing data points were represented with empty raster. It was expected that at the end of the imputation process all the empty raster layers will be filled with NDVI values to obtain a regular NDVI time series over the study period. After fitting the ARIMA model, the Kalman filter was applied to solve the linear optimal recursive filtering. The third and final stage was the filling in of the missing values using the estimated values from the Kalman filtering process. Since this process was pixel-based, the estimated NDVI values for each missing data point were written into the respective empty pixel. The imputation process was executed in R statistics and codes (Appendix B) were adapted from Moritz et al. (2015).

5.2.2.1 ARIMA Model

The autoregressive integrated moving average (ARIMA) model developed by Box and Jenkins (1976) is a univariate statistical model for forecasting future occurrences and also for prediction of missing values in a time series (Biswas *et al.*, 2014). It has gained popularity in the field of economics but recently, few references can be made to it in the field of remote sensing, although it has a great potential for performing short-term predictions (Fernández-Manso, Quintano and Fernández-Manso, 2011). The capabilities of ARIMA model such as moving average (MA), exponential smoothing, neural network, and its forecasting give it a huge advantage over the other models (Han *et al.*, 2010; Valipour, 2015).

Generally, an ARIMA model is described by the notation ARIMA (p, d, q) where, p, d and q stand for orders of non-seasonal auto-regression, integration (differentiation) and moving average, respectively. For a time series with polynomial trend of degree d, the trend can be eliminated by considering a process $\nabla^d Y_t$ obtained by differencing. The observed process $X_t = \nabla^d y_t$ is an ARMA (p,q) satisfying stationary process. The original (y_t) becomes autoregressive integrated moving average of order (p, d, q) if;

$$\varphi(B) = \emptyset_p(B)(1-B)^d y_t = \theta_0 + \theta_q(B)_{et} \qquad (5\text{-}1)$$

Where $\emptyset_p(B) = 1 - \emptyset_1 B - \ldots - \emptyset_p B^p$ is an autoregressive (AR) operator, $\theta_q(B) = 1 - \theta_1 B - \theta_2 B - \ldots - \theta_q B^q$ is a moving average (MA) operator, B is the backward shift operator, $\emptyset_p$ and θ_q are polynomials of order p and q respectively with all roots of polynomial equations outside the unit circle, e_t is the random errors.

If a time series contains a seasonal periodic component, the ARIMA model can be generalized to deal with seasonality by defining a general multiplicative Seasonal ARIMA model known as SARIMA. The ARIMA model is then transformed into;

$$\emptyset_p(B)\Phi_P(B^s)w_t = \theta_q(B)\Theta_Q(B^s)e_t \qquad (5\text{-}2)$$

Where, w_t is the differenced stationary series, $\emptyset_p$, Φ_P, θ_q and Θ_Q are polynomials of order p, P, q, Q respectively. P and Q are the order of seasonal auto-regression and moving average, respectively of the model. w_t is defined by;

$$w_t = \nabla^d \nabla_D y_t \qquad (5\text{-}3)$$

For $P = 1$, then $\Phi_p(B^s) = 1 = constant \times B^s$ which implies that w_t depends on w_{t-s} since $B^s w_t = w_{t-s}$ where w_t are formed from the original series y_t by simple differencing and also by seasonal differencing ∇_s to remove seasonality. For example, if $d = D = 1$ and $s = 12$, then

$$w_t = \nabla\nabla_{12} y_t = \nabla_{12} y_t - \nabla_{12} y_{t-1} \qquad (5\text{-}4)$$

$$= (y_t - y_{t-12}) - (y_{t-1} - y_{t-13}) \qquad (5\text{-}5)$$

After fitting the model, the missing values in the time series were then estimated using the Kalman filter.

5.2.2.2 Kalman Filter

Kalman filter is among the most popular and widely utilized state estimation technique (Pan *et al.*, 2016) in the assessment of linear systems. In essence, it is an ideal recursive filtering algorithm under linear and Gaussian assumptions (Pan *et al.*, 2016; Chen *et al.*, 2017). The main strength of the Kalman filter is in its ability to provide an intelligent guess of missing values and forecast future position of a given object in a dynamic system by using all available knowledge about the system (Pan *et al.*, 2016; Hamuda *et al.*, 2018). The Kalman filter can be implemented from the following deduction as shown in Chen et al. (2017). For example, for a linear system defined by the state and measurement equations;

$$\boldsymbol{x}(k) = \boldsymbol{F}(k-1)\boldsymbol{x}(k-1) + \boldsymbol{q}(k-1) \tag{5-6}$$

$$\boldsymbol{y}(k) = \boldsymbol{H}(k)\boldsymbol{x}(k) + \boldsymbol{r}(k) \tag{5-7}$$

where $\boldsymbol{x}(k) \in \mathrm{R}^n$ denotes the n-dimensional state vector, $\boldsymbol{y}(k) \in \mathrm{R}^m$ represents the m-dimensional measurement vector at instant k. **F** and **H** stand for, respectively, the system matrix (or state transition matrix) and observation matrix. $\boldsymbol{q}(k-1)$ and $\boldsymbol{r}(k)$ are mutually uncorrelated process noise and measurement noise, respectively, with zero mean and covariance matrices

$$\mathrm{E}\,[\boldsymbol{q}(k-1)\boldsymbol{q}^T(k-1)] = \boldsymbol{Q}(k-1) \tag{5-8}$$

$$\mathrm{E}\,[\boldsymbol{r}(k)\boldsymbol{r}^T(k)] = \boldsymbol{R}(k) \tag{5-9}$$

Generally, Kalman filter is made up of two steps;

i. Predict: The prior mean and covariance matrix are given by;

$$\mathbf{X}(k|k-1) = \mathbf{F}(k-1)\mathbf{X}(k-1|k-1) \tag{5-10}$$

$$\mathbf{P}(k|k-1) = \mathbf{F}(k-1)\mathbf{P}(k-1|k-1)\mathbf{F}^T(k-1) + (k-1) \tag{5-11}$$

ii. Update: The Kalman filter gain is computed as; $\mathbf{K}(k) = \mathbf{P}(k|k-1)\mathbf{H}^T(k)\,(\mathbf{H}(k)\mathbf{P}(k|k-1)\mathbf{H}^T(k) + \mathbf{R}(k))^{-1}$

(5-12)

The posterior state is equal to the prior state plus the innovation weighted by the Kalman filter gain;

$$\mathbf{X}(k|k) = \mathbf{X}(k|k-1) + \mathbf{K}(k)\ (\boldsymbol{y}(k) - \mathbf{H}(k)\mathbf{X}(k|k-1)) \quad (5\text{-}13)$$

Additionally, the posterior covariance is recursively updated as follows;

$$\mathbf{P}(k|k) = (\mathbf{I} - \mathbf{K}(k)\mathbf{H}(k))\mathbf{P}(\mathrm{k}|\mathrm{k}-1)\ (\mathbf{I} - \mathbf{K}(k)\mathbf{H}(k))^{T} + \mathbf{K}(k)\mathbf{R}(k)\mathbf{K}^{T}(k) \quad (5\text{-}14)$$

5.2.3 Statistical Assessment

Imputation of NDVI time series using the proposed method is only meaningful if there is a statistically significant relationship between the raw data with missing values and the imputed/filled NDVI time series. In view of this, the Kendell's correlation test was performed on the two-time series. In addition, a student t-test was also performed to find out if there was a significant difference between their means. The Kendell's correlation test showed a high positive correlation (tau of 0.95) between the two-time series. The student t-test also showed that statistically, there is no difference between the means of the two-time series (Table 5-1).

Table 5-1: Statistics of raw and filled NDVI time series

Data	**Mean**	**SD**	**Correlation (Kendall's tau)**	**T-test**
Raw NDVI (with missing data)	0.304	0.162		
Filled NDVI	0.356	0.124		
Raw vrs Filled NDVI			0.96	0.00

5.2.4 Decomposition of NDVI Time Series

The NDVI time series analysis was performed using the break for additive seasonal and trend (BFAST) algorithm. The BFAST developed by Verbesselt, Hyndman, Newnham, et al. (2010) is an algorithm that involves the decomposition of time series into trend, seasonal, and remainder components with methods for detecting and characterizing abrupt changes within the trend and seasonal components. The BFAST therefore, differentiates temporal variations

from phenological change and executes a phenological change detection (Verbesselt, Hyndman, Newnham, *et al.*, 2010). The BFAST can perform analysis on several satellite data time series as well as other disciplines involving seasonal or non-seasonal time series data, for example, hydrology, climatology, and econometrics (Verbesselt, Hyndman, Newnham, *et al.*, 2010). The process was executed in the R statistical tools under the package 'bfast' (Appendix C).

5.2.5 NDVI Time series Trend Detection and Analysis

Changes in vegetation greenness can be characterized into seasonal change, gradual change and abrupt change (Verbesselt, Hyndman, Zeileis, *et al.*, 2010; Zhu and Woodcock, 2014). In most cases, the seasonal change has a recurring pattern that is often considered as a source of noise in the analysis. Gradual change arising as a result of vegetation growth, land degradation due to anthropogenic activities, climate change, extreme drought, pests infestation and other factors, change greenness slowly over long period of time (more than five years). Abrupt change on the other hand, generally caused by land use/cover change, may have a huge impact on greenness over a short period (between one and two years) (Zhu *et al.*, 2017). Linear regression method for trend detection has been widely utilized in vegetation dynamics with NDVI time series data (Ju and Masek, 2016).

The use of Mann-Kendall (Mann, 1945; Kendall, 1948) test have proven to be robust in detecting significant slope in vegetation trend and is particularly effective for estimating trends within small series. The Mann-Kendall test is a non-parametric and robust to outliers. It uses the Theil-Sen's slope estimator procedure (Theil, 1950; Sen, 1968), which is a rank-based test for estimating the slope and intercept in a time series by determining the median of all estimate of the slopes calculated between observation values at all pair-wise time steps (that is, a total of *n(n - 1)/2* slopes) (Neeti and Eastman, 2011; Liu *et al.*, 2015). The Theil-Sen technique has the capability of rejecting wild values (of up to 29%) without affecting the slope (Neeti and Eastman, 2011). The Theil-Sen's slope is calculated using the expression in equation 5-15.

$$Q = X\frac{\quad j-X_i}{j-i} \qquad (5\text{-}15)$$

Where Q is the slope between data points X_j and X_i.

X_j and X_i are the NDVI data measurements at time j and i respectively.

The Mann-Kendall statistic test the significance of the slope obtained from the Theil-Sen's approach. The Mann-Kendall test examines the slopes between all pair-wise combinations of samples. The data is ranked with reference to time and each data point is treated as the reference for the data points in successive time periods. Kendall's statistic, *S* is defined as;

$$S = \sum_{j=1}^{n-1} \sum_{j=j+1}^{n} sign(x_i - x_j) \quad (5\text{-}16)$$

$$sign(x_i - x_j) = \begin{cases} 1 & if \ x_i - x_j < 0 \\ 0 & if \ x_i - x_j = 0 \\ -1 & if \ x_i - x_j > 0 \end{cases}$$

Where *n* is the length of the time series data set and x_i and x_j are the observations at times *i* and *j*, respectively. Unlike the Theil-Sen slope measure, the Mann-Kendall statistic is a test for the presence of a monotonic trend and not strictly a linear trend. Therefore, it is interpreted as a test for the presence of a non-linear trend. When significant, the Mann-Kendall test indicates the presence of a monotonic trend while the Theil-Sen slope is a best linear estimate of its character (Neeti and Eastman, 2011). The Mann-Kendall statistic varies between −1 and +1. A value of +1 shows a continuous increasing trend that never decreases. The contrary is true when the value is −1 and a 0 value demonstrate a stable or no consistent trend (Lamchin *et al.*, 2018).

In this study, the Theil-Sen slope estimator was used to determine the median trend of the NDVI time series, and the Mann-Kendall test was then used to determine if the time series exhibited a significant mono-tonic increasing or decreasing trend using a p-value of less than 0.05 (95% CI). The non-significant trends were not considered for further analysis.

5.2.6 Detecting Trend Change (breakpoint) within NDVI Time Series

Depending on the vegetation type, NDVI time series may contain a strong seasonal component linked with the growing seasons (de Jong *et al.*, 2012). Most standard NDVI trend detection algorithms are unable to account for the seasonal variation in NDVI time series and therefore uses a seasonal or yearly aggregation or do a comparison of specific years (Coppin *et al.*, 2004). The BFAST algorithm which is a more robust method for NDVI time series breakpoint detection has been widely used for this task because of its ability to account for seasonality and

enables the detection of trend change within the time series (de Jong *et al.*, 2012; Watts and Laffan, 2014).

The BFAST process for time series breakpoint detection has two main components, a decomposition model and the iterative detection of change. For the decomposition model, a piecewise linear trend and a seasonal model is iteratively fitted using an additive decomposition model. The general decomposition model is;

$$Y_t = T_t + S_t + e_t \quad (t = 1, \dots, n) \tag{5-17}$$

Where, Y_t is the observed NDVI data at time t, T_t is the trend component as given in equation (5-18), S_t is the seasonal component, and e_t is the remainder component.

The assumption is that, Y_t is a piecewise linear trend with segment-specific slopes and intercepts on $m + 1$ different segments. Which implies that, there are *m* breakpoints $\tau_1^*, \dots, \tau_m^*$ so that,

$$T_t = \alpha_i + \beta_i t \quad (\tau_{i-1}^* < t \leq \tau_i^*) \tag{5-18}$$

Where, $i = 1, \dots, m$ and $\tau_0^* = 0$ and $\tau_{m+1}^* = n$

An estimate, S_t begins the iteration of the seasonal component using a non-parametric STL (Seasonal decomposition of Time series by Leoss) method (Cleveland *et al.*, 1990).

In the iterative detection of change, estimation of parameters (T_t and S_t) are done by iteration until the position and number of breakpoints remain unchanged. The iteration is described by a 4-step process outlined below;

Step 1: If the ordinary least square-moving sum (OLS-MOSUM) test shows the occurrence of breakpoint in the trend component, as well as its position and number ($\tau_1^*, \dots, \tau_m^*$) is estimated via least squares from the seasonally adjusted data $Y_t - S_t$.

Step 2: The estimation of the trend coefficients α_i and β_i (knowing the trend breakpoints) are done using a robust linear regression model based on M-estimation to take into consideration potential outliers. This produces the trend estimate using equation (5-18).

$$T_t = \hat{\alpha}_i + \beta_i t \quad (5\text{-}19)$$

Step 3: If the OLS-MOSUM test shows the existence of a breakpoint in the seasonal component, the position and number of the seasonal breakpoints represented as $\tau_1^{\neq}, \ldots, \tau_p^{\neq}$ (where p is the seasonal breakpoint) are estimated from the de-trended data $Y_t - T_t$ using least squares.

Step 4: The position and number of breakpoints are compared to the previous iteration and the fitting procedure is completed if they remain the same.

The above BFAST algorithm used in the study was executed in R statistics using the package 'bfast'. The algorithm has three different options ('dummy', 'harmonic' and 'none') for the seasonal model when fitting the seasonal component and detecting seasonal breaks (i.e. significant phenological change). In this study, the 'harmonic' seasonal pattern was used as the regression model at 0.05 significant level (95% CI). A value of 0.14 was used as the minimum segment size between potentially detected breaks in the trend model. This value is expressed as a fraction relative to the sample size (i.e. the minimum number of observations in each segment divided by the total length of the time series).

5.2.7 Comparison of NDVI Trends Between ECA and NECA

To compare the NDVI trends of both ECAs and NECAs the analysis of variance (ANOVA) test was used. The ANOVA test is used to test the significance of an experiment or a survey.

Because two independent variables is under consideration, the two-way ANOVA test was applied.

The test was conducted among the NDVI trends obtained from the four different study sites each of ECA and NECA (within groups) and between the NDVI trends from the ECA and the NDVI trends from the NECA (between groups). The results from this statistical analysis will reveal if there are differences or not in the NDVI trends of ECAs and NECAs.

5.3 Extraction of Crop Height using Photographs from UAV

The aerial photographs captured from May to September 2018 were used to estimate the crop heights of three crops (maize, millet and cotton) in two selected sites of ECA and NECA each. The timing of the UAV flights was planned to cover the growing period of the crops until it reaches its maximum height. The first data was collected right after land preparation (before crop were sown) was used to generate DTM which serves as the bases for obtaining the crop height from the DSM for each time step. The details of the height estimation process have been outlined in the subsequent sections (5.3.1 - 5.3.6). The first stage involves the use of Agisoft PhotoScan software for processing of photos to obtain the DEMs and the second stage involves the extraction of crop height from the DEMs using R statistic software. Figure 5-3 shows the flow chart of the process.

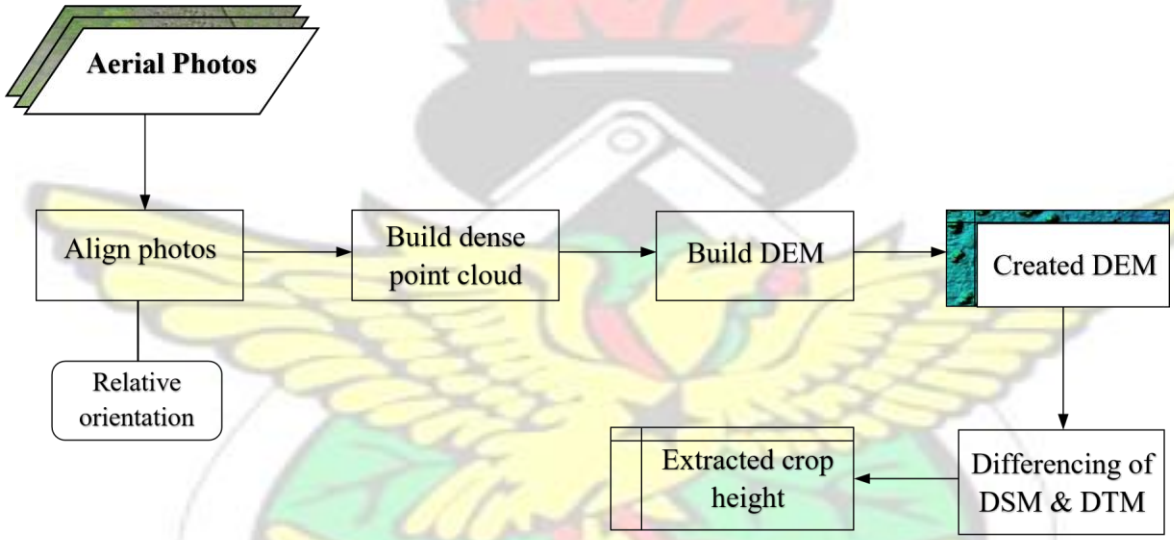

Figure 5-3: Flow chart for the extraction of crop height from UAV photographs

5.3.1 Photo Processing

After the acquisitions of images for all the time steps, the photos were processed using the Agisoft PhotoScan licensed under the Department of Remote Sensing, Julius Maximillians University of Wuerzburg, Germany. The Agisoft PhotoScan is an advanced image-based threedimensional (3D) modeling solution aimed at producing high quality 3D object from still images. Generally, the final goal of photographs processing with PhotoScan is to build a textured 3D model (Agisoft, 2018). The general workflow for the processing involves three stages; (i) align photos, (ii) build dense point cloud and (iii) build DEM.

The processing started by creating a new project and importing the images. A quality assurance checks was done to identify blurred and distorted images which may affect the results, but all the images passed the checks for all the photos processed. Also, none of the imported photos were automatically flagged by the software as not calibrated (NC) which indicates that the camera focal length cannot be estimated due to insufficient data in the EXIF (Exchangeable Image File Format) file.

After importing the photos and quality checks done, the next stage of the processing was to align the photos. To align the photos, the software first finds the approximate camera positions measured (with the help of the GNSS receiver on-board the UAV) during the data capture stored in the metadata of the photos. Secondly, the photos under-go relative orientation (oriented to each other). After subsequent trials, the following parameters was found to give the optimum results for the alignment procedure; the accuracy of the alignment process was set to *highest*, under pair preselection, *reference* option was used. Although setting the accuracy to *highest* increases the processing time, this was necessary because the software uses the original photo size to compute the camera positions the highest accuracy possible. Any other settings cause a downscaling of the original photo size. Also, since all the other processes (such as DEM and Orthophoto generation) are based on the aligned photo obtaining an optimum accuracy is vital. The *reference* option also helps to reduce processing time by determining the overlapping pairs of photos by their approximate position obtained from the GNSS receiver. In summary, the relative orientation is made up of, (i) the detection of feature points and (ii) selection and matching of overlapping image pairs. The final product of the alignment process is the generation of a *sparse point cloud*.

The second step of the photo processing in the Agisoft photoScan was the building of dense point cloud. Using the estimated camera positions the software computes the depth information for all the cameras to be joined into a single dense point cloud. The following parameters were set for the reconstruction process. Under *quality*, which specifies the desired reconstruction quality the option *high* was used. Parameters to achieve a high-quality results can be set, but this will require a high performance computer in other to achieve a shorter processing time. Interpretation of the quality parameters here is similar to that of accuracy settings given in the alignment process. The next parameter set was *depth filtering*. During dense point cloud generation, Agisoft PhotoScan calculates depth maps for every image. In the presence of noisy or badly focused images, there can be some outliers among the points. To remove the outliers, the software has many in-built filtering algorithms suitable for different projects. The option

mild was used under the depth filtering so that small important details which are spatially distinguish in the scene to be reconstructed are not sorted out as outliers.

The third and final stage of the photo processing was the creation of the DEM. During the creation of the DEM the dense point cloud was used as the input data the option *enabled* interpolation mode was selected so that the gaps in the dense point cloud are filled by interpolated points. The created DEM was then exported as a TIFF file for further processing in R statistics software. The above processing mode and parameters was used to processing all the photos captured in this research.

5.3.2 Accuracy Assessment

During the photo processing, an accuracy assessment report was generated after the relative orientation. An error obtained from the difference between the camera position from the approximate coordinates and the camera position according to the relative orientation was generated. In all cases, the total error was less than 6m. Also, the RMSE per-pixel was calculated from the re-projection. The values were within a range of 0 to 0.70 in all the processing.

5.3.3 Geo-referencing of Generated DEMs

Although the single-frequency GNSS receiver of the drone did not give a high position accuracy (accuracy can reach up to 10m), no exterior orientation using ground control points (GCPs) was done. This is primarily because no GCPs were laid during data capture. Secondly, considering the nature of the research, a positional accuracy of about 10m was considered ok although the generated DEMs for the same area in each time step had a considerable shift from each other. To mitigate the shift in the DEMs, the DTM from the first data capture was used to geo-reference the subsequent DEMs. The RMSE for the geo-referencing was less than $9.0e^{-5}$ in all cases.

5.3.4 Extraction of Crop Height

To obtain the crop height for each time step, the normalized surface model (nDSM) was calculated. The nDSM helps to differentiate elevated objects from the terrain or near-ground objects (Haala and Walter, 1999). To calculate the nDSM, the DTM obtained from the UAV

photos captured before the crops were sown was subtracted from the DSMs obtained when the crops were growing (equation 5-20). The resultant nDSMs represents the crop height at each time step. This process was executed in R statistic software using the 'overlay' function under the 'raster' package.

$$nDSM = DTM - DSM \quad (5\text{-}20)$$

5.3.5 Validation of Extracted Crop Height

The crop heights measured on the field during each UAV flight was used to validate the respective extracted crop height (nDSM). This was done to quantify the error in the crop height extracted. Random heights were selected from the generated nDSMs and two error statistics, Mean Absolute Error (MAE) and Root Mean Square Error (RMSE) were calculated for the two different sites of stone bunds erosion control and without stone bunds erosion control. The above statistics are defined in equations 5-21 and 5-22.

$$MAE = n^{-1} \sum_{i=1}^{n} |P_i - O_i| \quad (5\text{ -}21)$$

$$RMSE = \left[n^{-1} \sum_{i=1}^{n} (P_i - O_i)^2 \right]^{1/2} \quad (5\text{-}22)$$

Where *P* and *O* are the extracted and measure crop height respectively, and *n* is the number of measured samples.

5.3.6 Comparison of Crop Height between ECA and NECA

To compare the crop heights of areas with stone bunds erosion control and areas without, a graph was plotted to show the trends of the crop height for millet and cotton in two different areas. A Mann-Kendall's ranked correlation test was used to test for the correlation between the

two trends of crop height. Also, the student t-test was used to ascertain if there is a difference between the means of the crop heights of the two areas.

5.4 Time Series Analysis of Climate Variables (Rainfall and Temperature)

Time series analysis of climate variables specifically, rainfall and temperature are essential to know whether there have been changes in the trends of rainfall and temperature which has a big impact on primary productivity. Rainfall and temperature trend analysis, on different spatial and temporal scales, have been a topical issue in the past century because of the attention given to global climate change from the scientific community (Akinsanola and Ogunjobi, 2015). In order to ascertain if there have been changes in the trend of rainfall and temperature in the study area, a time series analysis from 2004 to 2017 was performed using climate station data from Dano. The analysis was executed in R statistics using the 'forecast' library (Appendix D). The total monthly and yearly rainfall were analyzed. For temperature, the minimum, mean and maximum values between the period of study were analyzed.

5.4.1 Trend Analysis of Climate Variables

In order to determine the trend of rainfall and temperature from 2004 to 2017 of the study area, the Mann-Kendall's test was used to determine if the rainfall and temperature time series exhibited a significant mono-tonic increasing or decreasing trend using a p-value of less than 0.05 (95% CI). The Mann-Kendall's test has been described in section 5.2.5 above. The analysis was executed in R statistics environment (Appendix D).

5.4.2 Pixel-wise Relationship between NDVI and Climate Variables

To examine the relationship of the spatial responds of NDVI to climate variables (rainfall and temperature) from 2004 to 2017, a non-parametric Kendall's ranked correlation test was used. The Kendall's ranked correlation coefficient referred to as the Kendall's tau (τ), lies on a scale of -1 to 1, where values of 1, -1 and 0 signifies a perfect positive, a perfect negative relationship, and no overall ordinal relationship at all, respectively. But due to the use of concordance and discordance ratio in calculating the Kendall's τ, it is sometimes scaled from 0 to ∞, with values of 1 in the case of statistical independence. Where the value of 1 represents a perfect relationship and 0 no relationship. The Kendall's ranked correlation coefficient is expressed in equation 5-23.

$$\tau = \frac{n_c - n_d}{n_c + n_d} \qquad (5\text{-}23)$$

Where n_c and n_d are the total numbers of concordant and discordant pairs respectively.

To perform a pixel-wise correlation between NDVI and climate variables, the total monthly rainfall and the average monthly temperature obtained from the Dano climate station were converted to a grid data of 30m spatial resolution. The 30m spatial resolution was appropriate in order to conform to the spatial resolution of the NDVI data. The relationships were computed from the strength of the linear correlation between NDVI-rainfall and NDVI-temperature. Subsequently, areas with a statistically significant relationship (95% CI) between NDVI and the climate variables were extracted. The process was implemented in R statistics environment and is listed in Appendix E.

6.0 CHAPTER 6: RESULTS

6.1 NDVI Time Series Analysis

6.1.1 The whole Ioba Province

Based on the average monthly NDVI time series analysis, the overall trend of vegetation phenology of the Ioba province from 2004 to 2017 has been obtained (Figure 6-1). The average monthly NDVI had a minimum value of about 0.12 to a maximum of about 0.68 with high values corresponding to the period of rainfall (April to October). The results of the trend

analysis produced a significant increasing trend in NDVI over the period (0.00037 ΔNDVI/month, p-value = 0.043).

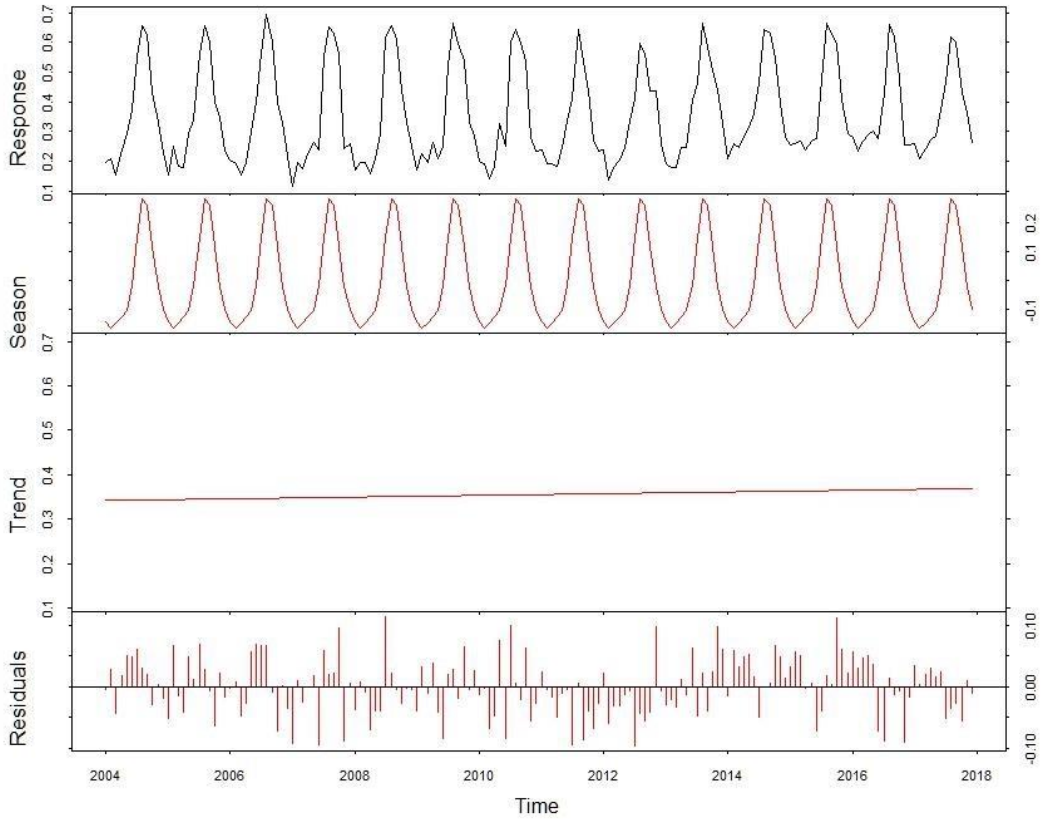

Figure 6-1: The bfast decomposition of monthly NDVI time series into seasonal, trend and residuals components. The sum of the three components equals the response or raw data series. The seasonal amplitude is approximately 0.5 NDVI.

6.1.1.1 Break Point Detection and Characterization

Figure 6-2 shows a detected change in the decomposed components (seasonal, trend and residual) within the NDVI time series using the 'bfast01' function in the bfast package. The change was statistically significant at 95% confidence interval (α=0.05) with a magnitude of about 0.40 in the trend component. Because this research focused on the long-term trend, only the trend component was considered for further analysis. A classification of the trends of the two segments using the 'bfast01classify' function in the bfast package revealed that the type of shift in the trend is caused by an interruption. Furthermore, only the trend of the second segment was significant at 95% confidence interval producing a p-value of 0.001.

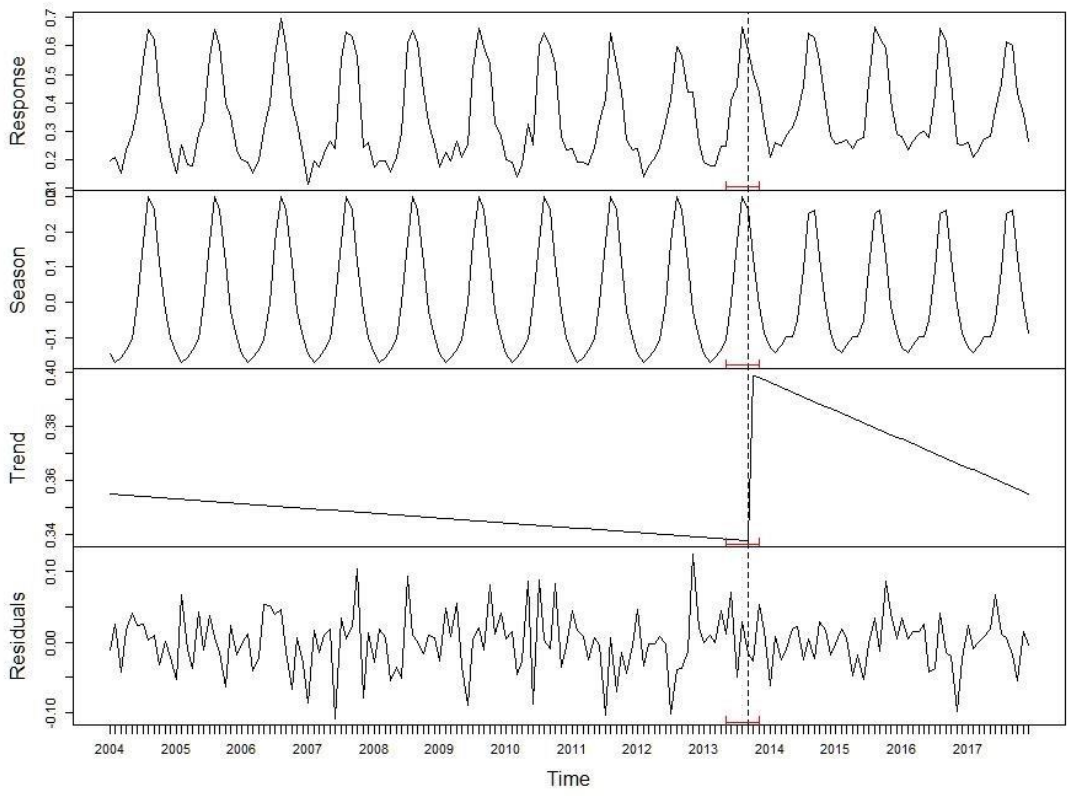

Figure 6-2: Monthly NDVI time series with one abrupt change. The magnitude of change in trend is about 0.40. The time of the change is indicated by the vertical dotted line. The confidence interval of the estimated time of change is shown in red.

6.1.1.2 Pixel-based Trend Analysis

To explore the trends of NDVI of the study area in a smaller scale, a pixel-wise trend analysis was performed. Figure 6-3 illustrates spatial distribution of the trends obtained from the pixelwise analysis of NDVI time series from 2004 to 2017 using the Theil-Sen estimator. The trend values range from -0.001 to a maximum of 0.002 ΔNDVI/month with value above and below 0 representing a positive and negative trend respectively and 0 shows a stable or no-trend. From Figure 6-3, areas showing stable/no-trend to negative trends were wide spread especially in the northern and the central parts of the study area. Areas of positive trends were more prominent in the southern, western and eastern fringes and were also interspersed with negative and stable trends in other parts of the study area. Positive trends were mostly found in irrigated areas, afforestation areas and along rivers/streams. Those found along rivers/streams depicts the linear shape of the rivers/streams.

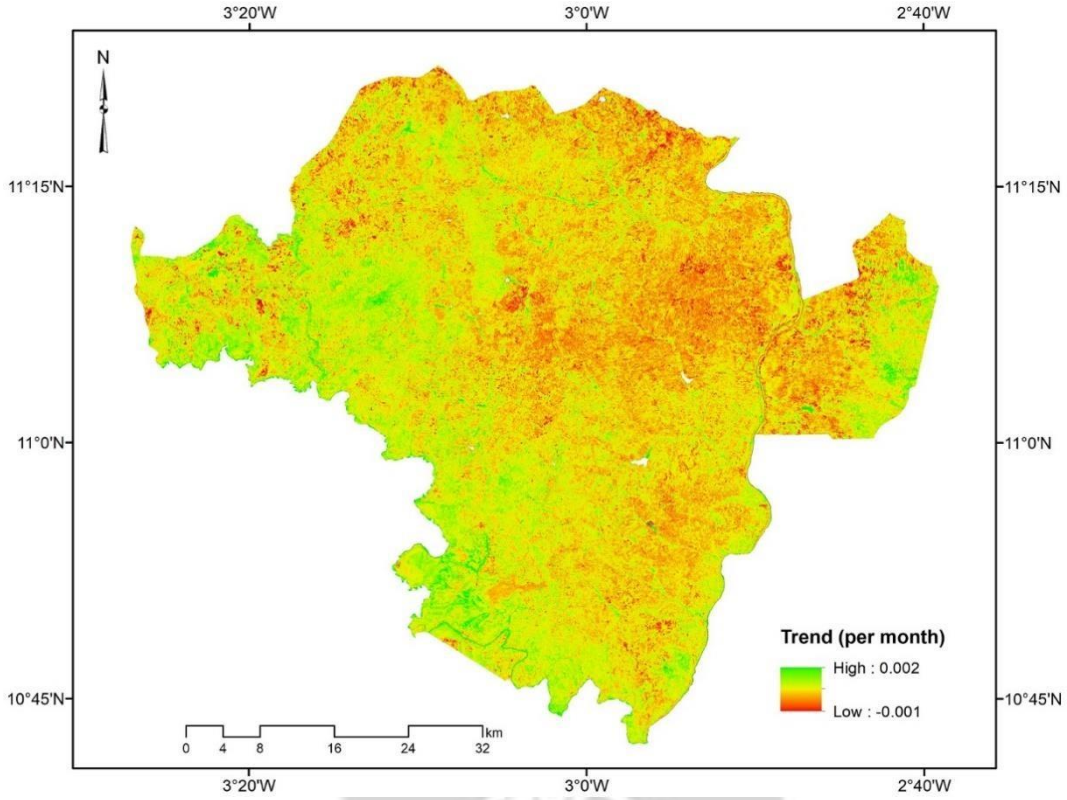

Figure 6-3: Slope values for trends derived from monthly NDVI observations from 2004 to 2017.

In order to determine the significance of the trends, analysis of their variability was performed using the Mann-Kendall test. Figure 6-4 shows the p-value map of the trend for the whole area which aided in the extraction of the significant trend map at 95% confidence interval ($\alpha = 0.05$). Figure 6-5 shows only trends with significant monotonic regression slope values. From Figure 6-5, it can be observed that some areas with positive trends were excluded from the significant trend map. Areas of stable trends were widespread across the whole study areas while areas of negative trends were few and could hardly be seen on the map. On the whole, areas of significant NDVI trends were about 10.6% of the total land size.

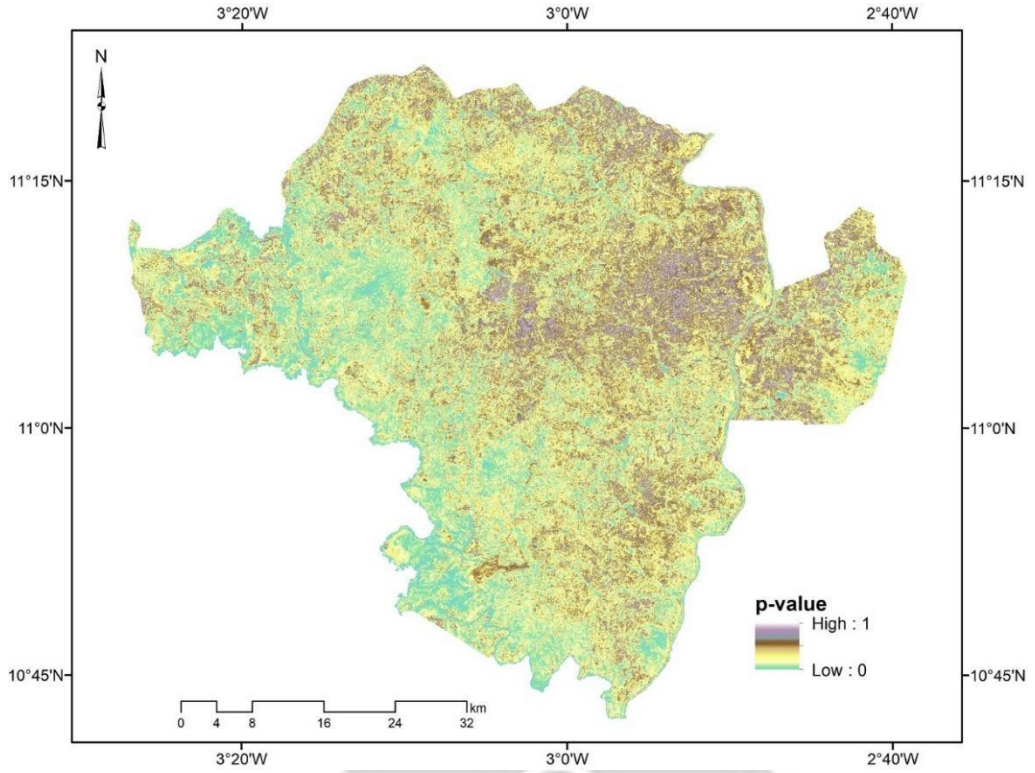

Figure 6-4: P-value map for trends of monthly NDVI observations from 2004 to 2017.

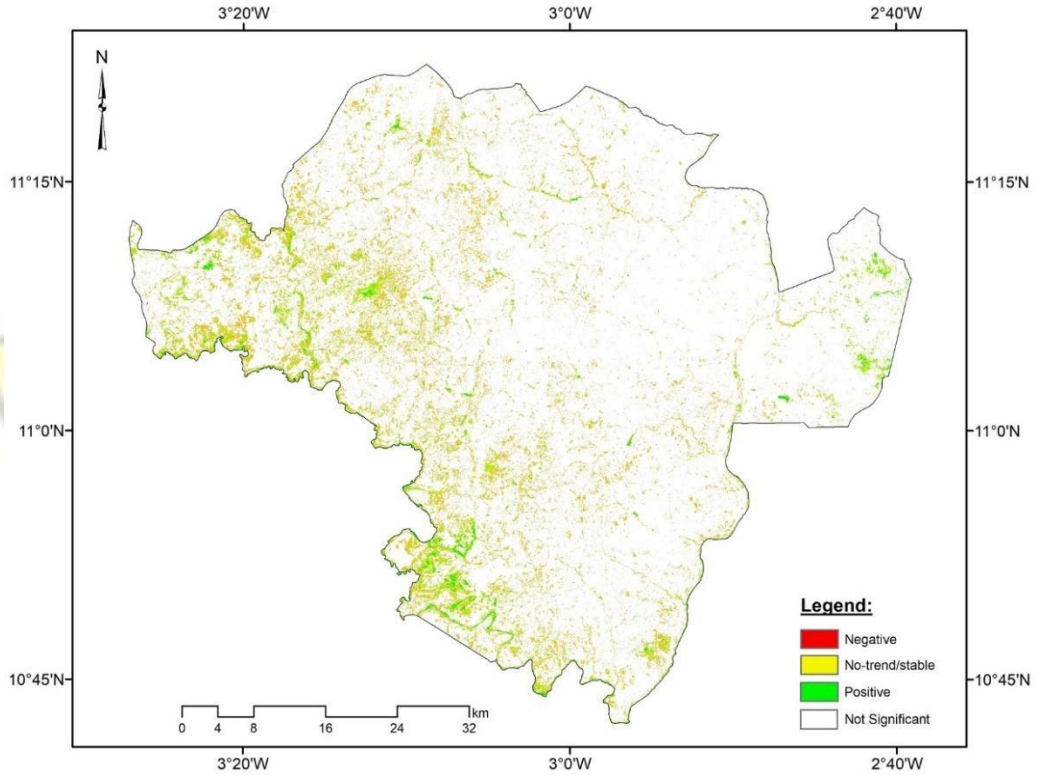

Figure 6-5: Significant slope values for trends at 95% confidence interval derived from monthly NDVI observations from 2004 to 2017.

6.1.2 Areas with stone bunds Erosion control measure

Figure 6-6 shows the spatial distribution of NDVI trends in four different sites (Badiere, Batiara, Dibogh and Namere) with stone bunds erosion control from 2004 to 2017. All the four sites had similar NDVI trend values ranging from -0.002 to 0.002 ΔNDVI/month. The spatial pattern of NDVI trends for Badiere and Batiara site looks more similar visually with a mixture of positive, stable and negative trends. However, the trends for the Dibogh and Namere sites were different. The Dibogh site showed more positive trends compared to the other three sites with few prominent areas of negative trends and dispersed areas of stable trends. Figure 6-8 shows the significant trend map extracted using the p-value map in Figure 6-7. From Figure 6-8 all the three trends (Positive, Stable and Negative) were represented in the significant trend map although positive trends were more prominent and continuous compared to the others. The Dibogh site had few significant negative trends compared to the other three sites. At 95% confidence interval, areas characterized by significant change in NDVI were generally small in all the four sites.

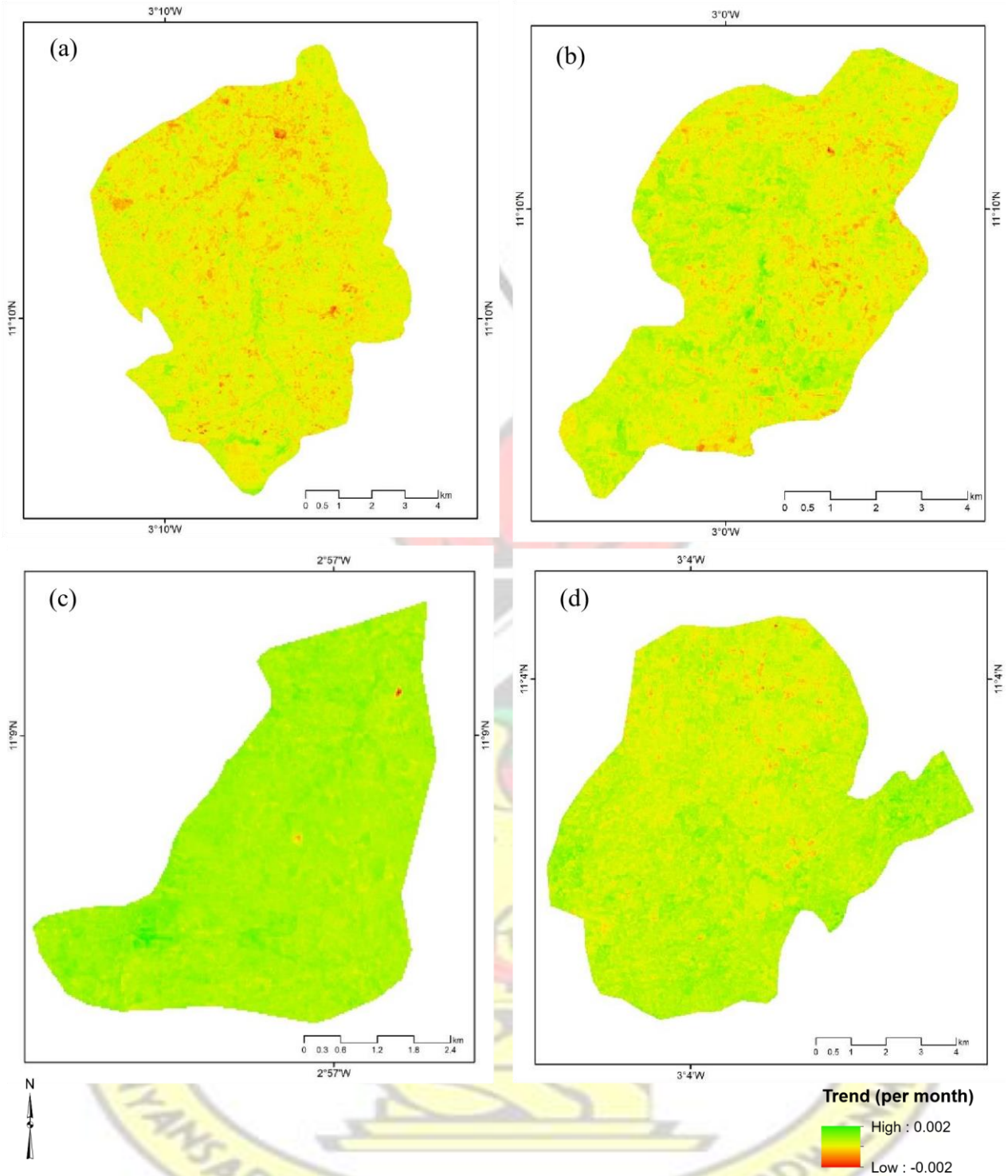

Figure 6-6: Slope values for trends derived from monthly NDVI observations of sites with stone bunds erosion control measure from 2004 to 2017, a, b, c & d represent Badiere, Batiara, Dibogh and Namere sites with stone bunds erosion control.

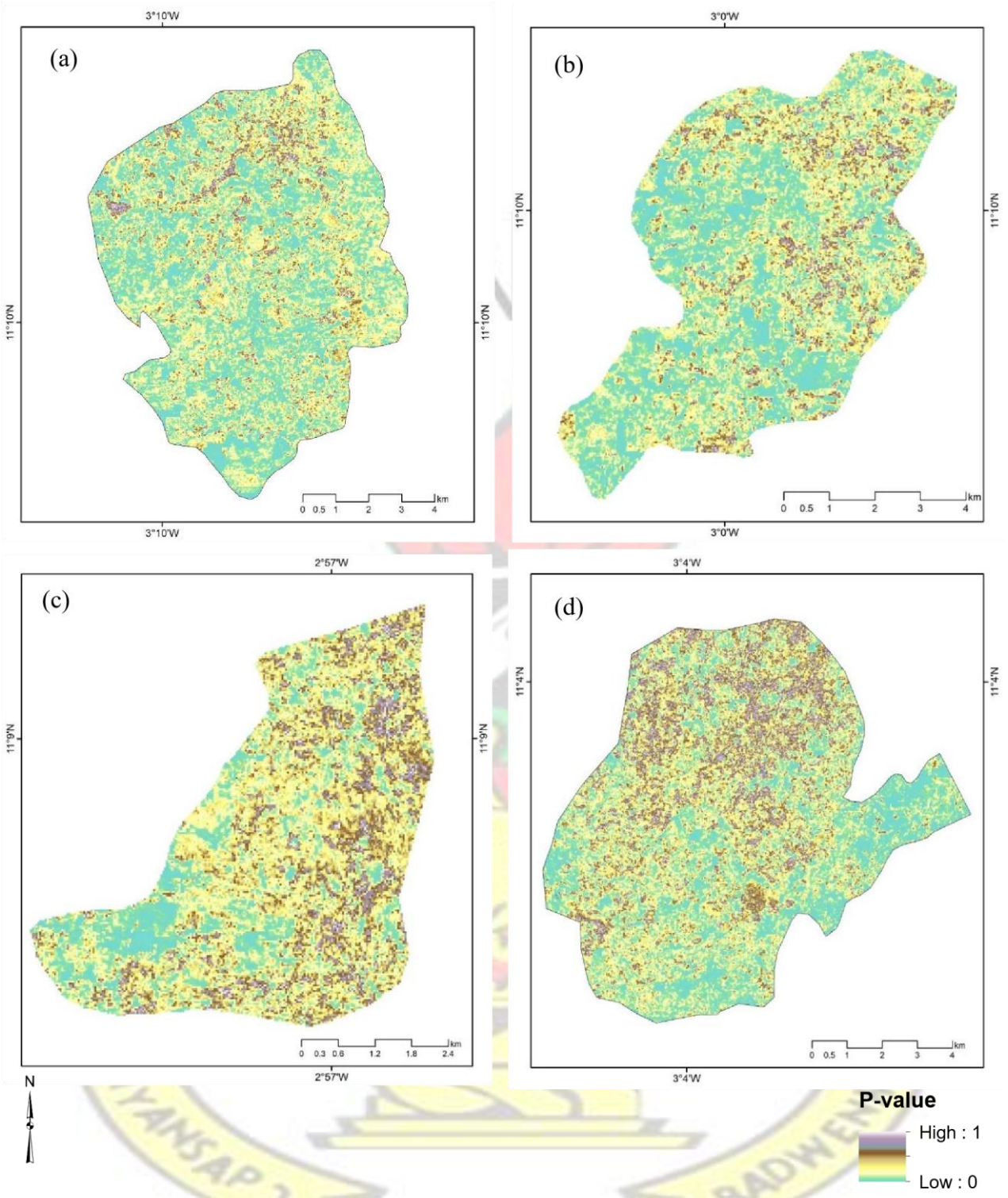

Figure 6-7: P-value map for trends of monthly NDVI observations of four sites with stone bunds erosion control measure from 2004 to 2017. The names of a, b, c & d represent Badiere, Batiara, Dibogh and Namere sites with stone bunds erosion control.

The Batiara site produced the highest area of significant trend of about 29.98% followed by the Badiere site with 28.9%. The Namere and Dibogh sites had 21.1% and 12.8% respectively of the total area being significant.

Overall, the results of the Theil-Sen slope estimator showed a positive increasing trend ranging from 3.14 x 10^{-4} to 3.95 x 10^{-4} ΔNDVI/month for all the four sites, but the Mann-Kendall trend test showed that only the trends of Badiere, Batiara and Namere were statistically significant at 95% confidence interval producing a p-value of 0.036, 0.035 and 0.044, respectively (Table 6-1).

Table 6-1: Statistics of the overall NDVI trend of sites in areas with stone bunds erosion control measure

Site	**Sen's slope (x 10^{-4} / month)**	**Lower Bound (x 10^{-4})**	**Upper Bound (x 10^{-4})**	**P-value (95% CI)**
Badiere	3.95	0.300	7.51	0.036
Batiara	3.77	0.329	6.86	0.035
Dibogh	3.14	-0.219	6.01	0.066
Namere	3.82	0.125	7.21	0.044

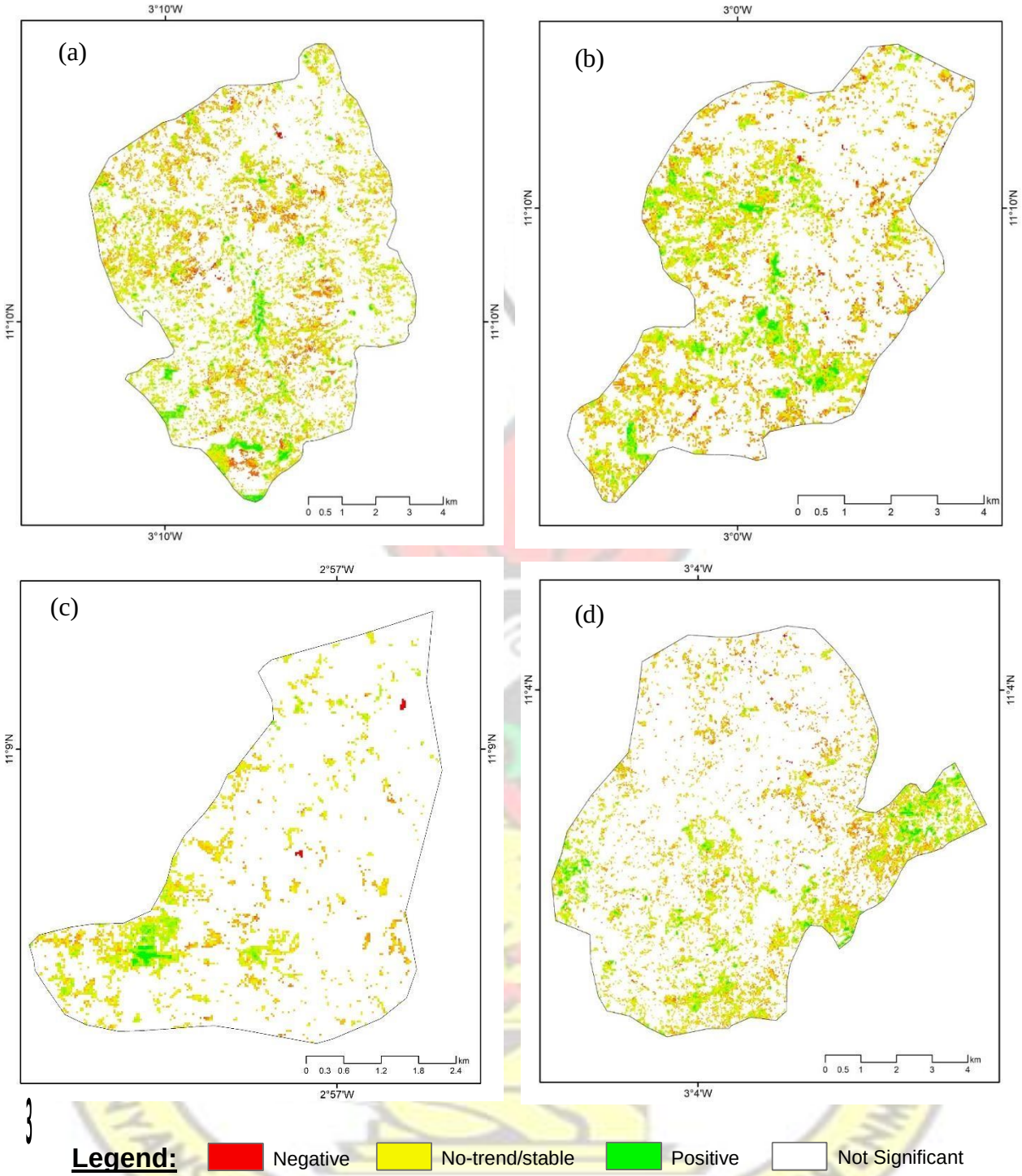

Figure 6-8: Significant slope values for trends at 95% confidence interval derived from monthly NDVI observations of four sites with stone bunds erosion measure from 2004 to 2017. The names of a, b, c & d represent Badiere, Batiara, Dibogh and Namere sites with stone bunds erosion control.

6.1.3 Areas without Stone Bunds Erosion Control Measures

Figure 6-9 shows the spatial distribution of NDVI trends in the four sites without stone bunds erosion control, namely, Bankandi, Biengane, Bisserke and Wizini from 2004 to 2017. Like

the areas with stone bunds erosion control, the areas without stone bunds control also had similar NDVI trend values ranging from -0.002 to 0.002 per month. The spatial pattern of NDVI trends for Bankandi and Bisserke shows a widespread of stable and negative trends with few areas of positive trends unlike the Biengane and Wizini sites. The negative trends in the Bisserke site is more prominent than the other three sites. Figure 6-10 shows the p-value map used to extract the areas of significant trends. At a 95% confidence interval, areas characterized by significant trend are shown in Figure 6-11. From the figure, areas of positive trend were more significant in all the four sites. Most of the negative trends in the Bisserke site were eliminated in the significant trend map. Like that of areas with stone bunds erosion control, the areas covered by significant NDVI trends forms about one-third of the total area. The Bisserke site obtained the highest coverage of significant trend (about 32.7%), followed by Bankandi with 31.8% and 23.2% for the Wizini site. The Biegane site recorded the lowest percentage of significant area coverage.

On the whole, all the four sites in areas without stone bunds erosion control reported a positive increasing trends in NDVI from the Theil-Sen's slope estimator test and the Mann-Kendall trend test showed that all the four sites were statistically significant at 95% confidence interval producing a p-value of less than 0.042 in all cases Table 6-2.

Table 6-2: Statistics of the overall NDVI trend of sites in areas without stone bunds erosion control measure

Site	**Sen's slope (x 10^{-4} / month)**	**Lower Bound (x 10^{-4})**	**Upper Bound (x 10^{-4})**	**P-value (95% CI)**
Bankandi	3.86	0.377	7.05	0.034
Biengane	3.91	0.196	7.24	0.041
Bisserke	3.87	0.329	7.34	0.035
Wizini	3.83	0.285	7.10	0.035

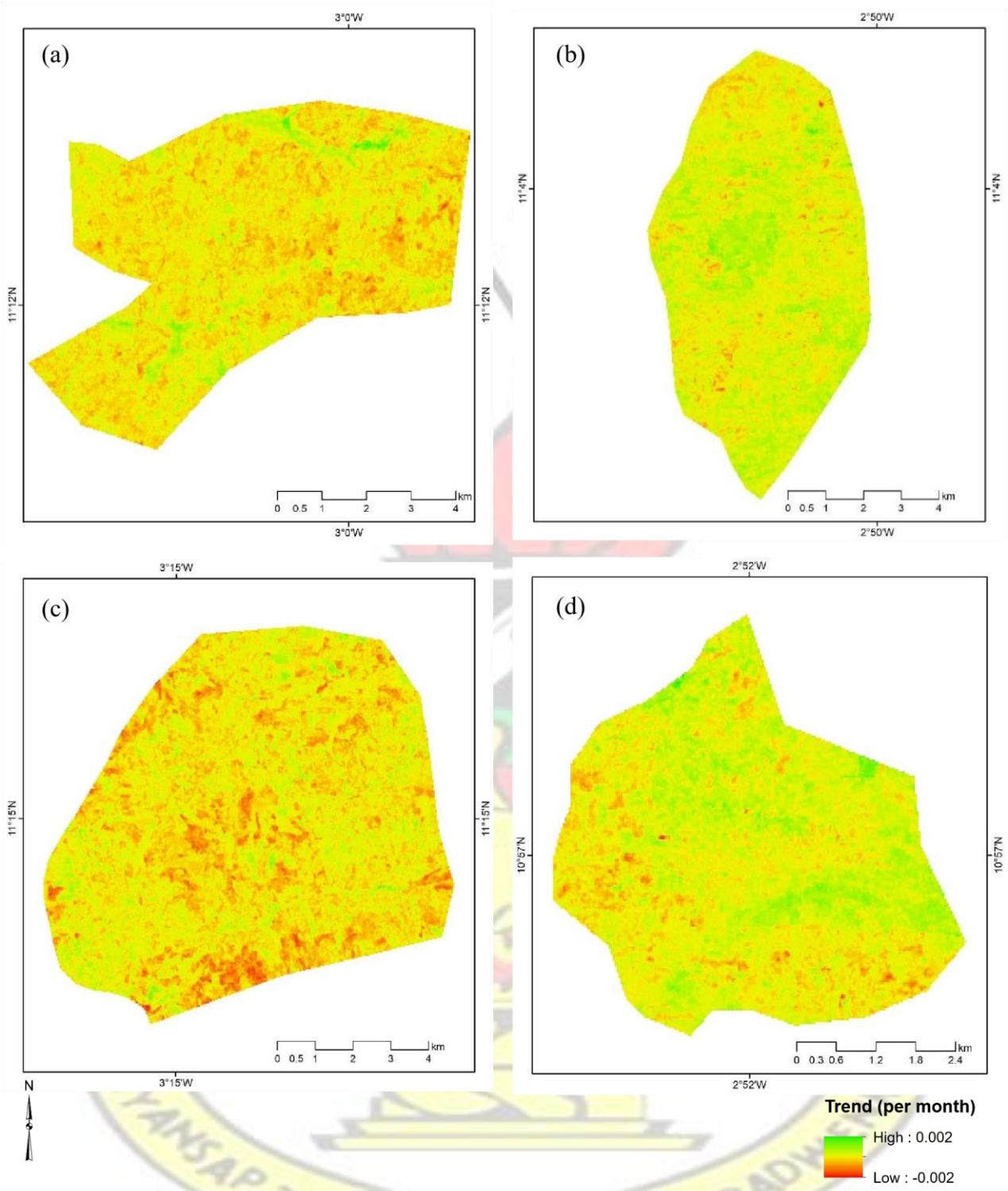

Figure 6-9: Slope values for trends derived from monthly NDVI observations of four sites without stone bunds erosion control measure from 2004 to 2017, a, b, c & d represent Bankandi, Biengane, Bisserke and Wizini sites without stone bunds erosion control.

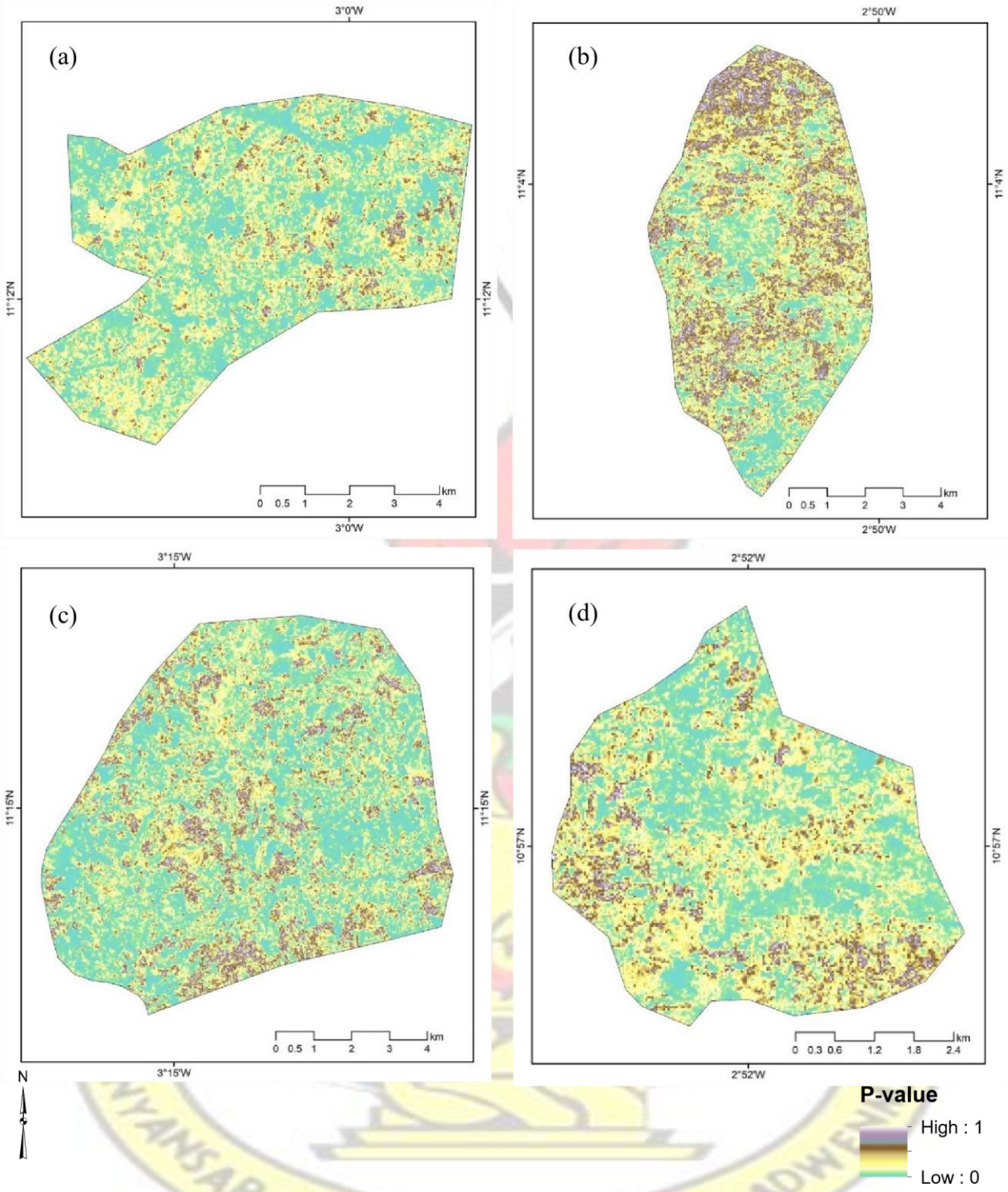

Figure 6-10: P-value map for trends of monthly NDVI observations of sites without stone bunds erosion control measure from 2004 to 2017. The names of a, b, c & d represent Bankandi, Biengane, Bisserke and Wizini sites without stone bunds erosion control.

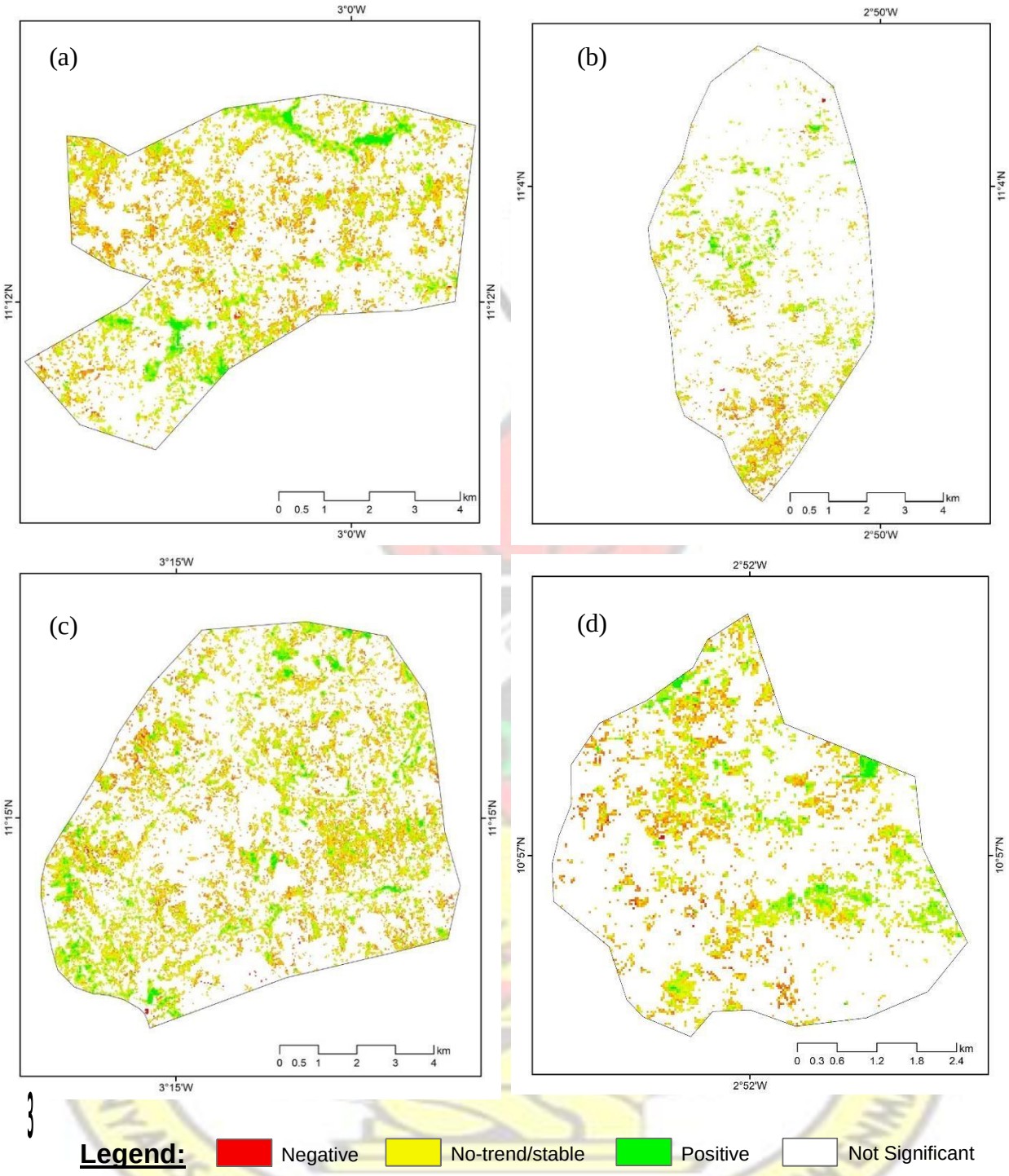

Figure 6-11:Significant slope values for trends at 95% confidence interval derived from monthly NDVI observations of four sites without stone bunds erosion measure from 2004 to 2017. The names of a, b, c & d represent Bankandi, Biengane, Bisserke and Wizini sites without stone bunds erosion control.

6.1.4 Comparison between Areas with and without Stone Bunds Erosion Control Measures

Figure 6-12 shows the trend lines of areas with stone bunds erosion control and areas without

stone bunds erosion control. From the Figure, the overall NDVI trends of areas with stone bunds were similar to those of areas without stone bunds.

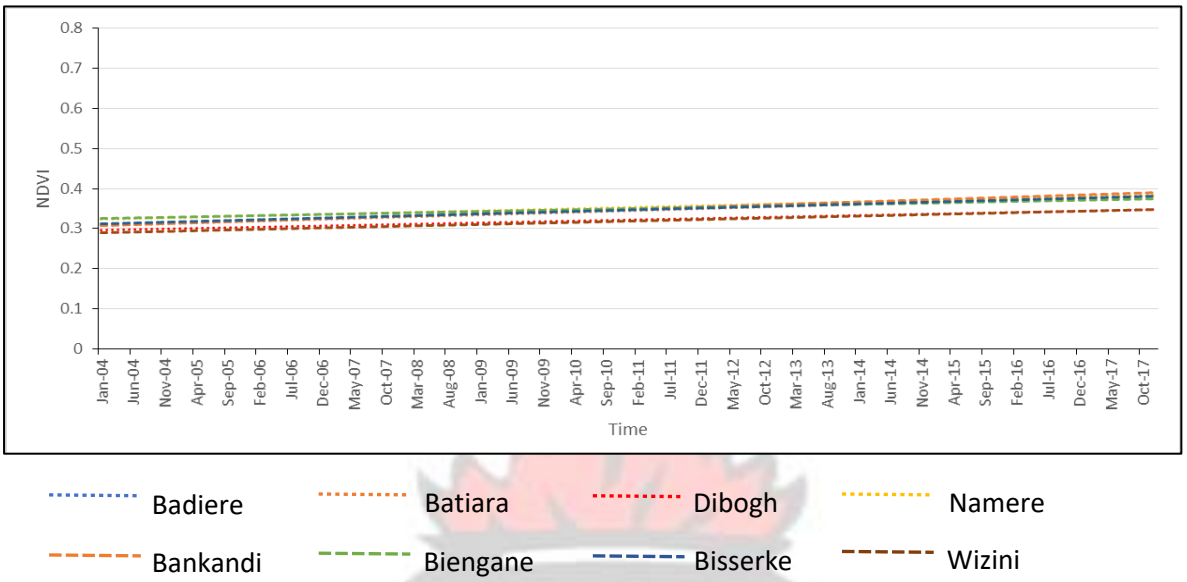

Figure 6-12: Comparison of overall NDVI trends in areas with stone bunds erosion control and areas without from 2004 to 2017. Badiere, Batiara, Dibogh and Namere are areas with stone bunds erosion control and Bankandi, Biengane, Bisserke, and Wizini are areas without stone bunds erosion control.

Table 6-3 shows the results of the ANOVA test to compare the difference between the NDVI trends of areas with stone bunds erosion control and areas without stone bunds erosion control. From the results, the p-value (0.319) is greater than the alpha level ($\alpha = 0.05$). This suggest that there is no significant difference between the NDVI trend of areas with stone bunds erosion control and areas without stone bunds erosion control. Also, a p-value of 0.406 within rows means that, there are no differences in NDVI trends among the four different sites with stone bunds erosion control likewise the four different sites without stone bunds erosion control measure.

Table 6-3: Results of the ANOVA test between NDVI trends of areas with stone bunds erosion control and areas without

SUMMARY	*Count*	*Sum*	*Average*	*Variance*

1	2	0.12815	0.06408	1.192E-06
2	2	0.12987	0.06494	1.397E-06
3	2	0.11700	0.05850	6.694E-05
4	2	0.13145	0.06573	8.887E-07
ECA	4	0.24651	0.06163	3.702E-05
NECA	4	0.25996	0.06499	3.766E-07

Source of Variation	***SS***	***df***	***MS***	***F***	***P-value***	***F crit***
Rows	6.438E-05	3	2.146E-05	1.34706	0.40621	9.27663
Columns	2.262E-05	1	2.262E-05	1.41994	0.31909	10.12796
Error	4.780E-05	3	1.593E-05			
Total	0.00013	7				

6.2 Extraction of Crop Height using Photographs from UAV

6.2.1 Generated DEMs

Figure 6-13 shows a sample of the DEMs created from the UAV images. Figure 6-13(a) is the DEM obtained from the photos taken during land preparation in an area with stone bunds erosion control measure, whiles Figure 6-14(a) is for an area without stone bunds erosion control measure. These were used to obtain the DTM of the crop fields. Figure 6-13(b) and Figure 6-14(b) shows a sample of the DEMs obtained during crop growth for both areas with and without stone bunds erosion control respectively. These DEMs were used to obtain the DSM of the crop fields. Figure 6-15 and Figure 6-16 shows a sample of the DTM and DSM of crop fields in an area with stone bunds erosion control measure and area without respectively, used for analysis.

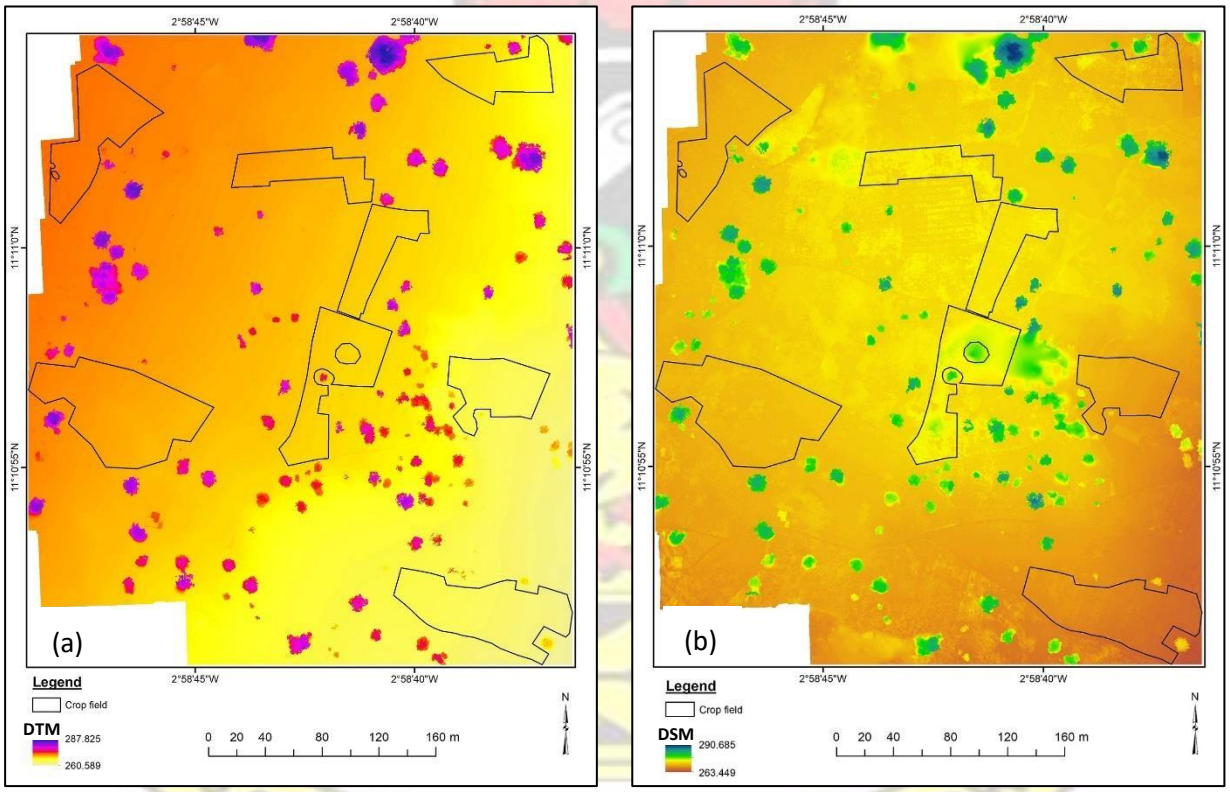

Figure 6-13: DEMs generated from UAV photos in an area with stone bunds erosion control measure; (a) DTM during land preparation, (b) DSM when crops were growing. Units of DTM and DSM is metres

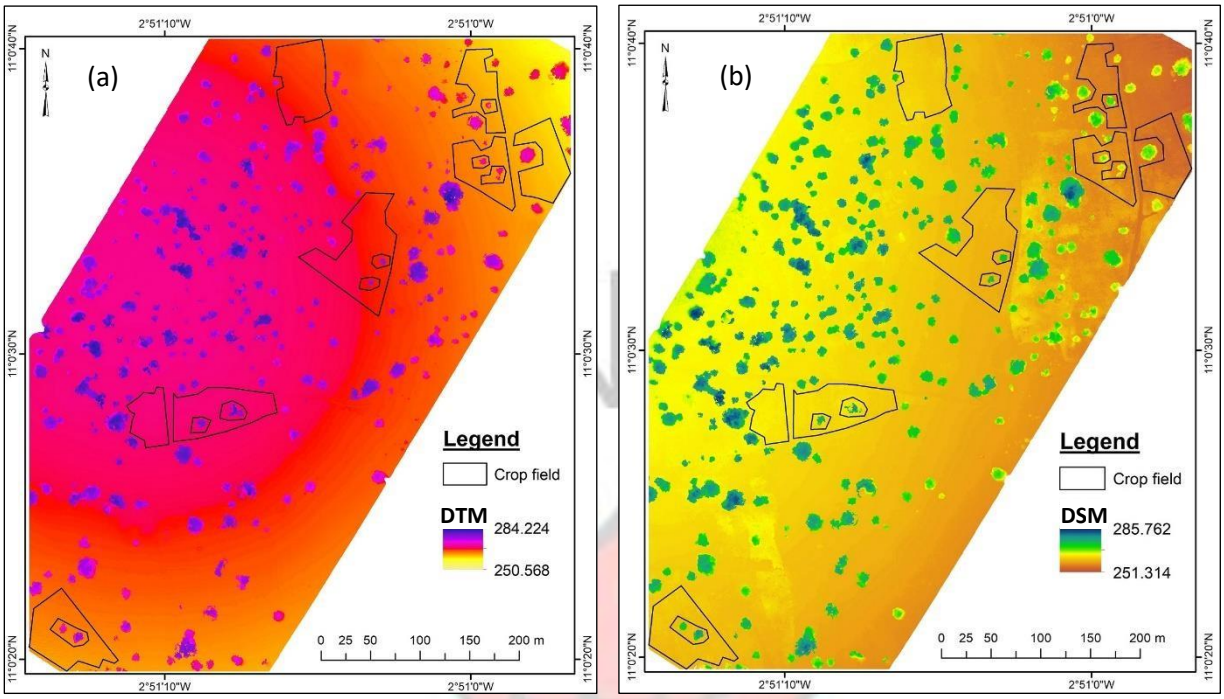

Figure 6-14: DEMs generated from UAV photos in an area without stone bunds erosion control measure; (a) DTM during land preparation, (b) DSM when crops were growing

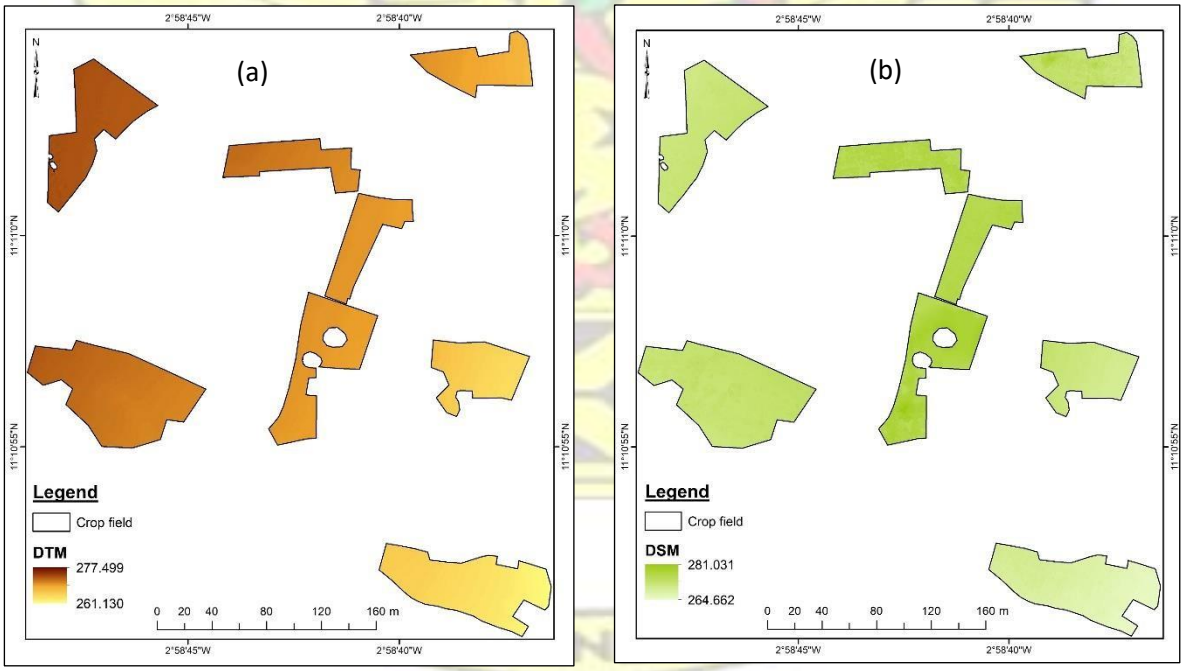

Figure 6-15: DEMs of crop fields in an area with stone bunds erosion control; (a) DTM of crop fields, (b) DSM of crop fields

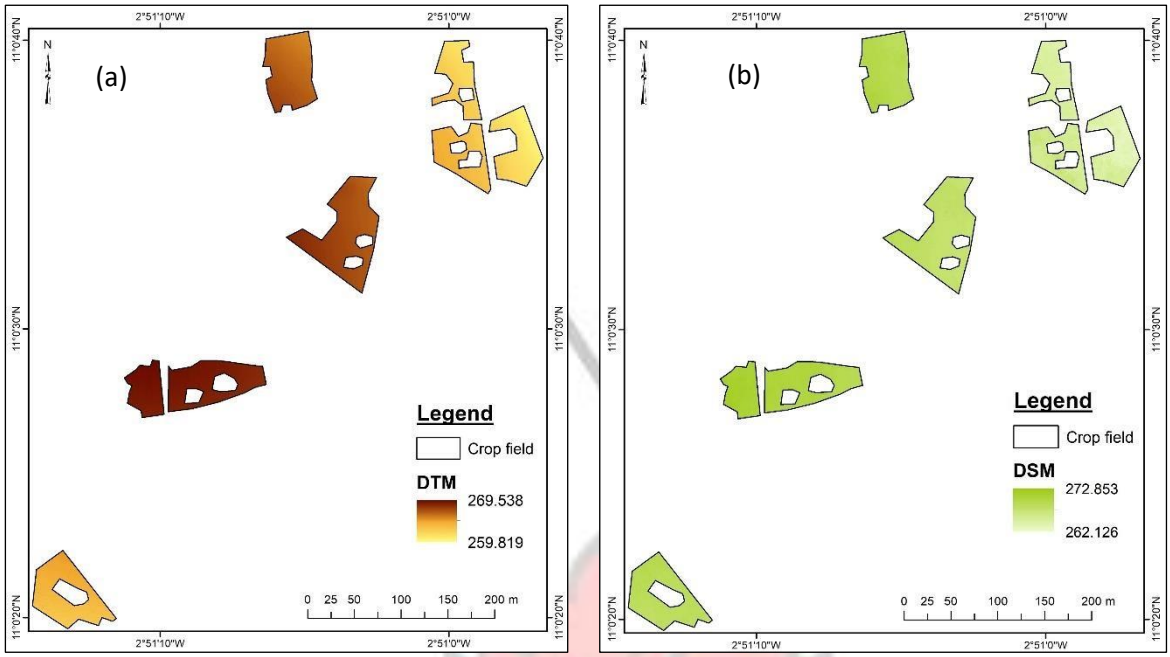

Figure 6-16: DEMs of crop fields in an area without stone bunds erosion control; (a) DTM of crop fields, (b) DSM of crop fields.

6.2.2 Extracted Crop Height

Figure 6-17 show the extracted crop height (nDSM) of cotton fields in an area with stone bunds erosion control measure and an area without, whiles Figure 6-18 show that of millet in both areas.

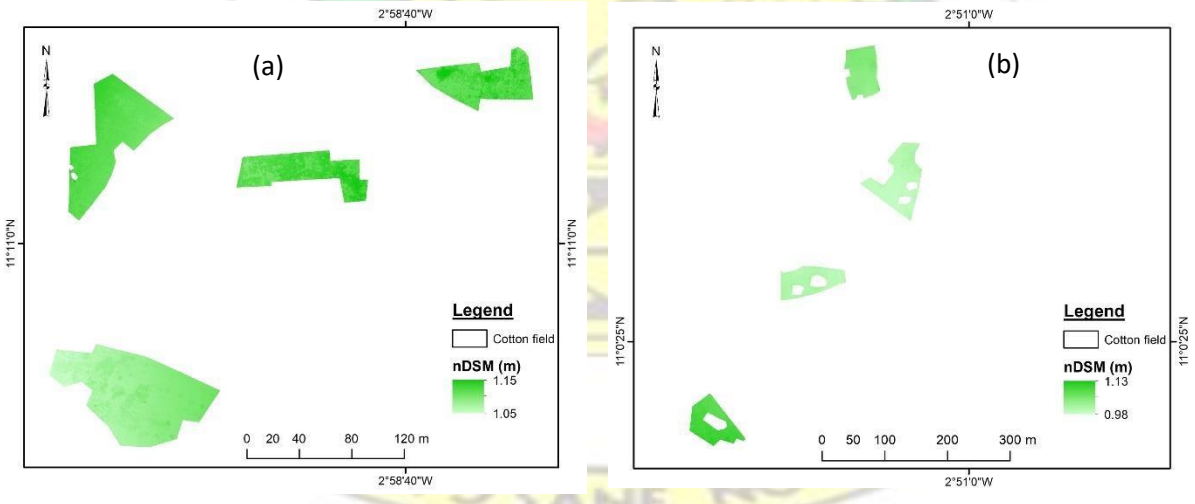

Figure 6-17: A sample of extracted crop heights (nDSM) of cotton at 16 weeks old; (a) ECA, (b) NECA

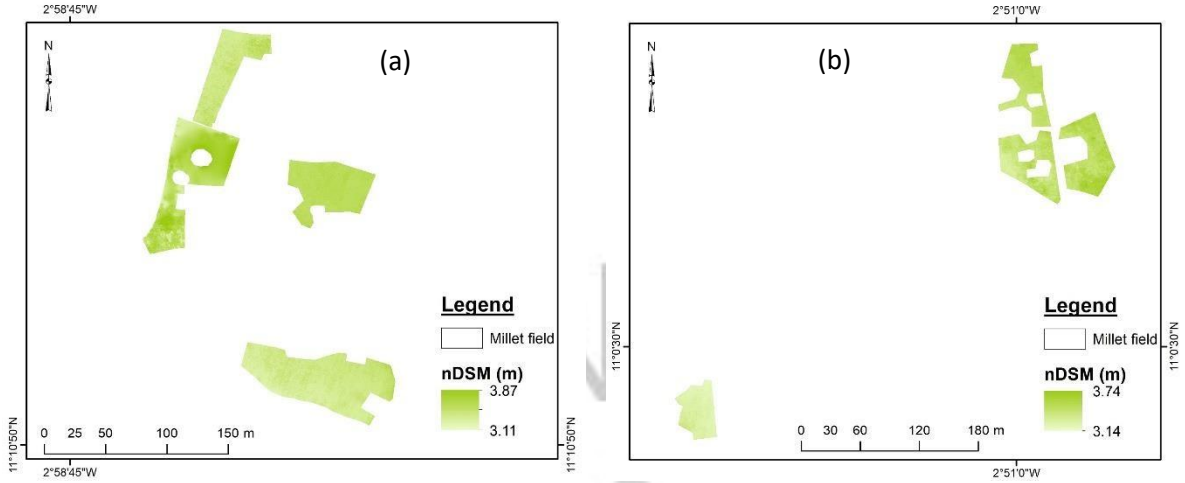

Figure 6-18: A sample of extracted crop heights (nDSM) of millet at 16 weeks old; (a) ECA, (b) NECA

Table 6-4 shows the values of extracted crop heights of millet and cotton in areas with stone bunds erosion control measure and areas without for various time steps. From the Table, it is evident that the crops in areas with stone bunds erosion control measure and those in areas without stone bunds erosion control have similar crop height for each time step. Millet in areas with stone bunds erosion control had a mean height of 0.15 m at 2 weeks old and grew up to 3.47m at 16 weeks while at areas without stone bunds erosion control, it had a mean of 0.13m at 2 weeks old to 3.44 at 16 weeks old. In the case of cotton in areas with stone bunds erosion control, the mean heights values at age 2 weeks and 16 weeks were 0.13m and 1.10m respectively whiles 0.14 and 1.06 were obtained in areas without stone bunds erosion control.

Table 6-4: Extracted crop height (in metres) of millet and cotton for growth season in areas with stone bunds erosion control and areas without.

Crop type	Age of crop (wks)	ECA			NECA		
		Min(m)	Max(m)	Mean(m)	Min(m)	Max(m)	Mean(m)
Millet	2	0.12	0.17	0.15	0.11	0.15	0.13
	5	0.31	0.39	0.35	0.32	0.41	0.37
	7	0.82	0.85	0.84	0.79	0.87	0.83
	10	1.16	1.28	1.22	1.2	1.34	1.27
	13	1.85	2.34	2.10	1.8	2.45	2.13
	16	3.11	3.87	3.49	3.14	3.74	3.44
Cotton	2	0.11	0.15	0.13	0.11	0.16	0.14
	5	0.19	0.26	0.23	0.2	0.25	0.23
	7	0.36	0.45	0.41	0.34	0.43	0.39
	10	0.51	0.59	0.55	0.50	0.60	0.55
	13	0.70	0.77	0.74	0.69	0.76	0.73
	16	1.05	1.15	1.10	0.98	1.13	1.06

6.2.3 Validation of Extracted Crop Height

Table 6-5 shows the error statistics obtained by validating the UAV extracted crop heights of millet and cotton using the measured heights from the field. The MAE, RMSE and the coefficient of determination (R^2) are presented for each crop type in areas with stone bunds erosion control and areas without. From the Table, it can be observed that similar values of MAE and RMSE were obtained from the extracted heights of both areas with stone bunds erosion control and areas without stone bunds erosion control.

Table 6-5: Accuracy estimates derived from the validation of extracted crop height in areas with stone bunds erosion control (ECA) and areas without (NECA)

Site	Crop type	MAE	RMSE	R_2
ECA	Millet	0.107	0.108	0.93
	Cotton	0.105	0.106	0.96
NECA	Millet	0.108	0.111	0.92
	Cotton	0.105	0.109	0.95

6.2.4 Comparison of Crop Heights between Areas with Stone Bunds and Areas without Figure 6-19 shows the trend of crop heights for millet in areas with stone bunds erosion control and areas without. From the graph it can be observed that the trend of crop height for areas with and without stone bunds erosion control measure are similar with overlapping segments in most cases. However, a very slight differences can be observed when the crops were 10 to 16 weeks old.

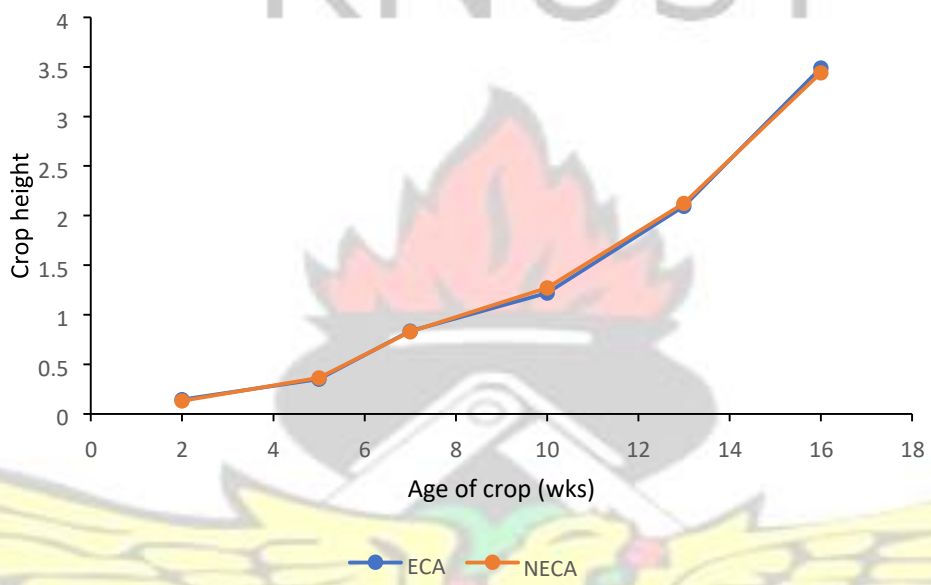

Figure 6-19: Comparison of growth trend of millet between areas with and without stone bunds erosion control measure

Similar to the trend of in millet growth, the trend of cotton in both areas with stone bunds and areas without stone bunds also had similar trends (Figure 6-20). With the exception of the 7th and the 16th weeks all the other time steps had crop heights very similar.

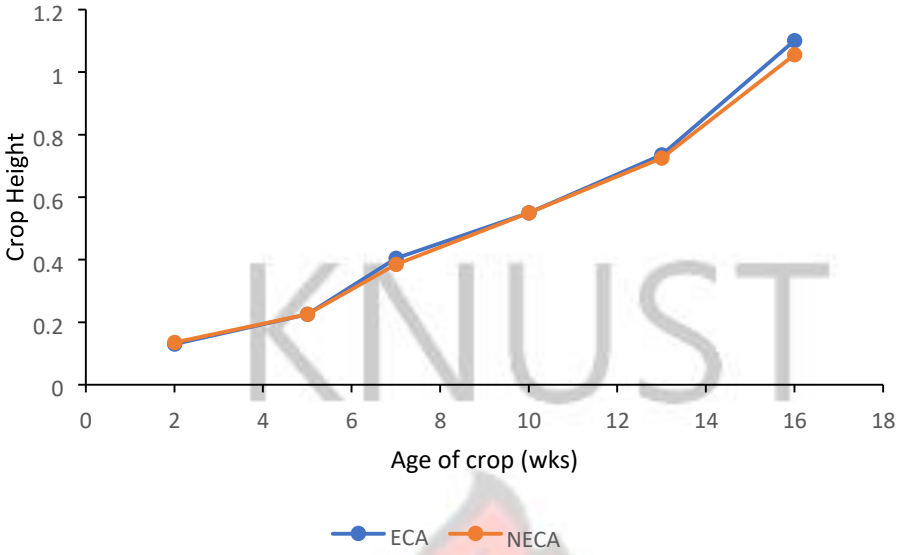

Figure 6-20: Comparison of growth trend of millet between areas with and without stone bunds erosion control measure

The results from the Mann-Kendall's ranked correlation test shows that the crop height of both cotton and millet in areas with stone bunds erosion control and areas without are highly correlated. A kendall τ of 0.969 and 0.954 were obtained for cotton and millet respectively with p-value of 0.000 in both cases.

The student t-test also gave a value of 0.0008 and a p-value 0.884 for millet in areas with stone bunds erosion control and areas without, whiles cotton had -0.005 and a p-value of 0.389, all at 95% confidence interval.

6.3 Time Series of Climate Variables and their Relationship with NDVI

6.3.1 Rainfall Analysis

A preliminary analysis of the rainfall data shows that, the distribution of monthly rainfall is mainly concentrated in the period of April to October. Also, high rainfall values were recorded in the months of August and September in the period of the study. The three highest total monthly rainfall values of 308.8, 305.6 and 303.9 mm were recorded for August 2008, September 2015 and September 2006 respectively. Although the months of November to February are noted to be months of little or no rainfall, a substantial amount of rainfall was recorded in November 2004 (69.5 mm). The results from the rainfall analysis revealed a positive trend in the avarage monthly rainfal from 2004 to 2017 at a rate of 0.12 mm/month (Figure 6-21). But the Mann-kendall test showed that the trend of rainfall is not statistically significant at 95% confidence interval (z-score of 0.91 at a p-value of 0.36). Also, no break point(s) were observed in the time series for the period of study.

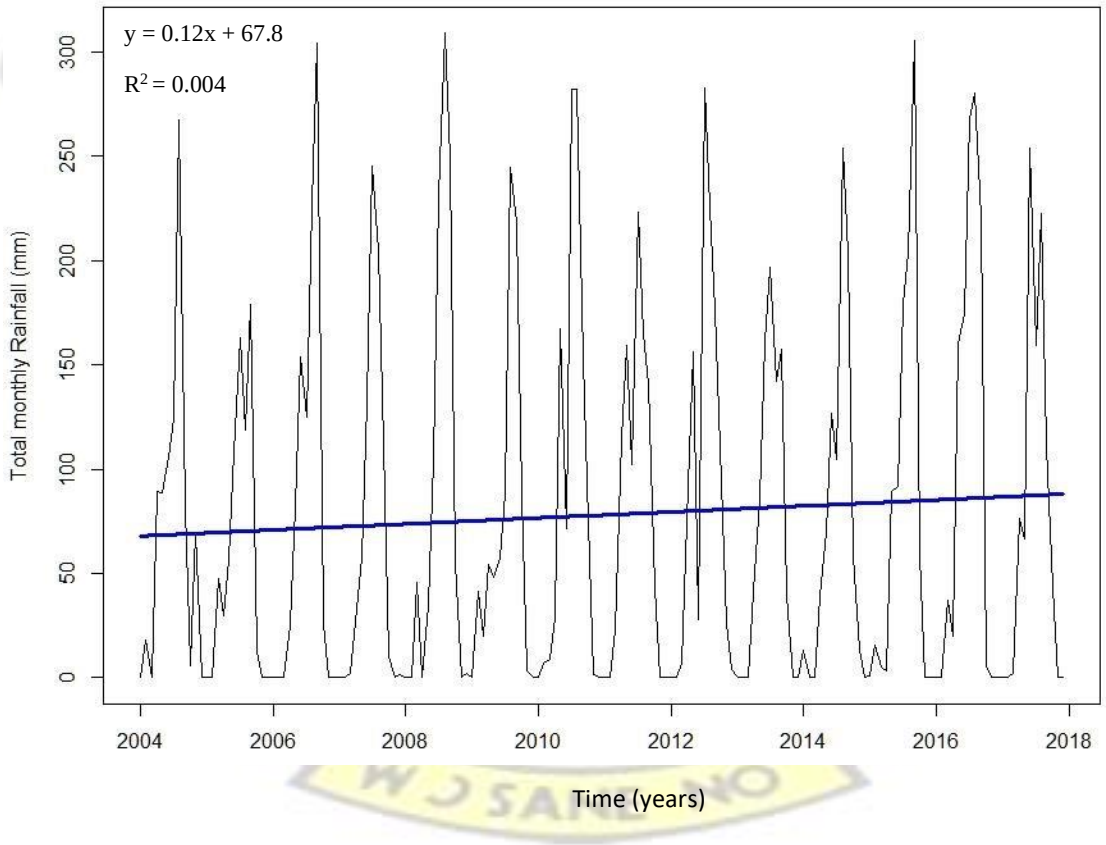

Figure 6-21: Monthly variation of rainfall from 2004 to 2017

Although the analysis reported a positive trend in rainfall which is not statistically significant, a critical look at the rainfall anomalies (Figure 6-22) over the period showed a slightly higher total increase (682.3 mm) above the average for the 14-year period compared to the total decrease (681.7 mm) over the period. The difference between the total increase and the total decrease is 0.6mm. It may be therefore a bit misleading to conclude that rainfall trends are increasing over the period of the study judging the positive trend (0.12 mm/month).

Within the 14-year period, seven years (2006, 2008, 2010, 2011, 2012, 2015 and 2016) had a total annual rainfall above the period's (14 years) average baseline of 935.7mm whiles the other seven years (2004, 2005, 2007, 2009, 2013, 2014 and 2107) also had a total annual rainfall below the baseline. The first four years (2004-2007) on the average experienced a marginal decrease in rainfall whiles on the average, an increase was also observed from 2008 to 2012. The highest value (of 230.5 mm) above the 14-year average baseline was observed in the year 2016 while the lowest (of -220.1 mm) occurred in 2005. Throughout the study period, the longest consecutive values above the period's average baseline of 935.7 mm was three years and this was observed from 2010 - 2012. Two consecutive years of values below the baseline were also recorded in 2004 - 2005 and 2013 - 2014.

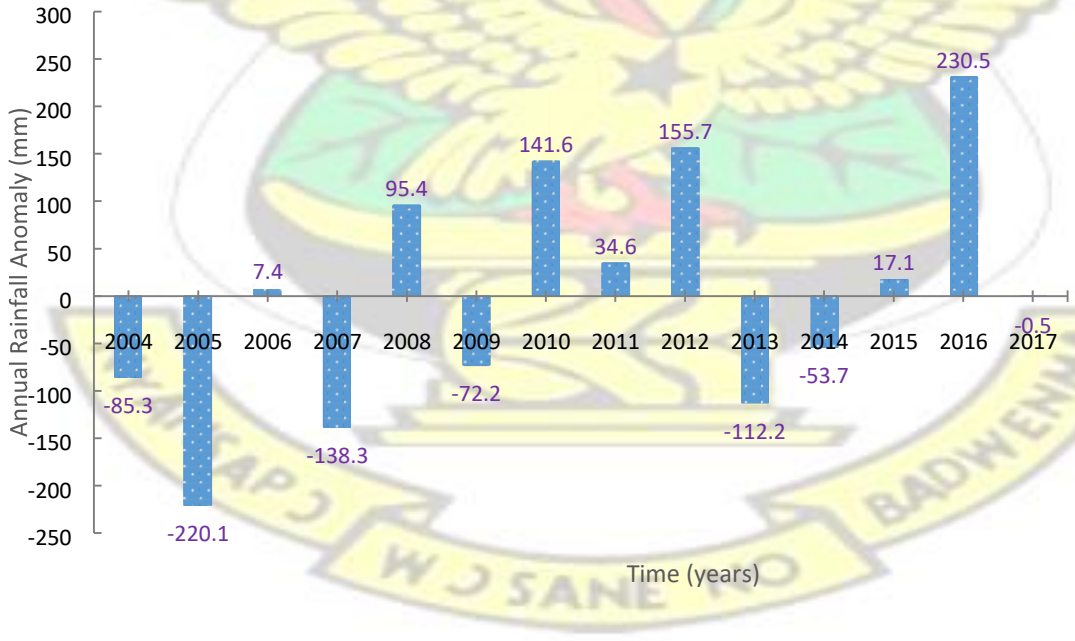

Figure 6-22: Mean annual rainfall anomaly from 2004 to 2017 for the study area (Mean annual rainfall value is 935.7 mm, calculated from the Dano climate station data)

The Theil-Sen slopes estimator and significant Mann-Kendall test results for rainfall time series for individual month are shown in Table 6-6. Overall, the months, May, June, July, September

and October showed a positive trend of 0.952, 4.02, 2.662, 2.656 and 2.877 mm/month respectively in rainfall within the period of study and whiles the months March, April and August showed a negative trend (-0.10, -0.20 and -0.25 mm/year) in rainfall. However, none of these trends were statistically significant at 95% confidence interval (Z-score between 0.99 and -0.33). The months, January, February, November and December reported no consistent trend in rainfall over the study period. However, the consistent trend of January was statistically significant at 95% confidence interval with a Z-score of 2.28.

Table 6-6: Results of Mann-Kendall's and Theil-Sen's statistics of total rainfall for each month. Confidence interval = 95% (α=0.05). Total number of years = 14 (Beginning year; 2004, Ending year; 2017).

Month	Z-score	p-value	Intercept	Trend (mm/year)
January	2.28	0.022	0	0
February	0.37	0.714	0	0
March	-0.33	0.739	6.2	-0.010
April	0	1	37.6	-0.200
May	0.77	0.443	76.9	0.952
June	0.66	0.511	92.2	4.02
July	0.44	0.661	163.9	2.662
August	-0.11	0.913	227.7	-0.250
September	0.44	0.661	163.3	2.656
October	0.99	0.324	18.8	2.877
November	0	1	0.1	0
December	-0.77	0.440	0	0

Generally, there is an increase in total yearly rainfall from 2004 to 2017. Apart from 2005 and 2013 which recorded lower values of 715.6 mm and 823.5 mm, all the other years had rainfall values more than 850mm. Out of the 14-year period, the years 2008, 2010, 2012 and 2016 recorded a total annual rainfall of more than 1000 mm with 2016 being the wettest year with a value of 1166.2 mm. The avaerage annual rainfall from 2004 to 2017 was 935.7 mm. Half of the years under consideration obtained annual rainfall values above the average and the other

half was below the average. The results from the Theil-Sen's slope estimator reveals a positve trend of inter-annual rainfall with a trend value of 13.80 mm/year but the Mann-kendall test shows that the trend is not statistically significant at 95% confidence interval producing a zscore of 1.64 at a p-value of 0.10.

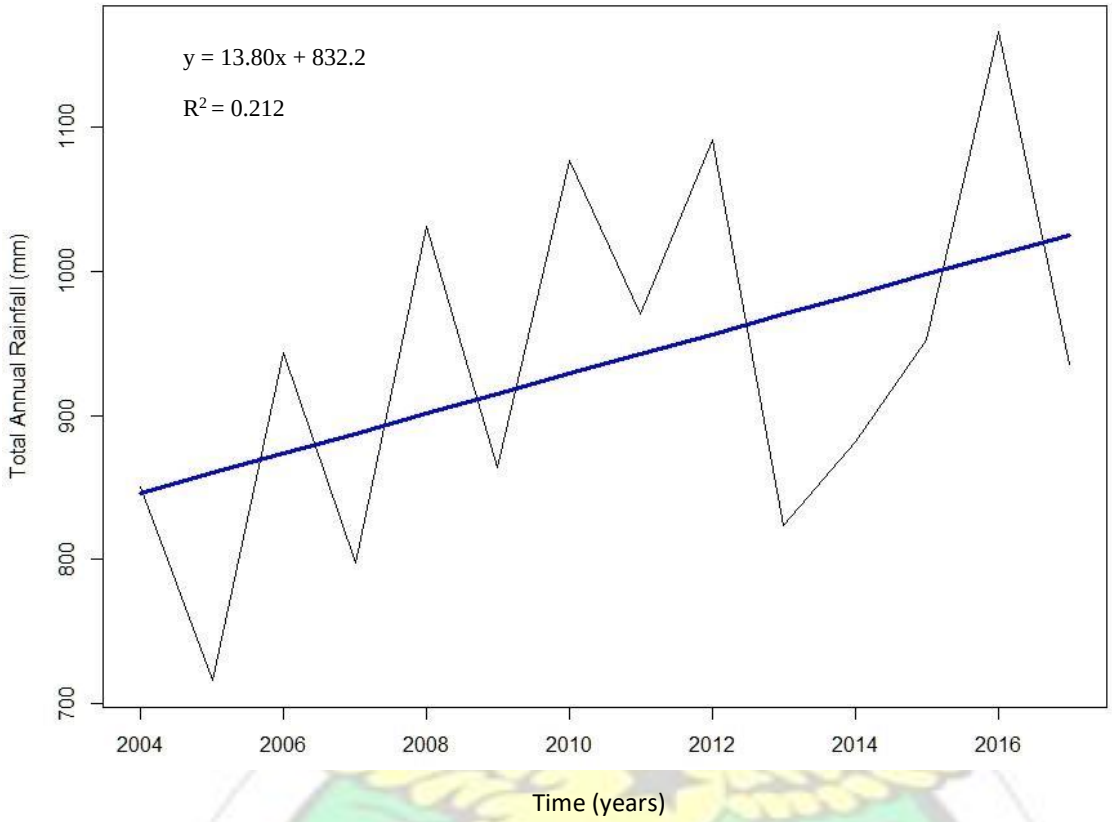

Figure 6-23: Yearly rainfall variation from 2004 to 2017

6.3.2 Temperature Analysis

Figure 6-24 shows the variations in monthly temperature from 2004 to 2017. The series shows that, average monthly temperature gradually increases at a rate of 0.01 °C/month over the period. A critical look at the temperature series reveals that high temperature values of more than 30 °C were mostly recorded in the months of February, March, April and May whiles low values of about 24 °C were recorded in January and December. For the period, the highest (33.95 °C) and lowest (23.30 °C) monthly averages were recorded in April 2016 and January 2008 respectively. Although the Theil-Sen's slope estimator gave a positive trend in temperature over the period, the Mann-kendall test shows that the temperature trend is not

statistically significant at 95% confidence interval (z-score of 1.72 at a p-value of 0.16). Also, no break point(s) were observed in the time series for the period of study.

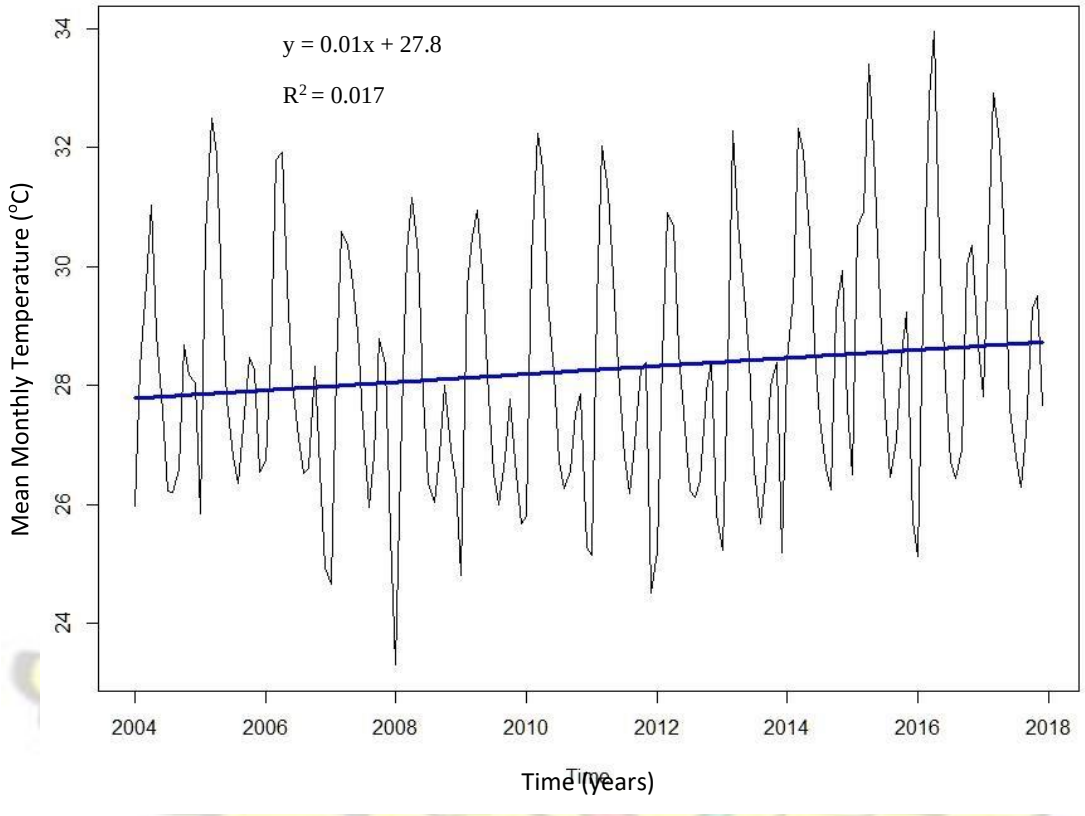

Figure 6-24: Monthly temperature variability from 2004 to 2017 (mean values)

Figure 6-25 presents the temperature anomaly from 2004 to 2017. It can be observed that the temperature anomaly is different each year, and the fluctuation range is between −0.7 and 0.8 °C with the obvious negative anomalies occurring before 2013. Overall, nine out of 14 years had annual temperature values below the mean value of 28.26 °C calculated from the station data from 2004 to 2017. Positive anomalies were consistent each year at the later part of the period (from 2014 to 2017). The highest value (of 0.79 °C) above the 14-year average baseline was observed in the year 2016 while the highest value below the baseline (lowest value) of -0.70 °C occurred in 2010.

0.8

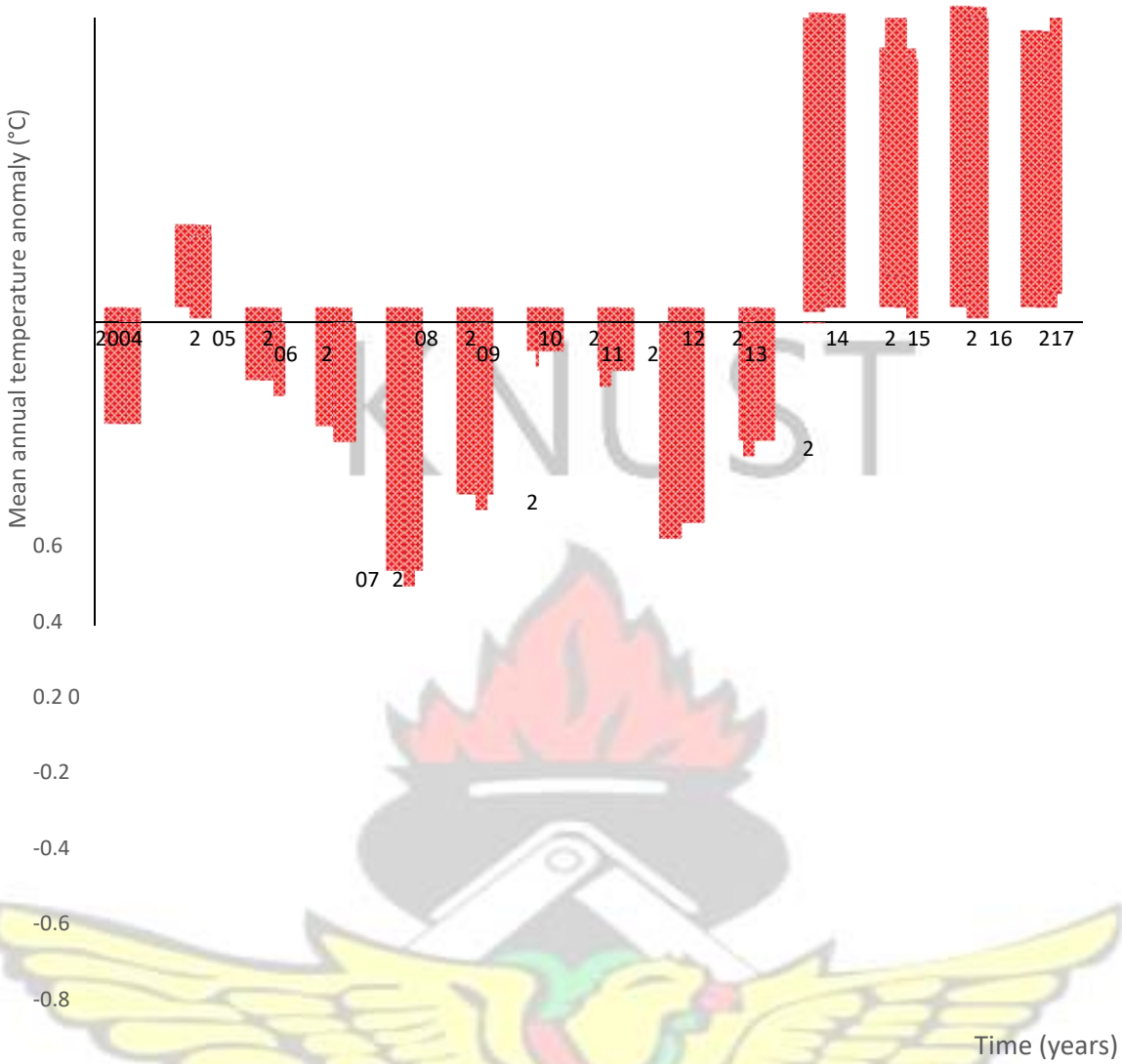

Figure 6-25: Mean annual temperature anomalies from 2004 to 2017 for the study area (Mean annual temperature value is 28.26°C, calculated from the Dano climate station data)

The results of temperature analysis for individual months from 2004 to 2017 obtained from the Mann-Kendall's and Theil-Sen's test are presented in Table 6-7. The average temperature values of the month were used in the analysis. It can be observed that generally all the months exhibit a positive trend in temperature between the period under study. A minimum slope of 0.005 ^{o}C/year was recorded in the month of September and this value increased steadily through other months to a maximum of 0.209 ^{o}C/year for the month of November. Although all the months recorded a positive trend in average temperature, only the months, March, May and November had trends (0.12, 0.094 and 0.209 ^{o}C/year with z-score of 2.30, 2.08 and 3.07 respectively) which are statistically significant at 95% confidence interval.

Table 6-7: Results of Mann-Kendall's and Theil-Sen's statistics of mean temperature for each month. Confidence interval = 95% (α=0.05). Total number of years = 14 (Beginning year; 2004, Ending year; 2017). Months with bold values were statistically significant.

Month	Z-score	p-value	Intercept	Trend (°C/year)
January	0.77	0.443	24.9	0.076
February	0.99	0.324	28.3	0.100
March	**2.30**	**0.021**	**31.0**	**0.126**
April	1.53	0.125	30.9	0.088
May	**2.08**	**0.038**	**29.2**	**0.094**
June	1.20	0.228	27.8	0.049
July	0.99	0.324	26.4	0.039
August	0.55	0.584	26.2	0.012
September	0	1	26.8	0.005
October	0.88	0.381	28.0	0.051
November	**3.07**	**0.002**	**26.7**	**0.209**
December	0.55	0.584	25.3	0.054

6.3.3 Relationship between NDVI and Climate Variables

6.3.3.1 Overall monthly correlation and regression between NDVI and climate variables

The results from the Mann-Kendall ranked correlation test gave a Kendall score of 7005, tau (τ) of 0.513 with a 2-sided p-value of =< 2.22e-16. This (τ = 0.513) shows that there is a positive association between NDVI and rainfall in the study area from 2004 to 2017. The scatter plot in Figure 6-26 illustrate the linear association between mean monthly NDVI and total monthly rainfall over the duration of the study with a slope of 0.0013. The regression model produced a coefficient of determination, R^2 of 0.54, which implies that if a time series of total monthly rainfall is provided the assumed model (linear relationship in Figure 6-26) will be able to predict approximately 54% of the variance of mean monthly NDVI fluctuations.

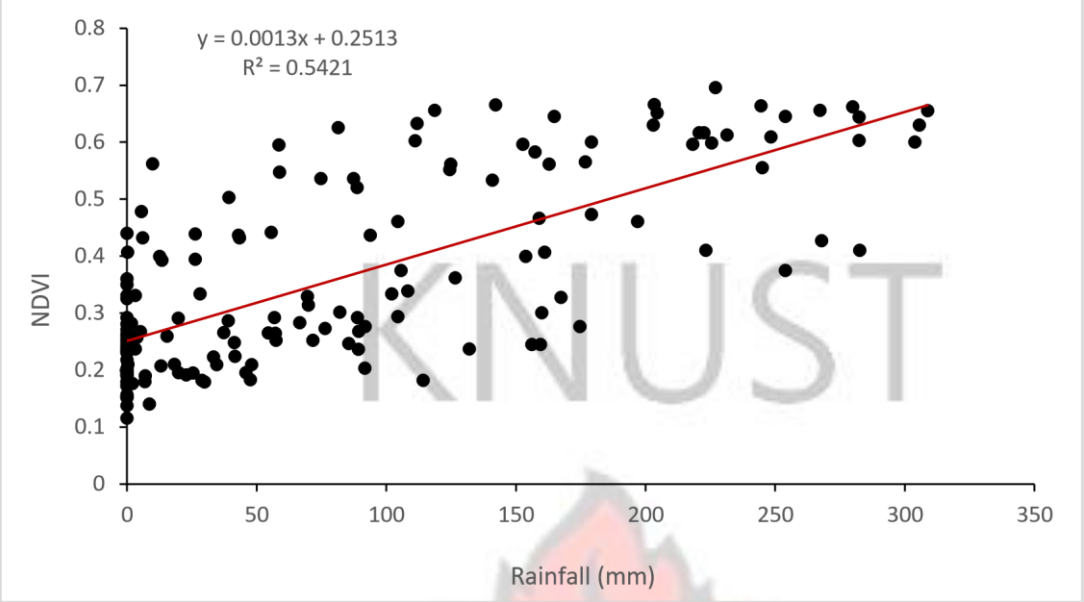

Figure 6-26: The overall relationship between mean monthly NDVI and total monthly rainfall from 2004 to 2017

In the case of temperature, Mann-Kendall ranked correlation test gave a Kendall score of -4515, tau (τ) of -0.322 with a 2-sided p-value of =5.943e-10. The negative value of τ (-0.322) is an indication that there is a negative association between NDVI and temperature in the study area from 2004 to 2017. The scatter plot (Figure 6-27) illustrate the linear association between mean monthly NDVI and temperature over the 14-year study producing a negative slope of 0.0329. The regression model produced a coefficient of determination, R^2 of 0.18, which implies that the assumed model (linear relationship in Figure 6-27) will be able to predict approximately 18% of the variance of mean monthly NDVI fluctuations when given a time series of mean monthly temperature.

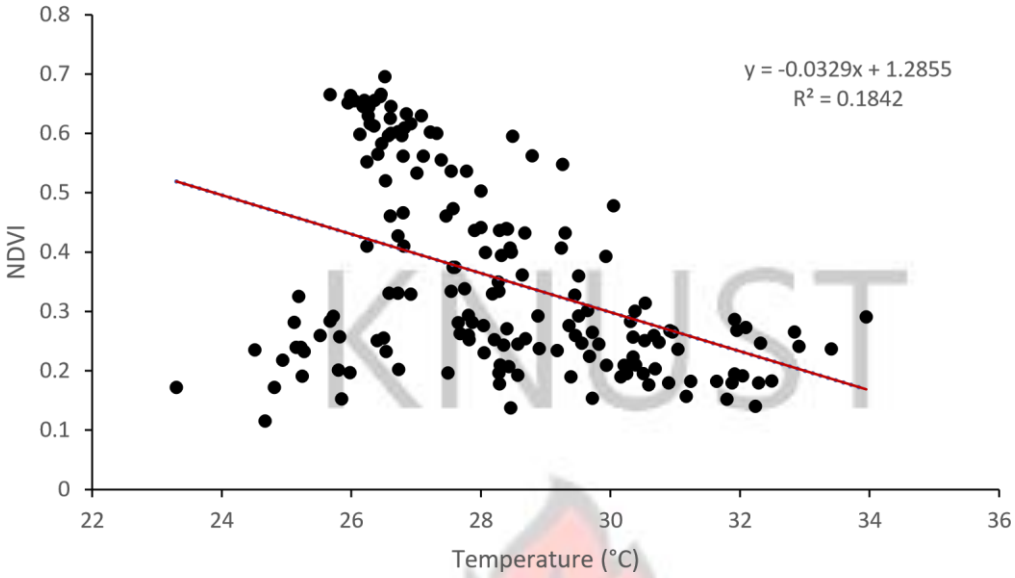

Figure 6-27: The overall relationship between mean monthly NDVI and mean monthly temperature from 2004 to 2017

From Figure 6-28 both precipitation and temperature correlate with NDVI, but the effect of rainfall seems more significant than that of temperature. This is because the variability of rainfall is high, and this correspond with NDVI whereas temperature has a low variability. Also, it can be observed that NDVI starts to increase in line with the onset of the rainfall and periods of high rainfall corresponds to high NDVI values in most cases but in terms of temperature, low values mostly correspond to high NDVI values.

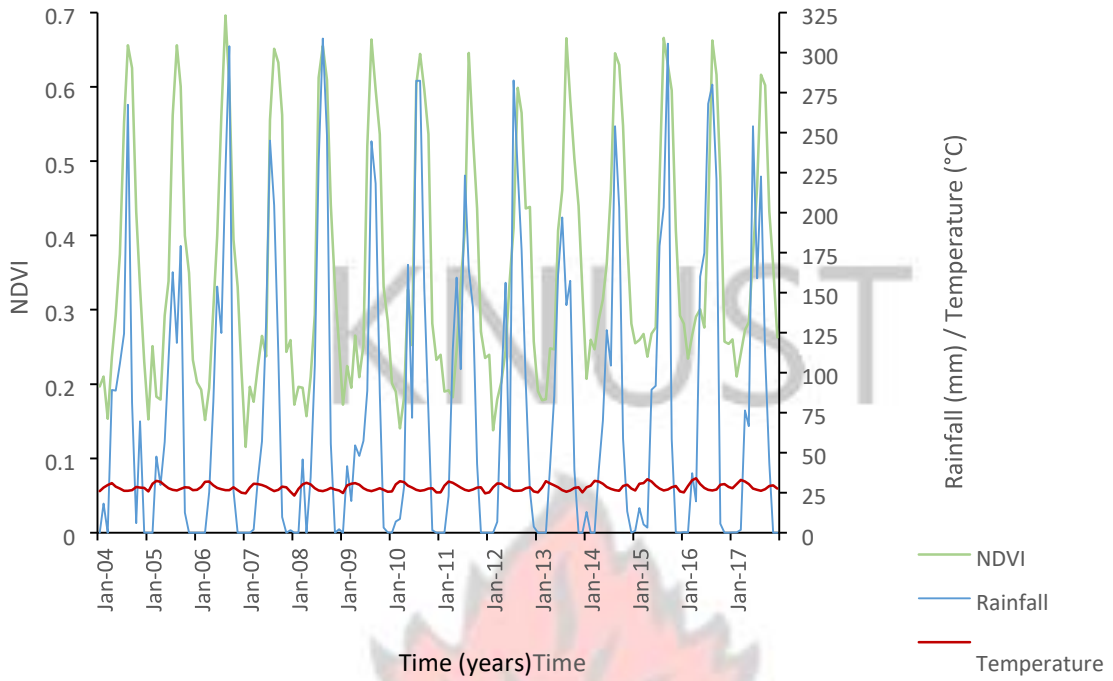

Figure 6-28: The overall relationship between NDVI and climate variables (total monthly rainfall and mean monthly temperature) from 2004 to 2017

6.3.4 Pixel-wise Correlation between NDVI and Climate Variables

Figure 6-29a represents the spatial patterns of Mann-Kendall's correlation coefficient (Kendall's τ) between NDVI and rainfall. From the results, it was observed that, NDVI and rainfall had a positive correlation across the whole study area producing a Kendall τ of 0.15 as the minimum to a maximum of 0.64 with a mean of 0.48. Although the NDVI of the whole study area correlated positively with rainfall only about 2% of the area was statistically significantly at 95% confidence interval (α = 0.05) (Figure 6-29b). In general, high positive correlations were mostly found in areas with rainfed croplands and natural vegetation whiles low positive correlations were found in riverine, wetlands and irrigated areas. From Figure 630a, unlike the correlation between NDVI and rainfall which is positive, NDVI correlates negatively to temperature throughout the study area. The correlation coefficients (τ) ranges from -0.08 to -0.47, with less than 1% being statistically significant at 95% confidence interval (α = 0.05) as shown in Figure 6-30b. Areas of high negative correlation was widespread compared to areas of low negative correlation.

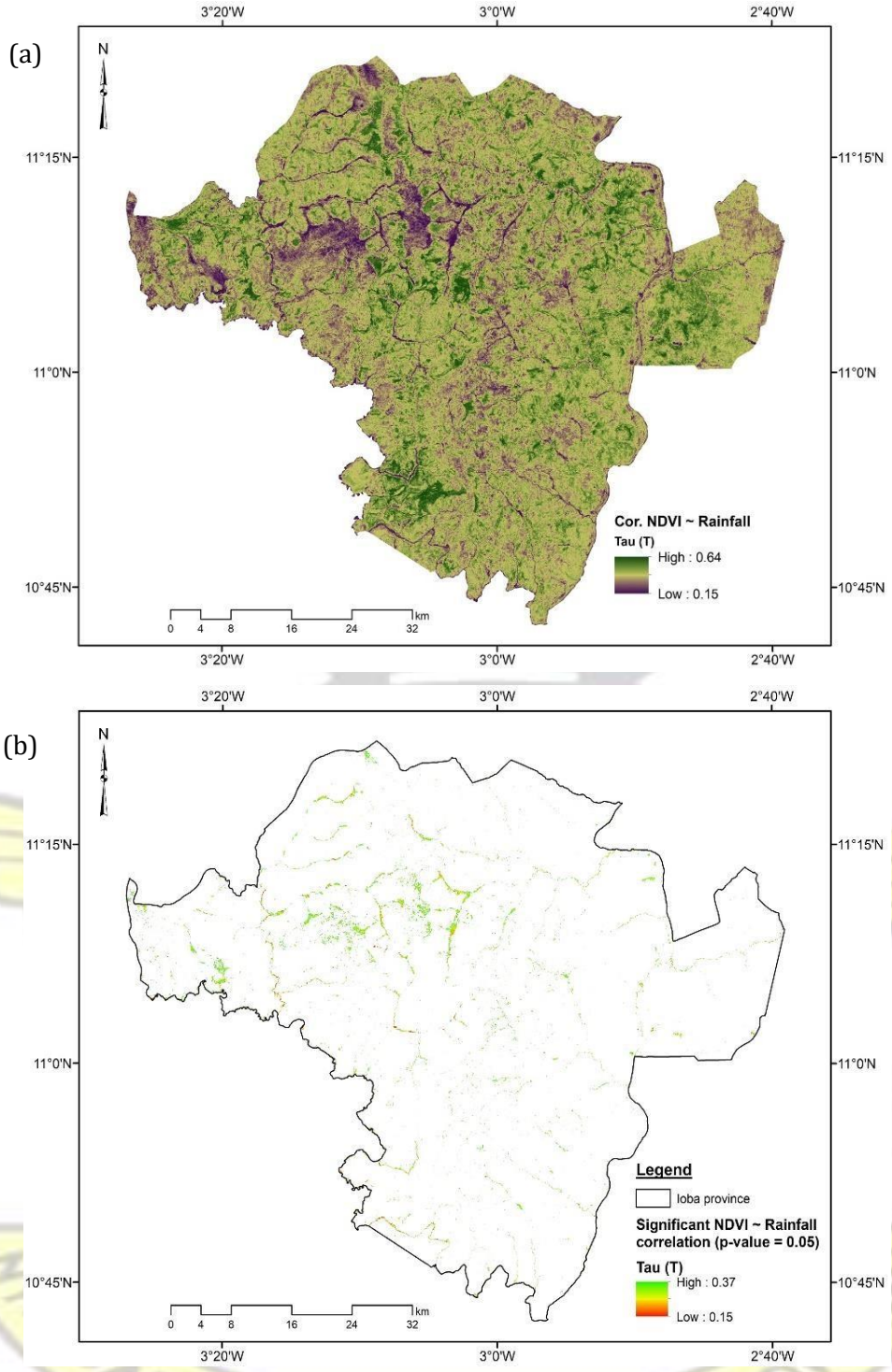

Figure 6-29: Relationship between NDVI and rainfall from 2004 to 2017; (a) Kendall's correlation coefficient (τ), (b) areas of significant correlation at 95% CI (α = 0.05)

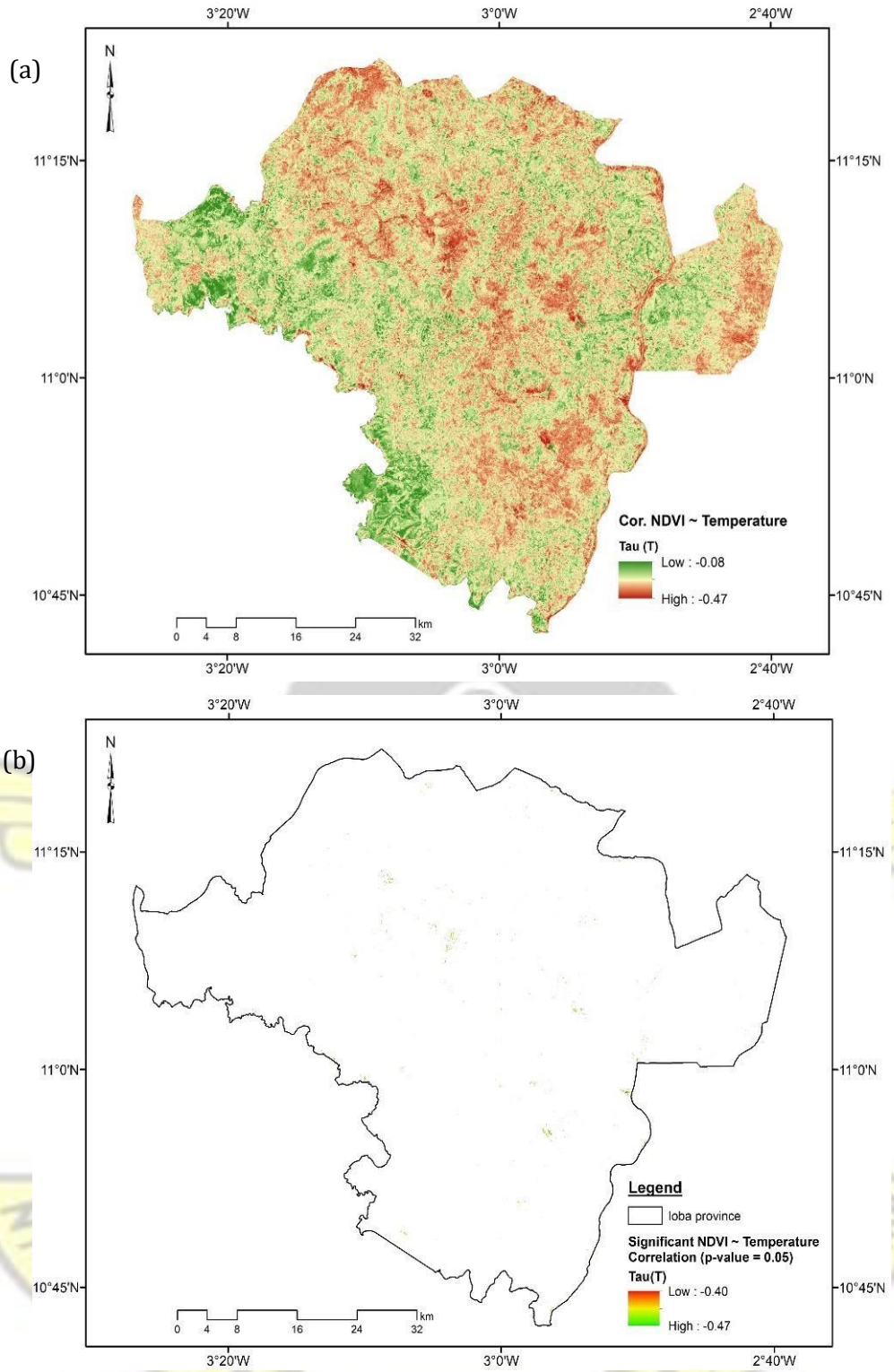

Figure 6-30: Relationship between NDVI and temperature from 2004 to 2017; (a) Kendall's correlation coefficient (τ), (b) areas of significant correlation at 95% CI (α = 0.05)

CHAPTER 7: DISCUSSION OF RESULTS

7.1 Introduction

This section discusses the results presented in chapter 6.0. The section is divided into three main sub-sections. Section 7.2 discusses the results obtained from the NDVI time series analysis for the Ioba province, ECA and NECA. It also discusses the comparison between the NDVI time series of ECA and NECA. The next sub-section (7.3) discusses results obtained from the extraction of crop height using UAV photographs for selected sites in areas with erosion control and areas without erosion control. The last sub-section (7.4) discusses the time series analysis of climate variables (rainfall and temperature). It also discusses the relationship that exist between the NDVI time series and the climate variables.

7.2 NDVI Trend Analysis

7.2.1 The whole Ioba province

From the result presented in section 6.1.1.1 the breakpoint occurred in June 2013. This date represents the start of Landsat 8 data in the time series. Therefore, this break in the time series can be associated with the difference in the NDVI values of Landsat 8 compared to that of Landsat 5 & 7. In a research to compare the difference between NDVI from Landsat 8 OLI and Landsat 7 ETM+ conducted by Li, Jiang and Feng (2014), Xu and Guo (2014) and Ke *et al.*, (2015), they found out that though there are differences in the NDVI values of Landsat 8 and Landsat 7 the magnitude is small and the two datasets have a high linear correlation coefficient (R^2 from 0.84 to 0.98). They also concluded that vegetated land cover types were found to have better NDVI agreement than non-vegetated land cover types. Based on the results from the characterization of the break in the trend and the works of the above researchers, the breakpoint was not considered for further analysis.

The vegetation trend in the study area may relate to different triggers either natural or anthropogenic, but since the study area is located in a semi-arid environment, vegetation greenness is strongly related to the seasonal rainfall cycle (Herrmann, Anyamba and Tucker, 2005). Therefore, changes in the rainfall trends, amount and distribution may have a huge impact on the NDVI values. Although there has been variability in the rainfall trends in the study area from 2004 to 2017, the overall NDVI trend still showed a significant positive increase with a value of $3.7x10^{-4}$ ΔNDVI/month at a p-value of 0.043. This may be attributed to the quick responds of vegetation to a moderate amount of rainfall in the area.

From the pixel-wise analysis, significant positive trends were mostly observed along water bodies, irrigated areas and afforestation areas. This is as a result of the continuous all year photosynthetic activities occurring in these areas as a result of the presence of soil moisture. Few areas of negative significant trends occurred along water bodies whiles most of them occurred on rainfed croplands and open vegetation. The negative trends in rainfed croplands can be associated with the variability of annual rainfall as a result of climate change. The 10.6% area of significant NDVI trend in the whole study area implies that almost 90% of the NDVI trend from 2004 to 2017 in the Ioba province is not statistically significant at 95% confidence interval. The low level of significant NDVI trends may be highly associated to human activities. For instance, since agriculture is the main occupation for rural dwellers, the high population in the rural areas has caused an expansion in agriculture resulting in the fast conversion of other land use/cover types to crop lands and encroachment on reserved forest (Ouattara, 2007).

Secondly, because of reduction in farm size, farmers do not allow trees to grow in their farm. From the field interviews, seeds dispersed by either water or wind are cleared immediately they sprout. This is done because too many trees will reduce their farm size and consequently their yield because for them yield is relative to farm size.

Also, the emergence of illegal small-scale mining in the area has led to the conversion of natural vegetation and crop land to bare surfaces and pools of water after rainfall. Soils excavated by the miners are left in heaps and pits dug are left uncovered even after mining.

7.2.2 Areas with Stone Bunds Erosion Control Measure

Generally, all the four sites in areas with stone bunds erosion control measure saw a significant positive trend in NDVI trend from 2004 to 2017 with slope values ranging 3.14×10^{-4} to 3.95×10^{-4} ΔNDVI/month. This indicates that the vegetation cover in these areas has improved within the period of the study. This improvement in vegetation may be as a result of the erosion intervention that has been implemented. Although, the mean NDVI trends for each of the sites gave a positive trend, the results from the pixel-based analysis shows that, positive, stable and negative NDVI trends were widespread in all the sites. overall, only about 23.15% of the total area under stone bunds erosion control showed significant trends in NDVI from 2004 to 2017.

7.2.3 Areas without Stone Bunds Erosion Control Measure

Similar to areas under stone bunds erosion control measure, the areas without stone bunds erosion control also recorded significant positive trends in NDVI from 2004 to 2017 with slope values from 3.83 x 10^{-4} to 3.91 x 10^{-4} ΔNDVI/month. Again, this is an indication of improved vegetation cover trends in the study area. This improvement in vegetation may be as a result of good farming practices and reduced vegetation cover in the area. The pixel-wise analysis also revealed a reasonable amount of negative and stable NDVI trends in some areas, although on the average, a positive trend was observed for all the four sites in areas without stone bunds erosion control. Overall, about 25.48% of the total area under areas without stone bunds erosion control showed significant trends in NDVI from 2004 to 2017.

7.2.4 Comparison between Areas with and without Stone Bunds Erosion Control

Although it is expected that areas under stone bunds erosion control measure should have a better and improved vegetation cover than areas without stone bunds erosion control, the results from the ANOVA test showed that, the absence of stone bunds erosion control measure in the Bankandi, Biengane, Bisserke and Wizini sites did not have any impact on the NDVI trends within the period of study. Areas without stone bunds erosion control had NDVI trends similar to that of areas (Badiere, Batiara, Dibogh and Namere) with stone bunds erosion control measure. During the field campaign, evidences of reduced soil erosion and re-germination of plants in areas which were seriously affected by erosion was eminent. Also, farmers whose farms have stone bunds erosion control also attested to improved crop growth and increased yield. Nonetheless, the results didn't show better NDVI trends in areas under stone bunds erosion control.

On the whole, the inability to differentiate between the NDVI trends of these two areas may be attributed to the fact that although erosion control using stone bunds is the widely practiced soil erosion control in the Ioba province, areas without stone bunds erosion control due to the peoples inability to afford the labour and cost of transporting stone (Zougmoré *et al.*, 2004) makes them look for other options to minimize soil erosion. During the field visits, areas without stone bunds erosion control were seen to have other measures such as mulching and earth mounds to minimize soil erosion. In this respect, though some areas do not have implemented stone bunds erosion control measures, they may not be totally unprotected from water induced soil erosion.

7.3 Comparison of Crop Heights between Areas with Stone Bunds and Areas without The results of the crop height extraction using UAV photos in section 6.2 revealed similar values of millet and cotton heights in areas with stone bunds and areas without stone bunds. This is evident in the height values obtained for each time step in Table 6-4. Also, in Figure 6-19 and 6-20, the trends of both millet and cotton in areas with and without stone bunds are similar.

Again, the inability to distinguish between the crop heights in areas with stone bunds erosion control and areas without may be attributed to fact that, during the field visits, farmers in areas without stone bunds look for other erosion control measures such as mulching and planting on earth mounds as remedial measure to minimize soil erosion by water. As a result, the crops which are not washed are able to survive and grow although some of the soil nutrients may have been lost to erosion.

7.4 Time Series Analysis of Climate Variable and their Relationship with NDVI

7.4.1 Rainfall Analysis

The results from the rainfall analysis in section 6.3.1 shows that there is a noticeable increase in the rainfall from 2004 to 2017, which is evident in the positive trend of 0.12 mm/month obtained. Although recent studies in west Africa suggest that the wet conditions of the 1950s and 1960s have not been re-established (Sanogo *et al.*, 2015). There has been some partial recovery in rainfall with a significant spatial and temporal variability after the decrease in rainfall in West Africa in the 1970s and 1980s which led to severe droughts, famines and many socio-economic problems (Nicholson, 2013). Several research conducted in the study area and West Africa as a whole has also reported increase in rainfall after the dry periods (1970s and 1980s) until now (Riede *et al.*, 2016). For example, a research conducted by Sanogo et al. (2015), suggested a positive linear rainfall trend between 1980 and 2010 at majority of climate stations in West Africa, which establishes the existence of rainfall recovery from the dry period of the 1980s.

Although, the magnitude of rainfall trend over the period depicts an increase in rainfall, the undulating nature of monthly and annual rainfall was evident. This is because the climate of West Africa is characterized by a sensitive monsoon system that is associated with marked natural precipitation variability (Knippertz *et al.*, 2015). It has also been established that interannual variability of rainfall is linked to changes in higher-level circulation features such as African Easterly Jet (AEJ) and the Tropical Easterly Jet (TEJ) over the continent and the

West African Westerly Jet (WAWJ) over the Atlantic (Nicholson, 2013). Secondly, the effect of climate change due to increase in anthropogenic greenhouse gases emissions (Roudier *et al.*, 2011), atmospheric dust and sand storm (Knippertz *et al.*, 2015), global climate shift and a weakening of the global monsoon circulation (Basistha, Arya and Goel, 2009) may be the probable causes of the variation in rainfall.

7.4.2 Temperature Analysis

The results of the analysis of temperature presented in section 6.3.2 indicates that, average monthly temperature gradually increases at a rate of 0.01°C/month over the period of study. It is also evident that the later part of the study period (2014-2017) recorded higher temperature than the rest of the period (2004-2013), which might indicate a shift to a warmer climate. This results agrees with many other research (Gbobaniyi *et al.*, 2014) and the IPCC (2013) report that show an increase in the mean temperature over the last 50 years in West Africa and the Sahel. Moreover, there is strong evidence of an anthropogenic signal in a continent-wide temperature increases in the 21st century and beyond if no mitigation measures are implemented (Coffel, Horton and Sherbinin, 2018). It is projected that the temperature rise is very likely to exceed the 1986–2005 baseline by between 3 and 6 °C across the region by the end of the 21st century (Riede *et al.*, 2016).

7.4.3 Correlation between NDVI and Climate Variables

7.4.3.1 Overall Correlation between NDVI and Climate Variables

The result from the monthly aggregation analysis in section 6.3.3.1 showed a significant positive correlation (Kendall's τ of 0.513, $p = 0.000$) between NDVI and rainfall. This suggest that the increase in rainfall could promote vegetation growth. This result is comparable to several others research conducted in West Africa (Li *et al.*, 2004) and global (Ichii, Kawabata and Yamaguchi, 2010; Liu *et al.*, 2015; Kundu *et al.*, 2018), which show a positive correlation between NDVI and rainfall. For example, the work by Traore et al. (2015), in neighboring Mali, found a positive correlation between NDVI and rainfall in a similar landscape. Similarly, a study conducted by Rishmawi et al. (2016) in the northern arid to sub-humid zones of subSaharan Africa observed a strong relationship between NDVI and rainfall in the arid and semiarid regions. In the study area, the major land use is agriculture (crop production). Crop production is mainly rainfed and normally occurs from May to October. Therefore, high

correlation values between NDVI and rainfall was achieved due to the influence of rainfall on crop production and natural vegetation growth. This is also in line with a similar study by Camberlin et al. (2007) in tropical Africa, which concluded that high correlation values (> 0.60) were distinctly found in semi-arid, open grassland and cropland areas. Again, in Figure 6-26 it can be observed that during periods of no rainfall, there were some relatively high values (about 0.44) of monthly NDVI. This is an indication of the presence of vegetation during the times of no rainfall. Due to the agro-forestry parkland system of farming in the area, there are substantial number of economic trees scattered around the whole area, although some of them shed their leaves during the dry season. Secondly, there are a lot of riverine vegetation and few areas of afforestation which still undertakes photosynthetic activities during periods of no rain because of the presence of soil moisture. Lastly, the relatively high values of NDVI can also be attributed to the presence of irrigation cropping (mostly vegetables) during the dry season. Because rainfall in the study area has a short period (within May to October) followed by long dry season (November to April), there are some irrigation dams purposely for dry season cultivation.

In the case of temperature, a significant negative correlation (Kendall's τ of -0.322, $p = 0.000$) between NDVI and temperature was obtained. This implies that an increase in temperature may reduce vegetation growth due to excessive heat and high rate of evapotranspiration. Although a certain amount of temperature is also needed for plant growth. The negative correlation between NDVI and temperature obtained in the study is comparable to a study conducted by Rishmawi et al. (2016) which reported a negative correlation between NDVI and temperature in the arid region of West Africa. It is also in line with a study by Liu et al. (2015) and also partially supported by (Piao *et al.*, 2014). They show that the relationship between global temperature variability and NDVI has weakened especially in the Humid Temperate and Dry Domain Regions. Although the NDVI correlation with temperature change is negative compared to the positive correlation between NDVI and rainfall, both climate variables are of similar significance in determining vegetation growth change (Liu *et al.*, 2015).

7.4.4 Pixel-wise Correlation between NDVI and Climate Variables

From the results in section 6.3.4 the positive correlation between NDVI and rainfall realized is because, the study area falls within a semi-arid area and as such the vegetation in the area responds to rainfall. This result agrees with that of Rishmawi et al. (2016) and Traore et al. (2015) as stated earlier. From figure 6-29a it can be observed that areas with low positive correlation are much more localized and are places which still have some vegetation during the

period of no rainfall (dry season). These places are mostly found around rivers/streams (riverine), wetlands and irrigated lands. Also, another land use type with low correlation is areas with closed canopy vegetation. Since the study area falls within the Sudanian savanna climatic zone the natural forest vegetation mostly has open canopy. In this sense, closed canopy vegetation is mostly found in areas which have gone through afforestation and are protected. The presence of substantial soil moisture in the top soil in these areas support vegetation growth even when there is no rainfall. For example, an afforestation area in the town of Ouessa and Dano and some areas along some major river banks (the Black Volta river) do have high NDVI in the dry season (see Figure 7-1). High positive correlations between NDVI and rainfall were widespread across the area occurring mostly in dry lands (rainfed croplands and natural vegetation) where rainfall is a limiting factor to vegetation growth.

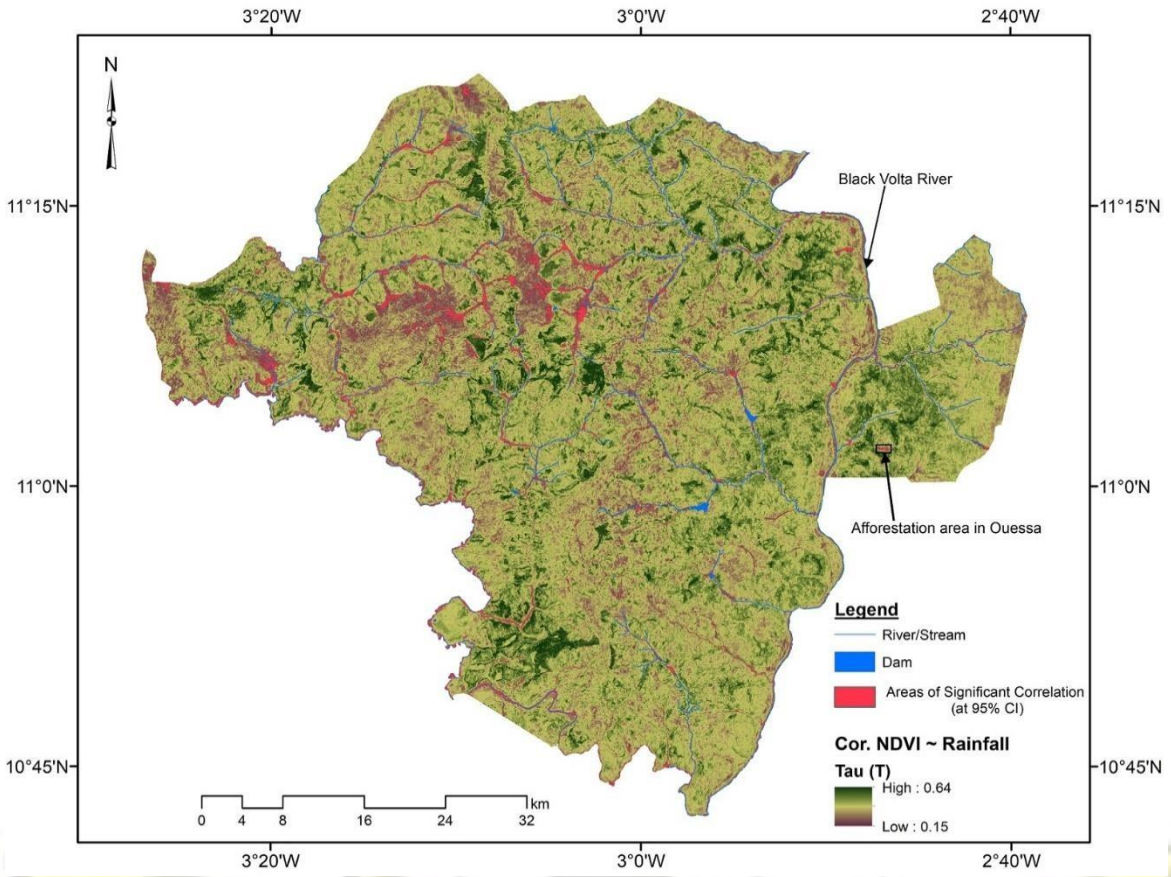

Figure 7-1: Analysis of NDVI and Rainfall correlation map

On the contrary, the results of the correlation between NDVI and temperature gave a negative trend throughout the study area with about 1% being statistically significant at 95% confidence interval (Figure 6-30). An increased in temperature trends in the study area may have caused a reduction in vegetation growth due to an increase in evapotranspiration. As stated earlier, the negative correlation between NDVI and temperature obtained in the study is comparable to other studies conducted by Rishmawi et al. (2016) in West Africa and Liu et al. (2015) and Piao et al., (2014) in other parts of the world.

CHAPTER 8: CONCLUSIONS AND RECOMMENDATIONS

8.1 Conclusions

Soil erosion has become a relevant worldwide issue due to its environmental and socioeconomic impacts. Currently, the impacts of soil erosion on sustainable agriculture and ecosystem services have become prominent in the light of rising concerns over climate change and food security. The implementation of organized and large-scale erosion control measures started in the early 1980's in West Africa as a response to a series of drought years, which had devastating consequences for the entire region in the 1970's. In West Africa, poor land use practices have exposed the vulnerability of many lands to erosion, most especially erosion by water. To minimize the impact of soil erosion by water in West Africa, several erosion control measures have been adopted and implemented. Although there are large scale implemented soil erosion controls, little has been done on evaluating the impact of these erosion controls on vegetation (crops and natural vegetation) improvement in West Africa using remote sensing data. In the quest to restore degraded lands by minimizing the effect of soil erosion, the use of remote sensing data more especially medium to high resolution data such as Landsat in evaluating and monitoring post implementation of erosion control on vegetation growth is vital in evaluating the recovery of degrading lands.

The evaluation of vegetation improvement after the implementation of erosion control measures in West Africa has been challenging due to several reasons. For example, the small scale and fragmented nature of implemented erosion control measures make it difficult to do a post implementation analysis using a medium to large spatial resolution satellite data. The use of high-resolution satellite data for such an analysis also has a huge cost implication. Again, optical satellite data availability is a big challenge in West Africa. The persistent cloud cover renders optical images which are capable for analyzing the vegetation improvements in these erosion control areas less appropriate for usage.

In line with the above, this research investigated the use of remote sensing data (Landsat NDVI data and UAV images) to analyze the effect of stone bunds erosion control measure on vegetation trend the Ioba Province of Burkina Faso. Landsat NDVI time series analysis was conducted for the whole study area to investigate the trend of vegetation from 2004 to 2017. Secondly, a comparative analysis was done to compare the vegetation trends of areas with stone bunds erosion control and areas without. The third objective also compared the crop heights extracted from UAV images for areas with and without stone bunds erosion control measure.

Finally, a correlation analysis was performed between climate variables (rainfall and temperature) and NDVI trends. Based on the above objectives, the following conclusions were made.

8.1.1 NDVI Time Series Analysis of Ioba Province

The NDVI time series of the Ioba province from 2004 to 2017 for vegetation trend was. Overall, the results produced a significant increasing trend in NDVI of about $3.7x10^{-4}$ ΔNDVI/month at 95% confidence interval over the period. This is an indication that overall the vegetation trend in the Ioba province has improved from 2004 to 2017. The pixel-wise analysis produced an NDVI trend values ranging from -0.001 to a maximum of 0.002 ΔNDVI/month. Stable to negative trends were widespread especially in the northern and the central parts of the study area. Positive trends were mostly found in irrigated areas, afforestation areas and along rivers/streams. This is as a result of the continuous all year photosynthetic activities occurring in these areas as a result of the presence of soil moisture. On the whole, areas of significant NDVI trends at 95% confidence interval were about 10.6% of the total land size (2,648 km^2). The low level of significant NDVI trends may be highly associated to human activities. The high number of missing data points in the time series could also be a factor. Although the missing data points were filled through interpolated, a better result may have been obtained if there were no missing data.

8.1.2 Comparison of NDVI Trends in Areas with and without Stone Bunds Erosion Control

A comparison between areas with and without stone bunds erosion control has been done. Generally, both areas with stone bunds erosion control and areas without stone bunds erosion control experienced a significant positive trend in NDVI from 2004 to 2017 with slope values ranging from $3.14 \times 10^{-4} - 3.95 \times 10^{-4}$ ΔNDVI/month and $3.83 \times 10^{-4} - 3.91 \times 10^{-4}$ ΔNDVI/month respectively. The results indicated that the overall the vegetation trends in these two areas have improved within the period of the study. Although, the mean NDVI trends for each of the two areas gave positive trends, the results of the pixel-wise analysis show that, positive, stable and negative NDVI trends were widespread in all the areas. Overall, about 23.15% of the total area under stone bunds erosion control showed significant trends in NDVI, whiles 25.48% of the total area without stone bunds erosion control showed significant trends of NDVI from 2004 to 2017. Comparing the NDVI trends of the two areas, the result from the

ANOVA test showed that there is no significant difference between the NDVI trends of areas with stone bunds erosion control and areas without stone bunds erosion control. The inability to differentiate between these two areas is because, though areas without stone bunds erosion control do not have implemented stone bunds erosion control measures, they are not totally unprotected from water induced soil erosion. This is because there were evidences of some other erosion control measures during the field visits.

8.1.3 Comparison between Crop Height in Areas with and without Stone Bunds Erosion Control

The extraction and comparison of crop heights in areas with stone bunds erosion control and areas without has been achieved. The results indicate that there is no significant difference between the crop heights in areas with and without stone bunds erosion control. A graph of the trends of cotton and millet in the two areas showed a similar trend. From the correlation test a high positive correlation (Kendall's τ) of 0.969 and 0.954 for cotton and millet respectively were observed between the trends of crop growth in these two areas. Finally, at 95% confidence interval, the t-test revealed that there is no significant difference between the means of the crop heights of cotton (mean of difference of 0.001) and millet (mean of difference of -0.005) in areas with stone bunds erosion control and areas without. The inability to distinguish between the crop heights in areas with stone bunds erosion control and areas without may be attributed to use of other erosion control measures by farmers in areas without stone bunds erosion control.

8.1.4 Trend of Climate Variables and their Relationship with NDVI Trend

In the analysis of rainfall pattern, the study found that, there was a noticeable positive increase in the monthly and annual rainfall patterns from 2004 to 2017 which was evident in the positive trend of 0.12mm/month and 13.80 mm/year obtained respectively. But a Mann-kendall test showed that both the monthly and annual trends of rainfall were not statistically significant at 95% confidence interval.

For temperature, the results suggest that, average monthly temperature gradually increases at a rate of 0.01°C/month with no breakpoints over the period of study. But this trend was not statistically significant at 95% confidence interval. Temperature anomaly was found to be different each year, and the fluctuation ranged between −0.7 and 0.8 °C with the obvious

negative anomalies occurring before 2013. Positive anomalies were consistent each year at the later part of the study period (from 2014 to 2017) which was an indication of a shift to a warmer climate.

The correlation between NDVI with climatic variables (rainfall and temperature) had been estimated. The correlation coefficients obtained describes the kind of relationships between NDVI and the climate variables. In terms of the correlation between NDVI and climate variables, the study showed that in general, there was a positive correlation between NDVI and rainfall in the study area from 2004 to 2017 with Kendall τ of 0.513 and a p-value of 0.000. This suggests that the increase in rainfall could promote vegetation growth. From the pixelwise analysis, it was observed that, NDVI and rainfall had a positive correlation across the whole study area producing a Kendall τ of 0.15 as the minimum to a maximum of 0.64 with a mean of 0.48. High positive correlations between NDVI and rainfall were widespread across the area occurring mostly in dry lands (rainfed croplands and natural vegetation) where rainfall is a limiting factor to vegetation growth. On the other hand, low positive correlations were found in riverine, wetlands and irrigated areas. The positive correlation between NDVI and rainfall realized can be attributed to the fact that the study area falls within a semi-arid area and as such the vegetation in the area responds to rainfall.

In the case of NDVI temperature correlation, a negative correlation ($\tau = -0.322$) was observed in the overall relationship. This implies that an increase in temperature may reduce vegetation growth due to excessive heat and high rate of evapotranspiration. From the pixel-wise analysis, NDVI correlates negatively to temperature throughout the study area. The correlation coefficients (τ) ranges from -0.08 to -0.47, with less than 1% being statistically significant at 95% confidence interval. Areas of high negative correlation was widespread compared to areas of low negative correlation.

8.2 Recommendations

8.2.1 Recommendations for Future Studies

(i) The major challenge of vegetation trend analysis in West Africa has been the availability of satellite data. Although the Landsat images are free of charge since 2008, its usability in West Africa has been hindered by excessive clouds and cloud shadow cover especially during the rainy season. As a result, to obtain a regular time series data for vegetation studies is almost impossible. With the launch of the Sentinel series of satellites through the Copernicus program in 2014, more optical data will be available for such studies. Although the problem of cloud cover will persist, combining satellite images from different sensors will help to bridge the problem of data availability for time series analysis. It is therefore recommended that future studies should look at combing data from different sensors rather than using mathematical models to impute missing time steps data in other to obtain a regular time series.

(ii) Secondly, although this study did not find any significant difference between the NDVI trend of areas with stone bunds erosion control and areas without stone bunds erosion control, evidence of re-germination of plants and improved crop growth and yield were eminent in areas with stone bunds erosion control. It is therefore recommended that future studies should use high resolution image in other to capture the little details that is happening in areas with stone bunds erosion control.

(iii) Again, from the field visits it was observed that farmers in areas without stone bunds look for other erosion control measures such as mulching and planting on earth mounds as remedial measure to minimize soil erosion by water. Future studies should consider setting up experimental sites for areas with and without stone bunds erosion control. In this case, it can be ensured that areas without stone bunds erosion control will not have other erosion control measures.

(iv) Although this study found a positive trend in the rainfall pattern and a negative trend of temperature, further researches are recommended in the future since these climate variables can change in the near future due to climate change. In addition, this study was based on a 14-year data due to data availability. It is therefore recommended that future studies should consider a longer period of data.

(v) Lastly, since the farming system in the study area and surrounding areas is agro-forestry parkland, the presence of the trees on crop lands do have a great impact on the NDVI of the area. In view of this, the use of high-resolution images is vital so that where the focus is on only crops, the trees in the cropland can be excluded from the analysis.

8.2.2 Recommendations for Policy

This study was conducted under the West African Science Service Center on Climate Change and Adapted Land use (WASCAL) program which is aimed among other to strengthen the research infrastructure and capacity in West Africa to tackle the issues of climate change. In line with the WASCAL agenda, the following recommendations have been made for policy and institutional action.

(i) In the quest to minimize erosion by water, several erosion control measures are being implemented in West Africa. It is therefore recommended that governments and NGOs should not only provide funds for the implementation but also fund post implementation assessment to ascertain whether or not the erosion control measures are yielding the needed results. For fast, efficient, large coverage and less expensive approach, the use of remote sensing data is highly recommended, because, this research has demonstrated the possibility of using remote sensing data for such assessment.

(ii) It is also recommended that data such as climate and topographic data should be made available and free of charge for such studies. Often at times, researchers and students will have to pay huge sums of money to obtain climate data. This hinders proper and accurate research because most of them may not be able to afford.

(iii) Finally, although governments and NGOs are putting in efforts to minimize the effects of climate change through soil erosion prevention, more efforts through funding and technical support are needed as there are still a lot of areas in South-west Burkina Faso that suffer severe soil erosion. Since a lot of the farmers are peasant farmers, they cannot afford the cost involved in putting up erosion interventions such as stone bunds. Also, education of the local farmers on the proper way of putting up these erosion interventions is vital.

REFERENCES

Adimassu, Z., Mekonnen, K., Yirga, C. and Kessler, A. (2014) 'Effect of soil bunds on runoff, soil and nutrient losses, and crop yield in the central highlands of Ethiopia', Land Degradation and Development, 25, pp. 554–564. doi: 10.1002/ldr.2182.

Agisoft (2018) ‘Agisoft PhotoScan User Manual Professional Edition’. Agisoft LLC. Available at: https://www.agisoft.com/pdf/photoscan-pro_1_4_en.pdf.

Akinsanola, A. A. and Ogunjobi, K. O. (2015) ‘Recent homogeneity analysis and long-term spatio-temporal rainfall trends in Nigeria’, Theoretical and Applied Climatology. doi: 10.1007/s00704-015-1701-x.

Aksoy, E., Özsoy, G. and Dirim, M. S. (2009) ‘Soil mapping approach in GIS using Landsat satellite imagery and DEM data’, African Journal of Agricultural Research, 4(11), pp. 1295–1302. Available at: http://www.academicjournals.org/AJAR.

Amri, R., Zribi, M., Lili-Chabaane, Z., Duchemin, B., Gruhier, C. and Chehbouni, A. (2011) ‘Analysis of Vegetation Behavior in a North African Semi-Arid Region, Using Spotvegetation Ndvi Data’, Remote Sensing, 3, pp. 2568–2590. doi: 10.3390/rs3122568.

Arhin, E., Zango, S. M. and Ruerrger, K. R. (2015) ‘Laterite Sampling Preparation for Gold Exploration Survey At Western Burkina Faso, Northern Extension of the Lawra Belt’, International Journal of Geography and Geology, 4(1), pp. 1–10.

Arnold, J. G., Srinivasan, R., Muttiah, R. S. and Williams, J. R. (1998) ‘Large area hydrologic modeling and assessment. Part I: model development’, Journal of the American Water Resources Association, 34(1), pp. 73–89.

Azabdaftari, A. and Sunar, F. (2016) ‘Soil Salinity Mapping Using Multitemporal Landsat Data’, The International Archives of the Photogrammetry, Remote Sensing and Spatial Information Sciences, XLI-B7. doi: 10.5194/isprsarchives-XLI-B7-3-2016.

Basistha, A., Arya, D. S. and Goel, N. K. (2009) ‘Analysis of historical changes in rainfall in the Indian Himalayas’, International Journal of Climatology, 29, pp. 555–572. doi: 10.1002/joc.

Bayala, J., Sileshi, G. W., Coe, R., Kalinganire, A., Tchoundjeu, Z., Sinclair, F. and Garrity, D. (2012) ‘Cereal yield response to conservation agriculture practices in drylands of West Africa: A quantitative synthesis’, Journal of Arid Environments, 78, pp. 13–25.

Begue, A., Vintrou, E., Saad, A. and Hiernaux, P. (2014) ‘Differences between cropland and rangeland MODIS phenology (start-of- season) in Mali International Journal of Applied Earth Observation and Geoinformation Differences between cropland and rangeland MODIS phenology (start-of-season) in Mali’, International Journal of Applied Earth Observations and Geoinformation. Elsevier B.V., 31(September), pp. 167–170. doi: 10.1016/j.jag.2014.03.024.

Bhandari, A. K., Kumar, A. and Singh, G. K. (2012) ‘Feature Extraction using Normalized Difference Vegetation Index (NDVI): a Case Study of Jabalpur City’, Procedia Technology, 6, pp. 612–621. doi: 10.1016/j.protcy.2012.10.074.

Bhatti, S. S. and Tripathi, N. K. (2014) ‘Built-up area extraction using Landsat 8 OLI imagery’, GIScience & Remote Sensing, 51(4), pp. 445–467. doi: 10.1080/15481603.2014.939539.

Birtwistle, A. N., Laituri, M., Bledsoe, B. and Friedman, J. M. (2016) ‘Using NDVI to measure precipitation in semi-arid landscapes’, Journal of Arid Environments. Elsevier Ltd, 131, pp. 15–24. doi: 10.1016/j.jaridenv.2016.04.004.

Biswas, B., Dhaliwal, L. K., Singh, S. O. M. P. A. L. and Sandhu, S. K. (2014) 'Forecasting wheat production using ARIMA model in Punjab', International Journal of Agricultural Sciences, 10(1), pp. 158–161.

Blackburn, G. A. (1998) 'Quantifying Chlorophylls and Caroteniods at Leaf and Canopy Scales : An Evaluation of Some Hyperspectral Approaches', Remote Sensing Environment, 66, pp. 273–285.

Blinkov, I., Kostadinov, S. and Marinov, I. T. (2013) 'Comparison of erosion and erosion control works in Macedonia, Serbia and Bulgaria', International soil and water conservation research, 1(3), pp. 15–28. doi: 10.1016/S2095-6339(15)30027-7.

Bobe, B. W. (2004) Evaluation of soil erosion in the Harerge region of Ethiopia using soil loss models, rainfall simulation and field trials. University of Pretoria.

Boegh, E., Soegaard, H., Broge, N., Hasager, C. B., Jensen, N. O., Schelde, K. and Thomsen, A. (2002) 'Airborne multispectral data for quantifying leaf area index , nitrogen concentration , and photosynthetic efficiency in agriculture', Remote Sensing of Environment, 81, pp. 179–193.

Boix-fayos, C., Vente, J. De and Albaladejo, J. (2009) 'Agriculture , Ecosystems and Environment Soil carbon erosion and stock as affected by land use changes at the catchment scale in Mediterranean ecosystems', Agriculture, Ecosystems and Environment, 133, pp. 75–85. doi: 10.1016/j.agee.2009.05.013.

Bouma, J. and Batjes, N. H. (2000) 'Trends of World-Wide Soil Degradation', Hohenheimer Umwelttagung, 32, pp. 33–44. Available at: http://www.isric.org/isric/webdocs/docs/HohenheimerUmwelttagung_2000v32_P3344.pdf.

Bridges, E. M. and Oldeman, L. R. (1999) 'Global assessment of human-induced soil degradation', Arid Soil Research and Rehabilitation, 13, pp. 319–325.

Bullock, P. (2005) 'Climate change impacts', in Hillel, D. (ed.) Encyclopedia of Soils in the Environment. Elsevier, pp. 254–262. doi: 10.1016/B0-12-348530-4/00089-8.

Butt, C. R. M. and Bristow, A. P. J. (2013) 'Relief inversion in the geomorphological evolution of sub-Saharan West Africa', Geomorphology. Elsevier B.V., 185, pp. 16–26. doi: 10.1016/j.geomorph.2012.11.024.

Callo-Concha, D., Gaiser, T. and Ewert, F. (2012) Farming and cropping systems in the West African Sudanian Savanna. 100. Bonn. Available at: http://hdl.handle.net/10419/88290.

Camberlin, P., Martiny, N., Philippon, N. and Richard, Y. (2007) 'Determinants of the interannual relationships between remote sensed photosynthetic activity and rainfall in tropical Africa', Remote Sensing of Environment, 106, pp. 199–216. doi: 10.1016/j.rse.2006.08.009.

Candiago, S., Remondino, F., Giglio, M. De, Dubbini, M. and Gattelli, M. (2015) 'Evaluating Multispectral Images and Vegetation Indices for Precision Farming Applications from UAV Images', Remote Sensing, 7, pp. 4026–4047. doi: 10.3390/rs70404026.

Cao, R., Chen, Y., Shen, M., Chen, J., Zhou, J., Wang, C. and Yang, W. (2018) 'A simple method to improve the quality of NDVI time-series data by integrating spatiotemporal

information with the Savitzky-Golay fi lter', Remote Sensing of Environment. Elsevier, 217, pp. 244–257. doi: 10.1016/j.rse.2018.08.022.

Carvalho, D. F. De, Durigon, V. L., Antunes, M. A. H., de Almeida, W. S. and de Oliveira, P. T. S. (2014) 'Predicting soil erosion using Rusle and NDVI time series from TM Landsat 5', Pesquisa Agropecuaria Brasileira, 49(3), pp. 215–224. doi: 10.1590/S0100204X2014000300008.

Chen, B., Liu, X., Zhao, H. and Principe, J. C. (2017) 'Maximum correntropy Kalman filter', Automatica. Elsevier Ltd, 76, pp. 70–77. doi: 10.1016/j.automatica.2016.10.004.

Chen, J., Zhu, X., Vogelmann, J. E., Gao, F. and Jin, S. (2011) 'A simple and effective method for filling gaps in Landsat ETM + SLC-off images', Remote Sensing of Environment. Elsevier B.V., 115(4), pp. 1053–1064. doi: 10.1016/j.rse.2010.12.010.

Chen, M. and Cihlar, J. (1996) 'Retrieving Leaf Area Index of Boreal Conifer Forests Using Landsat TM Images', Remote Sensing Environment, 55, pp. 153–162.

Chen, T. and Du, B. (2014) 'Regional soil erosion risk mapping using RUSLE , GIS , and remote sensing : A case study in Miyun Watershed , North China', Environmental Earth Sciences. doi: 10.1007/s12665-010-0715-z.

Chirwa, P. W. and Mahamane, L. (2017) 'Overview of restoration and management practices in the degraded landscapes of the Sahelian and dryland forests and woodlands of East and southern Africa', Southern Forests: a Journal of Forest Science. doi: 10.2989/20702620.2016.1255419.

Choi, J., Choi, Y., Lim, K. and Shin, Y. (2005) 'Soil erosion measurement and control techniques', in Chung, N., Kim, W., Kim, H., Kim, J., Eom, K., and Lee, I. (eds) InternationalWorkshop on Newly Developed Innovative Technology for Soil and Water Conservation. Rural Development Administration., pp. 1–12. Available at: http://www.fftc.agnet.org/htmlarea_file/library/20110808174828/eb568.pdf.

Cilek, A., Berberoglu, S., Kirkby, M., Irvine, B., Donmez, C. and Erdogan, M. A. (2015) 'Erosion Modelling In A Mediterranean Subcatchment Under Climate Change Scenarios Using Pan-European Soil Erosion Risk Assessment (PESERA)', XL, pp. 11–15. doi: 10.5194/isprsarchives-XL-7-W3-359-2015.

Cleveland, R. B., Cleveland, W. S., McRae, J. E. and Terpenning, I. (1990) 'STL: A SeasonalTrend Decomposition Procedure Based on Loess', Journal of Official Statistics, 6(1), pp. 3–73. Available at: http://www.nniiem.ru/file/news/2016/stl-statistical-model.pdf.

Coffel, E. D., Horton, R. M. and Sherbinin, A. De (2018) 'Temperature and humidity based projections of a rapid rise in global heat stress exposure during the 21st century', Environmental Research Letters, 13. doi: 10.1088/1748-9326/aaa00e.

Coppin, P., Jonckheere, I., Nackaerts, K., Muys, B. and Lambin, E. (2004) 'Digital change detection methods in ecosystem monitoring : a review', International Journal of Remote Sensing, 25(9), pp. 1565–1596. doi: 10.1080/0143116031000101675. Dang, Y., Ren, W., Tao, B., Chen, G., Lu, C., Yang, J., Pan, S., Wang, G., Li, S. and Tian, H.

(2014) 'Climate and land use controls on soil organic carbon in the Loess Plateau region of China', PLoS ONE, 9(5), p. e95548. doi: 10.1371/journal.pone.0095548.

DJI (2016) 'Phantom 4 Pro/Pro+ User Manual V1.0'. Available at: http://www.dji.com/product/phantom-4pro/info#video%0Ahttp://www.dji.com/phantom-4-pro/info#downloads.

DJI (2017) 'DJI Ground Station Pro', pp. 5–6. Available at: https://dl.djicdn.com/downloads/groundstation_pro/20171121/GS_Pro_User_Manual_EN_V2.0.pdf.

Dotterweich, M. (2013a) 'The history of human-induced soil erosion: Geomorphic legacies, early descriptions and research, and the development of soil conservation—A global synopsis', Geomorphology, 201, pp. 1–34. doi: https://doi.org/10.1016/j.geomorph.2013.07.021.

Dotterweich, M. (2013b) 'The history of human-induced soil erosion: Geomorphic legacies, early descriptions and research, and the development of soil conservation—A global synopsis', Geomorphology, 201, pp. 1–34. doi: https://doi.org/10.1016/j.geomorph.2013.07.021.

Eckert, S., Hüsler, F., Liniger, H. and Hodel, E. (2015) 'Trend analysis of MODIS NDVI time series for detecting land degradation and regeneration in Mongolia', Journal of Arid Environments. Elsevier Ltd, 113, pp. 16–28. doi: 10.1016/j.jaridenv.2014.09.001.

Esch, T., Himmler, V., Schorcht, G., Thiel, M., Wehrmann, T., Bachofer, F., Conrad, C., Schmidt, M. and Dech, S. (2009) 'Large-area assessment of impervious surface based on integrated analysis of single-date Landsat-7 images and geospatial vector data', Remote Sensing of Environment, 113, pp. 1678–1690. doi: 10.1016/j.rse.2009.03.012.

Ewen, J., Parkin, G. and O'Connell, P. E. (2000) 'SHETRAN: Distributed river basin flow and transport modeling system', Journal of hydrology and Engineering, 5, pp. 250–258.

Farhan, Y., Zregat, D. and Farhan, I. (2013) 'Spatial Estimation of Soil Erosion Risk Using RUSLE Approach, RS, and GIS Techniques: A Case Study of Kufranja Watershed, Northern Jordan', Journal of Water Resource and Protection, 5, pp. 1247–1261. doi: http://dx.doi.org/10.4236/jwarp.2013.512134.

Feng, M., Huang, C., Channan, S., Vermote, E. F., Masek, J. G. and Townshend, J. R. (2012) 'Quality assessment of Landsat surface reflectance products using MODIS data', Computers and Geosciences, 38(1), pp. 9–22. doi: 10.1016/j.cageo.2011.04.011.

Fensholt, R., Rasmussen, K., Theis, T. and Mbow, C. (2009) 'Evaluation of earth observation based long term vegetation trends — Intercomparing NDVI time series trend analysis consistency of Sahel from AVHRR GIMMS , Terra MODIS and SPOT VGT data', Remote Sensing of Environment. Elsevier Inc., 113(9), pp. 1886–1898. doi: 10.1016/j.rse.2009.04.004.

Fernández-Manso, A., Quintano, C. and Fernández-Manso, O. (2011) 'Forecast of NDVI in coniferous areas using temporal ARIMA analysis and climatic data at a regional scale', International Journal of Remote Sensing, 32(6), pp. 1595–1617. doi: 10.1080/01431160903586765.

Fernández, C. and Vega, J. A. (2016) 'Evaluation of RUSLE and PESERA models for predicting soil erosion losses in the first year after wildfire in NW Spain', Geoderma, 273. doi: 10.1016/j.geoderma.2016.03.016.

Fink, A. H., Vincent, D. G. and Ermert, V. (2006) 'Rainfall Types in the West African Sudanian Zone during the Summer Monsoon 2002', Monthly Weather Reviews, 134, pp. 2143– 2164. doi: doi.org/10.1175/MWR3182.1.

Foga, S., Scaramuzza, P. L., Guo, S., Zhu, Z., Dilley, R. D., Beckmann, T., Schmidt, G. L., Dwyer, J. L., Joseph Hughes, M. and Laue, B. (2017) 'Cloud detection algorithm comparison and validation for operational Landsat data products', Remote Sensing of Environment. Elsevier Inc., 194, pp. 379–390. doi: 10.1016/j.rse.2017.03.026.

Forkel, M., Carvalhais, N., Verbesselt, J., Mahecha, M. D., Neigh, C. S. R. and Reichstein, M. (2013) 'Trend Change detection in NDVI time series: Effects of inter-annual variability and methodology', Remote Sensing, 5(5), pp. 2113–2144. doi: 10.3390/rs5052113.

Forkuor, G. (2014) Agricultural Land Use Mapping in West Africa Using Multi-sensor Satellite Imagery. University of Wuerzburg. Available at: http://opus.bibliothek.uniwuerzburg.de/frontdoor/index/ index/docId/10868.

Forkuor, G., Thiel, M., Zoungrana, J.-B. and Dimobe, K. (2017) 'Overview of Key Satellite Missions', in Capacity Building Workshop – 22-24 August 2017. Ouagadougou, Burkina Faso.

Foth, H. D. (1990) Fundamentals of Soil Science. 8th ed. JOHN WILEY & SONS.

Frantz, D., Haß, E., Uhl, A., Stoffels, J. and Hill, J. (2018) 'Improvement of the Fmask algorithm for Sentinel-2 images: Separating clouds from bright surfaces based on parallax effects', Remote Sensing of Environment, 215(April 2017), pp. 471–481. doi: 10.1016/j.rse.2018.04.046.

Fraser, R. H., Olthof, I., Kokelj, S. V., Lantz, T. C., Lacelle, D., Brooker, A., Wolfe, S. and Schwarz, S. (2014) 'Detecting Landscape Changes in High Latitude Environments Using Landsat Trend Analysis: 1. Visualization', Remote Sensing, 6, pp. 11533–11557. doi: 10.3390/rs61111533.

Fu, S., Liu, B., Liu, H. and Xu, L. (2011) 'The effect of slope on interrill erosion at short slopes', Catena, 84, pp. 29–34. doi: 10.1016/j.catena.2010.08.013.

Gago, J., Douthe, C., Coopman, R. E., Gallego, P. P., Ribas-carbo, M., Flexas, J., Escalona, J. and Medrano, H. (2015) 'UAVs challenge to assess water stress for sustainable agriculture', Agricultural Water Management. Elsevier B.V., 153, pp. 9–19. doi: 10.1016/j.agwat.2015.01.020.

Ganasri, B. P. and Ramesh, H. (2016) 'Assessment of soil erosion by RUSLE model using remote sensing and GIS - A case study of Nethravathi Basin', Geoscience Frontiers, 7(6), pp. 953–961. doi: 10.1016/j.gsf.2015.10.007.

Gbobaniyi, E., Sarr, A., Sylla, B., Diallo, I., Kamga, A., Browne, A., Dosio, A., Dhi, A., Hewitson, B. and Lamptey, B. (2014) 'Climatology , annual cycle and interannual variability of precipitation and temperature in CORDEX simulations over West Africa', 2257(October 2013), pp. 2241–2257. doi: 10.1002/joc.3834.

Gebremichael, D., Nyssen, J., Poesen, J., Deckers, J., Haile, M., Govers, G. and Moeyersons, J. (2005) 'Effectiveness of stone bunds in controlling soil erosion on cropland in the Tigray Highlands, northern Ethiopia', Soil Use and Management, 21, pp. 287–297. doi:

10.1079/SUM2005321. Gobin, A., Jones, R., Kirkby, M., Campling, P., Govers, G., Kosmas, C. and Gentile, A. R.

(2004a) 'Indicators for pan-European assessment and monitoring of soil erosion by water', 7, pp. 25–38. doi: 10.1016/j.envsci.2003.09.004.

Gobin, A., Jones, R., Kirkby, M., Campling, P., Govers, G., Kosmas, C. and Gentile, A. R. (2004b) 'Indicators for pan-European assessment and monitoring of soil erosion by water', Environmental Science & Policy, 7, pp. 25–38. doi: 10.1016/j.envsci.2003.09.004.

Golosov, V. and Belyaev, V. (2013) 'The history and assessment of effectiveness of soil erosion control measures deployed in Russia', International soil and water conservation research. Elsevier Masson SAS, 1(2), pp. 26–35. doi: 10.1016/S2095-6339(15)30037-X.

Gómez, C., White, J. C. and Wulder, M. A. (2016) 'Optical remotely sensed time series data for land cover classification : A review', ISPRS Journal of Photogrammetry and Remote Sensing, 116, pp. 55–72. doi: 10.1016/j.isprsjprs.2016.03.008.

Gomiero, T. (2016) 'Soil Degradation , Land Scarcity and Food Security : Reviewing a Complex Challenge', Sustainability, 8, p. 281. doi: 10.3390/su8030281.

Haala, N. and Walter, V. (1999) 'Automatic classification of urban environments for database revision using lidar and color aerial imagery', International Archives of Photogrammetry and Remote Sensing, 32(7), pp. 3–4.

Hackney, C. and Clayton, A. I. (2015) 'Unmanned Aerial Vehicles (UAVs) and their application in geomorphic mapping', Geomorphological Techniques, 7, pp. 1–12. Available at: http://www.geomorphology.org.uk/sites/default/files/geom_tech_chapters/2.1.7_UAV.pdf.

Hamuda, E., Ginley, B. M., Glavin, M. and Jones, E. (2018) 'Improved image processingbased crop detection using Kalman filtering and the Hungarian algorithm', Computers and Electronics in Agriculture. Elsevier, 148, pp. 37–44. doi: 10.1016/j.compag.2018.02.027.

Han, P., Xin, P., Yu, S. and Zhu, D. H. (2010) 'Drought forecasting based on the remote sensing data using ARIMA models', Mathematical and Computer Modelling. Elsevier Ltd, 51(11–12), pp. 1398–1403. doi: 10.1016/j.mcm.2009.10.031.

Hardin, P. J., Lulla, V., Jensen, R. R. and Jensen, J. R. (2018) 'Small Unmanned Aerial Systems (sUAS) for environmental remote sensing : challenges and opportunities revisited', GIScience & Remote Sensing. Taylor & Francis, pp. 1–14. doi: 10.1080/15481603.2018.1510088.

Hellweger, F. L., Schlosser, P., Lall, U. and Weissel, J. K. (2004) 'Use of satellite imagery for water quality studies in New York Harbor', Estuarine, Coastal and Shelf Science, 61, pp. 437–448. doi: 10.1016/j.ecss.2004.06.019.

Herrmann, S. M., Anyamba, A. and Tucker, C. J. (2005) 'Recent trends in vegetation dynamics in the African Sahel and their relationship to climate', Global Environmental Change, 15, pp. 394–404. doi: 10.1016/j.gloenvcha.2005.08.004.

Herwitz, S. R., Johnson, L. F., Dunagan, S. E., Higgins, R. G., Sullivan, D. V., Zheng, J., Lobitz, B. M., Leunge, J. G., Gallmeyer, B. A., Aoyagi, M., Slye, R. E. and Brass, J. . (2004) 'Imaging from an unmanned aerial vehicle: agricultural surveillance and decision support', Computers and Electronics in Agriculture, 44(1), pp. 49–61. doi: 10.1016/j.compag.2004.02.006.

Hickler, T., Eklundh, L., Seaquist, J. W., Smith, B., Ardo, J., Olsson, L., Sykes, M. T. and Sjo, M. (2005) 'Precipitation controls Sahel greening trend', Geophysical Research Letters, 32(L21415). doi: 10.1029/2005GL024370.

Higginbottom, T. P. and Symeonakis, E. (2014) 'Assessing Land Degradation and Desertification Using Vegetation Index Data: Current Frameworks and Future Directions', Remote Sensing, 6, pp. 9552–9575. doi: 10.3390/rs6109552.

Hipt, O. D. F., Diekkrüger, B., Steup, G., Yira, Y., Hoffmann, T. and Rode, M. (2017) 'Applying SHETRAN in a Tropical West African Catchment (Dano, Burkina Faso)—Calibration, Validation, Uncertainty Assessment', Water, 9, p. 101. doi: 10.3390/w9020101.

Hird, J. N., Montaghi, A., Mcdermid, G. J., Kariyeva, J., Moorman, B. J., Nielsen, S. E. and Mcintosh, A. C. S. (2017) 'Use of Unmanned Aerial Vehicles for Monitoring Recovery of Forest Vegetation on Petroleum Well Sites', Remote Sensing, 9, p. 413. doi: 10.3390/rs9050413.

Hostert, P., Griffiths, P., Linden, S. van der and Pflugmache, D. (2015) 'Time Series Analyses in a New Era of Optical Satellite Data', in Kuenzer, C., Dech, S., and Wagner, W. (eds) Remote Sensing and Digital Image Processing. 22nd edn. Springer International Publishing Switzerland, pp. 25–42. doi: 10.1007/978-3-319-15967-6_2.

Hu, T., Yang, J., Li, X. and Gong, P. (2016) 'Mapping Urban Land Use by Using Landsat Images and Open Social Data', Remote Sensing, 8, p. 151. doi: 10.3390/rs8020151.

Hyndman, R. J. and Khandakar, Y. (2008) 'Automatic time series forecasting: The forecast package for R', Journal of Statistical Software, 26(3).

Ibrahim, Y. Z., Balzter, H., Kaduk, J. and Tucker, C. J. (2015) 'Land degradation assessment using residual trend analysis of GIMMS NDVI3g, soil moisture and rainfall in SubSaharan West Africa from 1982 to 2012', Remote Sensing. doi: 10.3390/rs70505471.

Ichii, K., Kawabata, A. and Yamaguchi, Y. (2010) 'Global correlation analysis for NDVI and climatic variables and NDVI trends : 1982-1990', 1161. doi: 10.1080/01431160110119416.

International Union of Soil Sciences(IUSS) working group (2006) World Reference Base for Soil Resources 2006. 2nd ed. Rome, Italy. Available at: http://www.fao.org/3/aa0510e.pdf.
IPCC (2000) 'Land Use, Land Use Change and Forestry'. Cambridge University Press, U.K. (IPCC special report).

IPCC (2001) Climate Change 2001: Synthesis Report. Contribution of Working Groups I, II, and III to the Third Assessment Report of the Intergovernmental Panel on Climate Change. Edited by R. T. Watson. Cambridge, UK: Cambridge Univ. Press.

Jain, E. G. and Mallick, B. (2017) 'A Study of Time Series Models ARIMA and ETS', International Journal of Modern Education and Computer Science, 4, pp. 57–63. doi: 10.5815/ijmecs.2017.04.07.

Jensen, J. R. and Im, J. (2007) 'Remote Sensing Change Detection in Urban Environments', in Jensen, R. R., Gatrell, J. D., and McLean, D. (eds) Geo-Spatial Technologies in Urban Environments. Berlin: Springer. doi: doi.org/10.1007/978-3-540-69417-5_2.

de Jong, R., Verbesselt, J., Schaepman, M. E. and de Bruin, S. (2012) 'Trend changes in global greening and browning: Contribution of short-term trends to longer-term change', Global Change Biology, 18(2), pp. 642–655. doi: 10.1111/j.1365-2486.2011.02578.x.

Ju, J. and Masek, J. G. (2016) 'The vegetation greenness trend in Canada and US Alaska from 1984 – 2012 Landsat data', Remote Sensing of Environment. Elsevier Inc., 176, pp. 1–16. doi: 10.1016/j.rse.2016.01.001.

Ju, J., Roy, D. P., Vermote, E., Masek, J. and Kovalskyy, V. (2012) 'Remote Sensing of Environment Continental-scale validation of MODIS-based and LEDAPS Landsat ETM + atmospheric correction methods', Remote Sensing of Environment. Elsevier Inc., 122, pp. 175–184. doi: 10.1016/j.rse.2011.12.025.

Kassam, A., Kueneman, E., Kebe, B., Ouedraogo, S. and Youdeowei, A. (2009) Enhancing crop-livestock systems in conservation agriculture for sustainable production intensification: a farmer discovery process going to scale in Burkina Faso. Rome, Italy. Available at: https://www.cabdirect.org/cabdirect/abstract/20103241700.

Kaufman, Y. J., Wald, A. E., Remer, L. A., Gao, B. C., Li, R. R. and Flynn, L. (1997) 'The MODIS 2.1-μm channel - correlation with visible reflectance for use in remote sensing of aerosol', IEEE Transactions on Geoscience and Remote Sensing, 35(5), pp. 1286–1298. doi: 10.1109/36.628795.

Ke, Y., Im, J., Lee, J., Gong, H. and Ryu, Y. (2015) 'Characteristics of Landsat 8 OLI-derived NDVI by comparison with multiple satellite sensors and in-situ observations', Remote Sensing of Environment. Elsevier Inc., 164, pp. 298–313. doi: 10.1016/j.rse.2015.04.004.

Kefi, M., Yoshino, K., Zayani, K. and Isoda, H. (2009) 'Estimation of Soil Loss by Using Combination of Erosion Model and GIS -Case of Study Watersheds in Tunisia', Journal of Arid Land Studies, 19(1), pp. 287–290.

Kendall, M. G. (1948) 'Rank Correlation Methods'. Oxford, England: Griffin.

Kiani-harchegani, M., Sadeghi, S. H. and Asadi, H. (2018) 'Comparing grain size distribution of sediment and original soil under raindrop detachment and raindrop-induced and flow transport mechanism', Hydrological Sciences Journal. Taylor & Francis, 63(2), pp. 312–323. doi: 10.1080/02626667.2017.1414218.

Kimball, J. (2014) 'Vegetation Phenology', in Njoku, E. G. (ed.) Encyclopedia of Remote Sensing. Encyclopedia of Earth Sciences Series. New York: Springe.

Klein, C., Heinzeller, D., Bliefernicht, J. and Kunstmann, H. (2015) 'Variability of West African monsoon patterns generated by a WRF multi - physics ensemble', Climate Dynamics. Springer Berlin Heidelberg, pp. 2733–2755. doi: 10.1007/s00382-015-2505-5.

Knippertz, P., Evans, M. J., Field, P. R., Fink, A. H., Liousse, C. and Marsham, J. H. (2015)

'The possible role of local air pollution in climate change in West Africa', Nature Publishing Group. Nature Publishing Group, 5(9), pp. 815–822. doi: 10.1038/nclimate2727.

Kuenzer, C., Dech, S. and Wagner, W. (2015) 'Remote Sensing Time Series Revealing Land Surface Dynamics: Status Quo and the Pathway Ahead', in Kuenzer, C., Dech, S., and Wagner, W. (eds) Remote Sensing Time Series. 22nd edn. Springer, pp. 1–24. doi: 10.1007/978-3-319-15967-.

Kundu, A., Denis, D. M., Patel, N. R. and Dutta, D. (2018) 'A Geo-spatial study for analysing temporal responses of NDVI to rainfall', Singapore Journal of Tropical Geography, 39, pp. 107–116. doi: 10.1111/sjtg.12217.

Kundzewicz, Z., Mata, L., Doll, P., Kabat, P., Jimenez, B., Miller, K., Oki, T., Sen, Z. and Shiklomanov, I. (2007) 'Freshwater resources and theirs management', in Parry, M., Canziani, O., Palutikof, J., van der Linden, P., and Hanson, C. (eds) Impacts, Adaptation and Vulnerability. Contribution of Working Group II to the Fourth Assessment Report of the Intergovernmental Panel on Climate Change. Cambridge: Cambridge University Press, p. 173e210.

Laili, N., Arafah, F., Jaelani, L. M., Subehi, L., Pamungkas, A., Koenhardono, E. S. and Sulisetyono, A. (2015) 'Development of Water Quality Parameter Retrieval Algorithms for Estimating Total Suspended Solids and Chlorophyll-A Concentration Using Landsat8 Imagery at Poteran Island Water', ISPRS Annals of the Photogrammetry, Remote Sensing and Spatial Information Sciences, II-2/W2. doi: 10.5194/isprsannals-II-2-W2-552015.

Lamchin, M., Lee, W., Jeon, S. W., Wang, S. W., Lim, C. H., Song, C. and Sung, M. (2018) 'Long-term trend and correlation between vegetation greenness and climate variables in Asia based on satellite data', Science of the Total Environment. Elsevier B.V., (October 2017). doi: 10.1016/j.scitotenv.2017.09.145.

Landsberg, H. E. (1972) 'World survey of climatology: Climates of Africa'. Amsterdam: Elsevier, p. 604. Available at: agris.fao.org.

Langbein, W. . B. and Schumm, S. A. . (1958) 'Yield of Sediment in Relation to Mean Annual Precipitation', Transactions, American Geophysical Union, 39(6). doi: 10.1029/TR039i006p01076.

Lausch, A., Erasmi, S., King, D. J., Magdon, P. and Heurich, M. (2016) 'Understanding Forest Health with Remote Sensing -Part I — A Review of Spectral Traits , Processes and Remote-Sensing Characteristics', Remote Sensing, 8, p. 1029. doi: 10.3390/rs8121029.

Laux, P., Kunstmann, H. and Bardossy, A. (2008) 'Predicting the regional onset of the rainy season in West', International Journal of Climatology, 28, pp. 329–342. doi: 10.1002/joc.

Leopold, L. B. (1951) 'Rainfall Frequency: An Aspect of Climate Variability', Transactions, American Geophysical Union, 32(3), pp. 347–357. doi: 10.1029/TR032i003p00347.

Leroux, L., Bégué, A., Lo, D., Jolivot, A. and Kayitakire, F. (2017) 'Driving forces of recent vegetation changes in the Sahel : Lessons learned from regional and local level analyses', Remote Sensing of Environment. Elsevier Inc., 191, pp. 38–54. doi: 10.1016/j.rse.2017.01.014.

Leslie, C. R., Serbina, L. O. and Miller, H. M. (2017) Landsat and Agriculture — Case Studies on the Uses and Benefits of Landsat Imagery in Agricultural Monitoring and Production. Virginia. doi: 10.3133/ofr20171034.

Li, J., Lewis, J., Rowland, J., Tappan, G. and Tieszen, L. L. (2004) 'Evaluation of land performance in Senegal using multi-temporal NDVI and rainfall series', Journal of Arid Environments, 59(3), pp. 463–480. doi: 10.1016/j.jaridenv.2004.03.019.

Li, P., Jiang, L. and Feng, Z. (2014) 'Cross-comparison of vegetation indices derived from landsat-7 enhanced thematic mapper plus (ETM+) and landsat-8 operational land imager (OLI) sensors', Remote Sensing, 6(1), pp. 310–329. doi: 10.3390/rs6010310.

Li, S., Yang, S., Liu, X., Liu, Y. and Shi, M. (2015) 'NDVI-Based Analysis on the Influence of Climate Change and Human Activities on Vegetation Restoration in the Shaanxi-GansuNingxia Region, Central China', Remote Sensing, 7, pp. 11163–11182. doi: 10.3390/rs70911163.

Li, Y., Yi, H. Q., Geng, X. C., Nguyen, M. L. and Funk, R. (2011) 'Assessment of Effectiveness of Soil Conservation Measures in Reducing Soil Erosion and Improving Soil Quality in China Using Fallout Radionuclide Techniques', in Dercon, G. (ed.) IAEA. TD-1665. Vienna: IAEA Press, pp. 207–224. Available at: http://www.iaea.org/books.

Li, Z. and Fang, H. (2016) 'Impacts of climate change on water erosion: A review', EarthScience Reviews, 163, pp. 94–117. doi: 10.1016/j.earscirev.2016.10.004.

Liu, H. Q. and Huete, A. (1995) 'A feedback based modification of the NDVI to minimize canopy background and atmospheric noise', IEEE Transactions on Geoscience and Remote Sensing, 33, pp. 457–465.

Liu, Y., Li, Y., Li, S. and Motesharrei, S. (2015) 'Spatial and Temporal Patterns of Global NDVI Trends: Correlations with Climate and Human Factors', Remote Sensing, 7, pp. 13233–13250. doi: 10.3390/rs71013233.

Liu, Z., Wimberly, M. C. and Dwomoh, F. K. (2017) 'Vegetation Dynamics in the Upper Guinean Forest Region of West Africa from 2001 to 2015', Remote Sensing, 9(5). doi: 10.3390/rs9010005.

Loveland, T. R. and Dwyer, J. L. (2012) 'Landsat : building a strong future', Remote Sensing of Environment. Elsevier B.V., 122, pp. 22–29. doi: 10.1016/j.rse.2011.09.022.

Lu, B. and He, Y. (2018) 'Optimal spatial resolution of Unmanned Aerial Vehicle (UAV) acquired imagery for species classification in a heterogeneous grassland ecosystem', GIScience & Remote Sensing. Taylor & Francis, 55(2), pp. 205–220. doi: 10.1080/15481603.2017.1408930.

Lu, D., Li, G., Valladares, G. S. and Batistella, M. (2004) 'Mapping soil erosion risk in Rondonia, Brazilian Amazonia: Using RUSLE, remote sensing and GIS', Land Degradation and Development, 15, pp. 499–512. doi: 10.1002/ldr.634.

Lu, D., Tian, H., Zhou, G. and Ge, H. (2008) 'Regional mapping of human settlements in southeastern China with multisensor remotely sensed data', Remote Sensing of Environment, 112, pp. 3668–3679. doi: 10.1016/j.rse.2008.05.009.

Luo, Y., Trishchenko, A. P. and Khlopenkov, K. V (2008) 'Developing clear-sky , cloud and cloud shadow mask for producing clear-sky composites at 250-meter spatial resolution for the seven MODIS land bands over Canada and North America', Remote Sensing of Environment, 112, pp. 4167–4185. doi: 10.1016/j.rse.2008.06.010.

MaCool, D. K. and Williams, J. D. (2008) 'Soil Erosion by Water', in Jørgensen, S. E. and Fath, B. D. (eds) Encyclopedia of Ecology. Academic Press, pp. 3284–3290. doi: 10.1016/B978-008045405-4.00296-2.

Maiersperger, T. K., Scaramuzza, P. L., Leigh, L., Shrestha, S., Gallo, K. P., Jenkerson, C. B. and Dwyer, J. L. (2013) 'Characterizing LEDAPS surface reflectance products by comparisons with AERONET , field spectrometer , and MODIS data', Remote Sensing of Environment, 136, pp. 1–13. doi: 10.1016/j.rse.2013.04.007.

Maisharou, A., Chirwa, P. W., Larwanou, M., Babalola, F. and Ofoegbu, C. (2015) 'Sustainable land management practices in the Sahel : review of practices , techniques and technologies for land restoration and strategy for up- -- scaling', International Forestry Review, 17(S3).

Mann, H. B. . (1945) 'Nonparametric Tests Against Trend', Econometrica, 13(3), pp. 245–259. Available at: https://www.jstor.org/stable/1907187.

Mariethoz, G., Renard, P. and Straubhaar, J. (2010) 'The direct sampling method to perform multiple-point geostatistical simulations', Water Resources Research, 46(11). doi: 10.1029/2008WR007621.

Masek, J. G., Vermote, E. F., Saleous, N. E., Wolfe, R., Hall, F. G., Huemmrich, K. F., Gao, F., Kutler, J. and Lim, T. (2006) 'A Landsat Surface Reflectance Data Set for North America, 1990–2000', IEEE Geoscience and Remote Sensing Letter, 3(1), pp. 68–72. doi: 10.1109/LGRS.2005.857030.

Maxwell, S. (2004) 'Filling Landsat ETM+ SLC-off Gaps Using a Segmentation Model Approach', Photogrammetric Engineering & Remote Sensing, pp. 1109–1111. Available at: http://www.ecognition.com/sites/default/files/305_pershighlight.pdf.

Maxwell, S. K., Schmidt, G. L. and Storey, J. C. (2007) 'A multi - scale segmentation approach to filling gaps in Landsat ETM + SLC - off images', International Journal of Remote Sensing, 28(33), pp. 5339–5356. doi: 10.1080/01431160601034902.

Mekonnen, M., Keesstra, S. D., Baartman, J. E., Ritsema, C. J. and Melesse, A. M. (2015) 'Evaluating sediment storage dams : Structural off-site sediment trapping measures in northwest Ethiopia', Cuadernos de Investigación Geográfica, 41(1), pp. 7–22. doi: 10.18172/cig.2643.

Mekuriaw, A., Heinimann, A., Zeleke, G. and Hurni, H. (2018) 'Factors in fluencing the adoption of physical soil and water conservation practices in the Ethiopian highlands', International Soil and Water Conservation Research. Elsevier B.V., 6(1), pp. 23–30. doi: 10.1016/j.iswcr.2017.12.006.

Meroni, M., Fasbender, D., Rembold, F., Atzberger, C. and Klisch, A. (2019) 'Remote Sensing of Environment Near real-time vegetation anomaly detection with MODIS NDVI : Timeliness vs . accuracy and e ff ect of anomaly computation options', Remote Sensing of Environment. Elsevier, 221, pp. 508–521. doi: 10.1016/j.rse.2018.11.041.

Mooij, W. M., Hülsmann, S., De Senerpont Domis, L. N., Nolet, B. A., Bodelier, P. L. E., Boers, P. C. M., Dionisio Pires, L. M., Gons, H. J., Ibelings, B. W., Noordhuis, R., Portielje, R., Wolfstein, K. and Lammens, E. H. R. R. (2005) 'The impact of climate change on lakes in the Netherlands: A review', Aquatic Ecology, 39(4), pp. 381–400. doi: 10.1007/s10452-005-9008-0.

Morgan, R. P. C. (1995) 'Soil Erosion and Conservation'. Harlow, UK: Longman Group.

Morgan, R. P. C., Quinton, J. N., Smith, R. E., Govers, G., Poesen, J. W. A., Auerswald, K., Chisci, G., Torri, D. and Styczen, A. M. E. (1998) 'The European Soil Erosion Model (EUROSEM): A Dynamic Approach for Predicting Sediment Transport from Fields and Small Catchments', Earth Surface Processes and Landforms, 23, pp. 527–544.

Moritz, S., Sardá, A., Bartz-Beielstein, T., Zaefferer, M. and Stork, J. (2015) 'Comparison of different Methods for Univariate Time Series Imputation in R'. Cologne University of Applied Sciences. Available at: http://arxiv.org/abs/1510.03924.

Mullan, D. (2013) 'Soil erosion under the impacts of future climate change: Assessing the statistical significance of future changes and the potential on-site and off-site problems', Catena. doi: 10.1016/j.catena.2013.03.007.

Myneni, R. B., Keeling, C. D., Tucker, C. J., Asrar, G. and Nemani, R. R. (1997) 'Increased plant growth in the northern high latitudes from 1981 to 1991', Nature, 386, pp. 698–702.

Narayanan, R. G. L. and Ibe, O. C. (2015) Wireless Public Safety Networks 1: Overview and Challenges. doi: 10.1016/B978-1-78548-022-5.50006-6.

Nash, M. S., Wickham, J., Christensen, J. and Wade, T. (2017a) 'Changes in Landscape Greenness and Climatic Factors over 25 Years (1989 – 2013) in the USA', Remote Sensing, 9(295), pp. 1–21. doi: 10.3390/rs9030295.

Nash, M. S., Wickham, J., Christensen, J. and Wade, T. (2017b) 'Changes in Landscape Greenness and Climatic Factors over 25 Years (1989 – 2013) in the USA', Remote Sensing, 9, p. 295. doi: 10.3390/rs9030295.

Nawar, S., Buddenbaum, H., Hill, J. and Kozak, J. (2014) 'Modeling and Mapping of Soil Salinity with Reflectance Spectroscopy and Landsat Data Using Two Quantitative Methods (PLSR and MARS)', Remote Sensing, 6, pp. 10813–10834. doi: 10.3390/rs61110813.

Nearing, M. A., Jetten, V., Baffaut, C., Cerdan, O., Couturier, A., Hernandez, M., Le Bissonnais, Y., Nichols, M. H., Nunes, J. P., Renschler, C. S., Souchère, V. and Van Oost, K. (2005) 'Modeling response of soil erosion and runoff to changes in precipitation and cover', in Catena, pp. 131–154. doi: 10.1016/j.catena.2005.03.007.

Nearing, M. A., Pruski, F. F. and O'Neal, M. R. (2004) 'Expected CC impacts on soil erosion Rates: A review', Journal of Soil and Water Conservation, 59(1), pp. 43–50.

Nearing, M. A., Yin, S., Borrelli, P. and Polyakov, V. O. (2017) 'Rainfall erosivity : An historical review', Catena, 157, pp. 357–362. doi: 10.1016/j.catena.2017.06.004.

Neeti, N. and Eastman, J. R. (2011) 'A Contextual Mann-Kendall Approach for the Assessment of Trend Significance in Image Time Series', 15(5), pp. 599–611. doi: 10.1111/j.14679671.2011.01280.x.

Nicholson, S. E. (2009) 'A revised picture of the structure of the "' monsoon '" and land ITCZ over West Africa', Climate Dynamics, 32, pp. 1155–1171. doi: 10.1007/s00382-0080514-3.

Nicholson, S. E. (2013) 'The West African Sahel : A Review of Recent Studies on the Rainfall Regime and Its Interannual Variability', ISRN Meteorology, 453521, p. 32. doi: 10.1155/2013/453521.

Nigussie, H., Poesen, J., Nyssen, J., Verstraeten, G., de Vente, J., Govers, G., Deckers, J. and Moeyersons, J. (2005) 'Specific sediment yield in Tigray-Northern Ethiopia: Assessment and semi-quantitative modelling', Geomorphology, 69, pp. 315–331.

Nikiema, A. (2005) Agroforestry parkland species diversity: uses and management in semiarid West Africa (Burkina Faso)., Agroforestry parkland species diversity: uses and management in semi-arid West Africa (Burkina Faso). Wageningen University, the Netherlands. Available at: https://www.researchgate.net/publication/35944725%0AAgroforestry.

Nyamekye, C., Thiel, M., Schönbrodt-stitt, S., Zoungrana, B. J. and Amekudzi, L. K. (2018) 'Soil and Water Conservation in Burkina Faso , West Africa', Sustainability, 10, p. 3182. doi: 10.3390/su10093182.

Nyeko-Ogiramoi, P., Willems, P. and Ngirane-Katashaya, G. (2013) 'Trend and variability in ob- served hydrometeorological extremes in the Lake Victoria basin', Journal of Hydrology, 489, pp. 56–73.

Nyssen, J., Poesen, J., Gebremichael, D., Vancampenhout, K., Margo, D., Yihdego, G., Govers, G., Leirs, H., Moeyersons, J., Naudts, J., Haregeweyn, N., Haile, M. and Deckers, J. (2007) 'Interdisciplinary on-site evaluation of stone bunds to control soil erosion on cropland in Northern Ethiopia', Soil & Tillage Research, 94, pp. 151–163. doi: 10.1016/j.still.2006.07.011.

O'Neal, M. R., Nearing, M. A., Vining, R. C., Southworth, J. and Pfeifer, R. A. (2005) 'Climate change impacts on soil erosion in Midwest United States with changes in crop management', Catena, 61, pp. 165–184. doi: 10.1016/j.catena.2005.03.003.

Omotosho, J. B. (2008) 'Pre-rainy season moisture build-up and storm precipitation delivery in the West African Sahel', 946(August 2007), pp. 937–946. doi: 10.1002/joc.

Omotosho, J. B. and Abiodun, B. J. (2007) 'A numerical study of moisture build-up and rainfall over West Africa', 225(July), pp. 209–225. doi: 10.1002/met.

Onojeghuo, A. O. and Onojeghuo, A. R. (2015) 'Mapping forest transition trends in Okomu reserve using Landsat and UK-DMC-2 satellite data', South African Journal of Geomatics, 4(4), pp. 486–501. doi: 10.4314/sajg.v4i4.9.

Ouattara, K. (2007) Improved Soil and Water Conservatory Managements for Cotton-Maize Rotation System in the Western Cotton Area of Burkina Faso. Swedish University of Agricultural Sciences. Available at: http://www.compost.org/CCC_Science_Web_Site/pdf/Corn/Improved Soil and Water Conservatory Managements for Cotton-Maize Rotation System in the Western Cotton Area of Burkina Faso.pdf.

Ouédraogo, E. (2004) Soil Quality Improvement for Crop Production in semi-arid West Africa. Wageningen University and Research Centre. Available at: https://library.wur.nl/WebQuery/wurpubs/337181.

Pajares, G. (2015) 'Overview and Current Status of Remote Sensing Applications Based on Unmanned Aerial Vehicles (UAVs)', Photogrammetric Engineering & Remote Sensing, 81(4), pp. 281–330. doi: 10.14358/PERS.81.4.281.

Pan, J., Yang, X., Cai, H. and Mu, B. (2016) 'Image noise smoothing using a modi fi ed Kalman fi lter', Neurocomputing, 173, pp. 1625–1629. doi: 10.1016/j.neucom.2015.09.034.

Paroissien, J. B., Darboux, F., Couturier, A., Devillers, B., Mouillot, F., Raclot, D. and Le Bissonnais, Y. (2015) 'A method for modeling the effects of climate and land use changes on erosion and sustainability of soil in a Mediterranean watershed (Languedoc, France)', Journal of Environmental Management. doi: 10.1016/j.jenvman.2014.10.034.

Parveen, R. and Kumar, U. (2012) 'Integrated Approach of Universal Soil Loss Equation (USLE) and Geographical Information System (GIS) for Soil Loss Risk Assessment in Upper South Koel Basin, Jharkhand', Journal of Geographic Information System, 4, pp. 588–596. doi: 10.4236/jgis.2012.46061.

Perez-sanz, F., Navarro, P. J. and Egea-cortines, M. (2018) 'Plant phenomics : an overview of image acquisition technologies and image data analysis algorithms', GigaScience, 6, pp. 1–18. doi: 10.1093/gigascience/gix092.

Piao, S., Nan, H., Huntingford, C., Ciais, P., Friedlingstein, P., Sitch, S., Peng, S., Ahlstrom, A., Canadell, J. G., Cong, N., Levis, S., Levy, P. E., Liu, L., Lomas, M. R., Mao, J., Myneni, R. B., Peylin, P., Poulter, B., Shi, X., Yin, G., Viovy, N., Wang, T., Wang, X., Zaehle, S., Zeng, N., Zeng, Z. and Chen, A. (2014) 'Evidence for a weakening relationship between interannual temperature variability and northern vegetation activity', Nature Communications, pp. 1–7. doi: 10.1038/ncomms6018.

Pimentel, D., Harvey, C., Resosudarmo, P., Sinclair, K., Kurz, D., Mcnair, M., Crist, S., Shpritz, L., Fitton, L., Saffouri, R. and Blair, R. (1995) 'Environmental and Economic Costs of Soil Erosion and Conservation Benefits', Science, 267, pp. 1117–1123. doi: 10.1126/science.267.5201.1117.

Posthumus, H., L.K.Deeks, Rickson, R. J. and Quinton, J. N. (2015) 'Costs and benefits of erosion control measures in the UK', Soil Use and Management, 31, pp. 16–33. doi: 10.1111/sum.12057.

Pouliot, D. and Latifovic, R. (2018) 'Reconstruction of Landsat time series in the presence of irregular and sparse observations: Development and assessment in north-eastern Alberta, Canada', Remote Sensing of Environment. Elsevier, 204, pp. 979–996. doi: 10.1016/j.rse.2017.07.036.

Pringle, M. J., Schmidt, M. and Muir, J. S. (2009) 'Geostatistical interpolation of SLC-off Landsat ETM+ images', ISPRS Journal of Photogrammetry and Remote Sensing, 64(6), pp. 654–664. doi: 10.1016/j.isprsjprs.2009.06.001.

Pruski, F. F. and Nearing, M. A. (2002a) 'Climate-induced changes in erosion during the 21st century for eight U . S . locations', Water Resources Research, 38(12), p. 1298. doi: 10.1029/2001WR000493.

Pruski, F. F. and Nearing, M. A. (2002b) 'Runoff and soil-loss responses to changes in precipitation: A computer simulation study', Journal of Soil and Water Conservation, 57(1).
Qi, S., Brown, D. G., Tian, Q., Jiang, L., Zhao, T. and Bergen, K. M. (2009) 'Inundation Extent and Flood Frequency Mapping Using LANDSAT Imagery and Digital Elevation Models', GIScience & Remote Sensing, 46(1), pp. 101–127. doi: 10.2747/1548-1603.46.1.101.

Qiang, L., H, F. Y., Zaichun, Z., Zhuo, L., Mengtian, H. and Ivan, J. (2016) 'Delayed autumn phenology in the Northern Hemisphere is related to change in both climate and spring phenology', Global Change Biology, 22(11), pp. 3702–3711. doi: 10.1111/GCB.13311.

Rao, Y., Zhu, X., Chen, J. and Wang, J. (2015) 'An Improved Method for Producing High Spatial-Resolution NDVI Time Series Datasets with Multi-Temporal MODIS NDVI Data and Landsat TM/ETM+ Images', Remote Sensing, 7(6), pp. 7865–7891. doi: 10.3390/rs70607865.

Rawat, S. K., Mishra, A. K. and Bhattacharyya, R. (2016) 'Soil erosion risk assessment and spatial mapping using LANDSAT-7 ETM + , RUSLE, and GIS—a case study', Arab Journal of Geosciences, 9(4), pp. 288–310. doi: 10.1007/s12517-015-2157-0.

Reij, C., Tappan, G. and Belemvire, A. (2005) 'Changing land management practices and vegetation on the Central Plateau of Burkina Faso (1968 – 2002)', Journal of Arid Environments, 63, pp. 642–659. doi: 10.1016/j.jaridenv.2005.03.010.

Renard, K. G., Foster, G. R., Weesies, G. A. and Porter, J. P. (1991) 'RUSLE, Revised Universal Soil Loss Equation', Journal of Soil and Water Conservation, 46(1), pp. 30–33.

Richardson, A. D., Keenan, T. F., Migliavacca, M., Ryu, Y., Sonnentag, O. and Toomey, M. (2013) 'Agricultural and Forest Meteorology Climate change , phenology , and phenological control of vegetation feedbacks to the climate system', Agricultural and Forest Meteorology. Elsevier B.V., 169, pp. 156–173. doi: 10.1016/j.agrformet.2012.09.012.

Riede, J. O., Posada, R., Fink, A. H. and Kaspar, F. (2016) 'What's on the 5th IPCC Report for West Africa?', in Yaro, J. A. and Hesselberg, J. (eds) Adaptation to Climate Change and Variability in Rural West Africa. Switzerland: Springer International Publishing, pp. 7–23. doi: 10.1007/978-3-319-31499-0.

Rishmawi, K., Prince, S. D. and Xue, Y. (2016) 'Vegetation Responses to Climate Variability in the Northern Arid to Sub-Humid Zones of Sub-Saharan Africa', Remote Sensing, 8(910). doi: 10.3390/rs8110910.

Romero-sanchez, M. E., Ponce-hernandez, R., Franklin, S. E. and Aguirre-salado, C. A. (2015) 'Comparison of data gap-filling methods for Landsat ETM + SLC-off imagery for monitoring forest degradation in a semi-deciduous tropical forest in Mexico', International Journal of Remote Sensing, 36(11), pp. 2786–2799. doi: 10.1080/01431161.2015.1047991.

Roudier, P., Sultan, B., Quirion, P. and Berg, A. (2011) 'The impact of future climate change on West African crop yields : What does the recent literature say ?', Global Environmental Change. Elsevier Ltd. doi: 10.1016/j.gloenvcha.2011.04.007.

Rouse Jr, W. J., Haas, H. R., Schell, A. J. and Deering, W. (1974) 'Monitoring vegetation systems in the great plains with erts .', NASA special publication, 351(309). Available at: https://ntrs.nasa.gov/archive/nasa/casi.ntrs.nasa.gov/19740022614.pdf.

Roy, D. P., Ju, J., Kline, K., Scaramuzza, P. L., Kovalskyy, V., Hansen, M., Loveland, T. R., Vermote, E. and Zhang, C. (2010) 'Web-enabled Landsat Data (WELD): Landsat ETM + composited mosaics of the conterminous United States', Remote Sensing of Environment. Elsevier Inc., 114(1), pp. 35–49. doi: 10.1016/j.rse.2009.08.011.

Roy, D. P., Ju, J., Mbow, C., Frost, P. and Loveland, T. (2010) 'Accessing free Landsat data via the Internet : Africa ' s challenge', Remote Sensing Letters, 1(2), pp. 111–117. doi: 10.1080/01431160903486693.

Sandwidi, W. J. P. (2007) Groundwater potential to supply population demand within the Kompienga dam basin in Burkina Faso. Rheinischen Friedrich-Wilhelms-Universität zu Bonn. Available at: http://hss.ulb.uni-bonn.de/2007/1231/1231.

Sanogo, S., Fink, A. H., Omotosho, J. A., Ba, A., Redl, R. and Ermert, V. (2015) 'Spatiotemporal characteristics of the recent rainfall recovery in West Africa', International Journal of Climatology, 35(March), pp. 4589–4605. doi: 10.1002/joc.4309.

Sawadogo, H. (2011) 'Using soil and water conservation techniques to rehabilitate degraded lands in northwestern Burkina Faso', International Journal of Agricultural Sustainability, 9(1), pp. 120–128. doi: 10.3763/ijas.2010.0552.

Scaramuzza, P., Micijevic, E. and Chander, G. (2004) SLC Gap-Filled Products Phase One Methodology. Available at: http://landsat.usgs.gov/documents/SLC_Gap_ Fill_Methodology.pdf. (Accessed: 7 September 2017).

Schmengler, A. C. (2010) Modeling soil erosion and reservoir sedimentation at hillslope and catchment scale in semi-arid Burkina Faso. Rheinischen Friedrich-Wilhelms-Universität zu Bonn.

Schroeder, T. A., Wulder, M. A., Healey, S. P. and Moisen, G. G. (2011) 'Remote Sensing of Environment Mapping wild fi re and clearcut harvest disturbances in boreal forests with Landsat time series data', Remote Sensing of Environment. Elsevier B.V., 115(6), pp. 1421–1433. doi: 10.1016/j.rse.2011.01.022.

Schulze, R. E. (2000) 'Transcending scales of space and time in impact studies of climate and climate change on agrohydrological responses', Agriculture, Ecosystems and Environment, 82, pp. 185–212. doi: 10.1016/S0167-8809(00)00226-7.

Sen, P. K. (1968) 'Estimates of the Regression Coefficient Based on Kendall's Tau', Journal of the American Statistical Association, 63(324), pp. 1379–1389. doi: 10.1080/01621459.1968.10480934.

She, X., Zhang, L., Cen, Y., Wu, T., Huang, C. and Biag, M. H. A. (2015) 'Comparison of the Continuity of Vegetation Indices Derived from Landsat 8 OLI and Landsat 7 ETM+ Data among Different Vegetation Types', Remote Sensing, 7, pp. 13485–13506. doi: 10.3390/rs71013485.

Singh, A. (1989) 'Digital change detection techniques using remotely-sensed data', International Journal of Remote Sensing, 10(6), pp. 989–1003. doi: 10.1080/01431168908903939.

Soille, P., Vogt, J. and Colombo, R. (2003) 'Carving and adaptive drainage enforcement of grid digital elevation models', Water Resources Research, 39(12), p. 1366. doi: 10.1029/200.

Stockle, C. O., Dyke, P. T., Williams, J. R., Jones, C. A. and Rosenberg, N. J. (1992) 'A method for estimating the direct and climatic effects of rising atmospheric carbon dioxide on growth and yield of crops: Part II - Sensitivity analysis at three sites in the Midwestern USA', Agricultural Systems, 38(3), pp. 239–256. doi: 10.1016/0308-521X(92)90068-Y.

Storey, J., Scaramuzza, P., Schmidt, G. and Barsi, J. (2005) 'Landsat 7 Scan Line CorrectorOff Gap-Filled Product Development Process', in In Proceedings of Pecora. Sioux Falls, South Dakota, pp. 23–27. Available at: http://www.asprs.org/a/publications/proceedings/pecora16/Storey_J.pdf.

Subhatu, A., Lemann, T., Hurni, K., Portner, B., Kassawmar, T., Zeleke, G. and Hurni, H. (2017) 'International Soil and Water Conservation Research Deposition of eroded soil on terraced croplands in Minchet catchment , Ethiopian Highlands', International Soil and Water Conservation Research. Elsevier B.V., 5(3), pp. 212–220. doi: 10.1016/j.iswcr.2017.05.008.

Sultan, B. and Janicot, S. (2000) 'Abrupt shift of the ITC Z over West Africa and intra-seasonal variability', Geophysical Research Letters, 27(20), pp. 3353–3356. doi: 10.1029/1999GL011285.

Tang, H., Li, Z., Zhu, Z., Chen, B., Zhang, B. and Xin, X. (2015) 'Variability and Climate Change Trend in Vegetation Phenology of Recent Decades in the Greater Khingan Mountain Area, Northeastern China', Remote Sensing, 7, pp. 11914–11932. doi:

10.3390/rs70911914.

Tang, Q., Xu, Y., Bennett, S. J. and Li, Y. (2014) 'Assessment of soil erosion using RUSLE and GIS: a case study of the Yangou watershed in the Loess Plateau, China', Environmental Earth Sciences. doi: 10.1007/s12665-014-3523-z.

Taye, G., Poesen, J., Vanmaercke, M., Wesemael, B. Van, Martens, L., Teka, D., Nyssen, J., Deckers, J., Vanacker, V., Haregeweyn, N. and Hallet, V. (2015) 'Evolution of the effectiveness of stone bunds and trenches in reducing runoff and soil loss in the semi-arid Ethiopian highlands Evolution of the effectiveness of stone bunds and trenches in reducing runoff and soil loss in the semi-arid Ethiopian highlan', Zeitschrift für Geomorphologie, 59(4), pp. 477–493. doi: 10.1127/zfg/2015/0166.

Theil, H. (1950) 'A Rank-Invariant Method of Linear and Polynomial', in In Proceedings of Koninalijke Nederlandse Akademie van Weinenschatpen A, p. Vol. 53, pp. 1397–1412. Available at: http://www.dwc.knaw.nl/DL/publications/PU00018789.pdf.

Tian, F., Brandt, M., Liu, Y. Y., Verger, A., Tagesson, T., Diouf, A. A., Rasmussen, K., Mbow, C., Wang, Y. and Fensholt, R. (2016) 'Remote sensing of vegetation dynamics in drylands: Evaluating vegetation optical depth (VOD) using AVHRR NDVI and in situ green biomass data over West African Sahel', Remote Sensing of Environment. Elsevier Inc., 177, pp. 265–276. doi: 10.1016/j.rse.2016.02.056.

Traore, S. S., Forkuo, E. K., Traore, P. C. S. and Landmann, T. (2015) 'Assessing the interrelationship between vegetation productivity , rainfall , population and land cover over

the Bani River Basin in Mali (West Africa)', IOSR Journal of Engineering, 05(06), pp. 10– 18.

Tucker, C. J. (1979) 'Red and Photographic Infrared linear Combinations for Monitoring Vegetation', Remote Sensing of Environment, 8, pp. 127–150.

UNEP (1986) Sands of change: why land becomes desert and what can be done about it. UNEP Brief #2. Nairobi, Kenya.

UNFCC (1997) 'Kyoto Protocol to the United Nations Framework Convention on Climate Change'. Bonn, Germany: UNFCC.

USGS (2013) 'Landsat — A Global Land-Imaging Mission', U.S. Geological Survey Fact Sheet. Available at: https://pubs.usgs.gov/fs/2012/3072/fs2012-3072.pdf (Accessed: 26 September 2017).

USGS (2017) Landsat Surface Reflectance-Derived Spectral Indices. Available at: https://landsat.usgs.gov/sites/default/files/documents/si_product_guide.pdf.

Valipour, M. (2015) 'Long-term runoff study using SARIMA and ARIMA models in the United States', Meteorological Applications, 22, pp. 592–598. doi: 10.1002/met.1491.

Vancampenhout, K., Nyssen, J., Gebremichael, D., Deckers, J., Poesen, J., Haile, M. and Moeyersons, J. (2006) 'Stone bunds for soil conservation in the northern Ethiopian highlands : Impacts on soil fertility and crop yield', Soil & Tillage Research, 90, pp. 1–15. doi: 10.1016/j.still.2005.08.004.

Vanlauwe, B., Coyne, D., Gockowski, J., Hauser, S., Huising, J., Masso, C., Nziguheba, G., Schut, M. and Asten, P. Van (2014) 'Sustainable intensification and the African smallholder farmer', Current Opinion in Environmental Sustainability. Elsevier B.V., 8, pp. 15–22. doi: 10.1016/j.cosust.2014.06.001.

Verbesselt, J., Hyndman, R., Newnham, G. and Culvenor, D. (2010) 'Detecting trend and seasonal changes in satellite image time series', Remote Sensing of Environment. Elsevier B.V., 114(1), pp. 106–115. doi: 10.1016/j.rse.2009.08.014.

Verbesselt, J., Hyndman, R., Zeileis, A. and Culvenor, D. (2010) 'Phenological change detection while accounting for abrupt and gradual trends in satellite image time series', Remote Sensing of Environment. Elsevier B.V., 114(12), pp. 2970–2980. doi: 10.1016/j.rse.2010.08.003.

Vermote, E. F., Tanre, D., Deuze, J. L., Herman, M. and Morcrette, J. (1997) 'Second Simulation of the Satellite Signal in the Solar Spectrum , 6S : An Overview', IEEE Geoscience and Remote Sensing Letter, 35(3), pp. 675–686. doi: 10.1109/36.581987.

Vermote, E., Justice, C., Claverie, M. and Franch, B. (2016) 'Preliminary analysis of the performance of the Landsat 8 / OLI land surface re fl ectance product', Remote Sensing of Environment. Elsevier B.V., 185, pp. 46–56. doi: 10.1016/j.rse.2016.04.008.

Vogel, E., Deumlich, D. and Kaupenjohann, M. (2016) 'Bioenergy maize and soil erosion — Risk assessment and erosion control concepts', Geoderma. Elsevier B.V., 261, pp. 80–92. doi: 10.1016/j.geoderma.2015.06.020.

Watts, L. M. and Laffan, S. W. (2014) 'Effectiveness of the BFAST algorithm for detecting vegetation response patterns in a semi-arid region', Remote Sensing of Environment. Elsevier Inc., 154(1), pp. 234–245. doi: 10.1016/j.rse.2014.08.023.

Weldeab, S., Schneider, R. R. and Andersen, N. (2007) '155,000 Years of West African Monsoon and Ocean Thermal Evolution', Science, 316, pp. 1303–1308.

White, J. C., Wulder, M. A., Hermosilla, T., Coops, N. C. and Hobart, G. W. (2017) 'A nationwide annual characterization of 25 years of forest disturbance and recovery for Canada using Landsat time series', Remote Sensing of Environment. Elsevier Inc., 194, pp. 303–321. doi: 10.1016/j.rse.2017.03.035.

Wijedasa, L. S., Sloan, S., Michelakis, D. G. and Clements, G. R. (2012) 'Overcoming limitations with landsat imagery for mapping of peat swamp forests in sundaland', Remote Sensing, 4(9), pp. 2595–2618. doi: 10.3390/rs4092595.

Williams, D. L., Goward, S. and Arvidson, T. (2006) 'Landsat : Yesterday , Today , and Tomorrow', Photogrammetric Engineering & Remote Sensing, 72(10), pp. 1171–1178. doi: 10.14358/PERS.72.10.1171.

Williams, J., Nearing, M. A., Nicks, A., Skidmore, E., Valentin, C., King, K. and Savabi, R. (1996) 'Using soil erosion models for global change studies', Journal of Soil and Water Conservation, 51(5), pp. 381–385.

Wischmeier, W. H. and Smith, D. D. (1978) 'Predicting Rainfall Erosion Loss: A Guide to Conservation Planning', in Agricultural Handbook. No. 537. Washington DC: US Department of Agricul- ture, Agricultural Research Service.

Wolka, K., Moges, A. and Yimer, F. (2011) 'Effects of level soil bunds and stone bunds on soil properties and its implications for crop production : the case of Bokole watershed , Dawuro zone , Southern Ethiopia', Agricultural Sciences, 2(3), pp. 357–363. doi: 10.4236/as.2011.23047.

Woodcock, C., Allen, R., Anderson, M., Belward, A., Bindschadler, R., Cohen, W., Gao, F., Goward, S., Helder, D., Helmer, E., Nemani, R., Oreopoulos, L., Schott, J., Thenkabail,

P., Vermote, E., Vogelmann, J., Wulder, M. and Wynne, R. (2008) 'Free Access to Landsat Imagery', Science, 320, p. 1011.

Wortley, L., Hero, J. and Howes, M. (2013) 'Evaluating Ecological Restoration Success : A Review of the Literature', Restoration Ecology, 21(5), pp. 537–543. doi: 10.1111/rec.12028.

Wulder, M. A., White, J. C., Goward, S. N., Masek, J. G., Irons, J. R., Herold, M., Cohen, W. B., Loveland, T. R. and Woodcock, C. E. (2008) 'Landsat continuity: Issues and opportunities for land cover monitoring', Remote Sensing of Environment, 112, pp. 955–969.

Wulder, M. A., White, J. C., Loveland, T. R., Woodcock, C. E., Belward, A. S., Cohen, W. B., Fosnight, E. A., Shaw, J., Masek, J. G. and Roy, D. . (2016) 'The Global Landsat Archive: Status, Consolidation, and Direction', Remote Sensing of Environment, 185, pp. 271–283. doi: 10.1016/j.rse.2015.11.032.

Xie, Y., Sha, Z. and Yu, M. (2008) 'Remote sensing imagery in vegetation mapping : a review', Journal of Plant Ecology, 1(1), pp. 9–23. doi: 10.1093/jpe/rtm005.

Xu, D. and Guo, X. (2014) 'Compare NDVI Extracted from Landsat 8 Imagery with that from Landsat 7 Imagery', American Journal of Remote Sensing, 2(2), p. 10. doi: 10.11648/j.ajrs.20140202.11.

Yengoh, G. T., Dent, D., Olsson, L., Tengberg, A. E. and Tucker, C. J. (2014) Use of the Normalized Difference Vegetation Index (NDVI) to assess land degradation at multiple scales : a review of the current status , future trends , and practical considerations. 1st edn. Lund: Springer. doi: 10.1007/978-3-319-24112-8.

Yin, G., Mariethoz, G., Sun, Y. and Mccabe, M. F. (2017) 'A comparison of gap-filling approaches for Landsat-7 satellite data', International Journal of Remote Sensing. Taylor & Francis, 38(23), pp. 6653–6679. doi: 10.1080/01431161.2017.1363432.

Yira, Y. and Diekkrüger, B. (2016) 'Modeling land use change impacts on water resources in a tropical West African catchment (Dano, Burkina Faso)', Journal of Hydrology, 537, pp. 187–199. doi: 10.1016/J.JHYDROL.2016.03.052.

Young, A. (1989) 'Agroforestry for Soil Conservation', in Hegyes, G. and Francis, C. A. (eds) Future Horizons : Recent Literature in Sustainable Agriculture Future. Volume 6. Lincoln, pp. 177–178. Available at: https://digitalcommons.unl.edu/cari-sustain/6.

Young, R. A. and Wiersma, J. L. (1973) 'The Role of Rainfall Impact in Soil Detachment and Transport', Water Resources Research, 9(6), pp. 1629–1636.

Yozgatligil, C., Aslan, S., Iyigun, C. and Batmaz, I. (2013) 'Comparison of missing value imputation methods in time series : the case of Turkish meteorological data', Theoretical and Applied Climatology, 112, pp. 143–167. doi: 10.1007/s00704-012-0723-x.

Zeng, C., Shen, H. and Zhang, L. (2013) 'Recovering missing pixels for Landsat ETM + SLCoff imagery using multi-temporal regression analysis and a regularization method', Remote Sensing of Environment, 131, pp. 182–194. doi: dx.doi.org/10.1016/j.rse.2012.12.012.

Zhang, C., Li, W. and Civco, D. (2014) 'Application of geographically weighted regression to fill gaps in SLC-off Landsat ETM + satellite imagery', International Journal of Remote Sensing. Taylor & Francis, 35(22), pp. 7650–7672. doi: 10.1080/01431161.2014.975377.

Zhang, C., Li, W. and Travis, D. (2007) 'Gaps - fill of SLC - off Landsat ETM + satellite image using a geostatistical approach', International Journal of Remote Sensing, 28(22), pp. 5103–5122. doi: 10.1080/01431160701250416.

Zhang, G., Liu, B., Liu, G., He, X. and Nearing, M. A. (2003) 'Detachment of Undisturbed Soil by Shallow Flow', Soil Science Society of America Journal, 67, pp. 713–719. doi: 10.2136/sssaj2003.7130.

Zhang, Y., Song, C., Band, L. E., Sun, G. and Li, J. (2017) 'Reanalysis of global terrestrial vegetation trends from MODIS products: Browning or greening?', Remote Sensing of Environment. Elsevier Inc., 191, pp. 145–155. doi: 10.1016/j.rse.2016.12.018.

Zhao, G., Mu, X., Wen, Z., Wang, F. and Gao, P. (2013) 'Soil erosion , conservation , and Eco-environment changes in the Loess Plateau of China', Land Degradation and Development, 24, pp. 499–510. doi: 10.1002/ldr.2246.

Zhong, Y., Wang, X., Xu, Y., Wang, S., Jia, T., Hu, X., Zhao, J., Wei, L. and Zhang, L. (2018)

'Mini-UAV-Borne Hyperspectral Remote Sensing', IEEE Geoscience and Remote Sensing Magazine. IEEE, 6, pp. 46–62. doi: 10.1109/MGRS.2018.2867592.

Zhu, X., Liu, D. and Chen, J. (2012) 'A new geostatistical approach for filling gaps in Landsat ETM+ SLC-off images', Remote Sensing of Environment. Elsevier Inc., 124, pp. 49–60. doi: 10.1016/j.rse.2012.04.019.

Zhu, Z., Fu, Y., Woodcock, C. E., Olofsson, P., Vogelmann, J. E., Holden, C., Wang, M., Dai, S. and Yu, Y. (2017) 'Including land cover change in analysis of greenness trends using all available Landsat 5 , 7 , and 8 images : A case study from Guang ....', Remote Sensing of Environment. Elsevier B.V., 185, pp. 243–257. doi: 10.1016/j.rse.2016.03.036.

Zhu, Z., Wang, S. and Woodcock, C. E. (2015) 'Improvement and expansion of the Fmask algorithm: cloud, cloud shadow, and snow detection for Landsats 4-7, 8, and Sentinel 2 images', Remote Sensing of Environment, 159, pp. 269–277. doi: 10.1016/j.rse.2014.12.014.

Zhu, Z. and Woodcock, C. E. (2012) 'Object-based cloud and cloud shadow detection in Landsat imagery', Remote Sensing of Environment. Elsevier Inc., 118, pp. 83–94. doi: 10.1016/j.rse.2011.10.028.

Zhu, Z. and Woodcock, C. E. (2014) 'Continuous change detection and classification of land cover using all available Landsat data', Remote Sens. Environ., 144, pp. 152–171. doi: 10.1016/j.rse.2014.01.011.

Zougmoré, R. (2003) 'Integrated water and nutrient management for sorghum production in semi-arid Burkina Faso', Tropical Resources Management Papers.

Zougmoré, R., Jalloh, A. and Tioro, A. (2014) 'Climate-smart soil water and nutrient management options in semiarid West Africa : a review of evidence and analysis of stone bunds and zaï techniques', Agriculture & Food Security, 3, p. 16. doi: 10.1186/2048-70103-16.

Zougmoré, R., Mando, A., Stroosnijder, L. and Ouédraogo, E. (2004) 'Economic benefits of combining soil and water conservation measures with nutrient management in semiarid Burkina Faso Economic benefits of combining soil and water conservation measures with nutrient management in semiarid Burkina Faso', Nutrient Cycling in Agroecosystems, 70, pp. 261–269. doi: 10.1007/s10705-004-0533-3.

Zoungrana, B., Conrad, C., Amekudzi, L., Thiel, M., Da, E., Forkuor, G. and Löw, F. (2015) 'Multi-Temporal Landsat Images and Ancillary Data for Land Use/Cover Change (LULCC) Detection in the Southwest of Burkina Faso, West Africa', Remote Sensing, 7(9), pp. 12076–12102. doi: 10.3390/rs70912076.

APPENDICES

Appendix A: Field Data Form for UAV Survey

DRONE SURVEY: FIELD DATA FORM

A. GENERAL INFORMATION

Field ID GPS		Coordinates (UTM)	Northings (N)	Eastings (E)
Name of locality				
Date & Time				

FIELD PHOTOGRAPHS

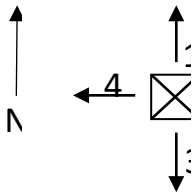

Photo No.	Direction

Relative position of photos from the centre of field

B. TERRAIN CHARACTERISTICS

Soil type

Evidence of erosion

Y	N

Slope

Flat to gentle slope (0 – 7 %)

Gentle to moderate slope (8 – 13 %)

Moderate to steep slope. Undulating terrain (14 – 20 %)

Steep to very steep. Undulating to hilly terrain (21 – 55 %)

Extremely steep. Hilly to mountainous terrain (56 – 100 %)

Presence of Duricrust

Y	N

C. LAND USE/COVER INFORMATION

General land use/cover type

☐ Agriculture (crop land) ☐ Natural vegetation

Agriculture (crop land)

Name of crop	Age (wks)	Height (m)					Planting Distance (m)					Density (/m^2)				
		1	2	3	4	Avg.	1	2	3	4	Avg.	1	2	3	4	Avg.

Farming practices

- ☐ Erosion controlled (with stone bunds)
- ☐ Non-erosion controlled
- ☐ Fertilizer application
- ☐ Mono cropping
- ☐ Intercropping

Natural vegetation

Vegetation type

- ☐ Grasses
- ☐ Shrubs
- ☐ Trees

Height of trees

- ☐ < 2m
- ☐ 2 – 5m
- ☐ > 5m

D. DRONE FLIGHT INFORMATION

Flight grid type

Flight height

Total no. of GCPs

Scene overlap

Camera angle

General Remarks

Appendix B: R Codes for Imputation of Missing NDVI Time Steps

Raster imputation using auto.arima and Kalman filter (adapted from: Moritz et al., 2015)
Required libraries (Raster, forecast)

```
NDVI_stack <- stack(NDVI)            #### stack all the NDVI raster files, create empty raster
                                     for missing time steps
filledNDVI_stack <- NDVI_stack    #### create a duplicate of the NDVI_stack to contain the
                                        final imputed raster stack for (i
in 1:nrow(NDVI_stack)) {
  print(i)
  for (j in 1:ncol(NDVI_stack)) {

    v <- as.vector(NDVI_stack[i,j])
    NDVI.ts <- ts(v, start=c(2004,1), end=c(2017,12), frequency= 12)
fit <- auto.arima(NDVI.ts)      kal <- KalmanRun(NDVI.ts,
fit$model)     tmp <- which(fit$model$Z == 1)
    id  <- ifelse(length(tmp) == 1, tmp[1], tmp[2])
id.na <- which(is.na(NDVI.ts))     NDVI.ts[id.na]
<- kal$states[id.na, id]     filledNDVI_stack[i,j]
<- NDVI.ts[ ]
     }
  }
```

Appendix C: R Codes for Time Series Analysis using 'bfast' package

Required libraries (raster, trend, forecast, bfast)

```
Raster-TS <- brick("location of rater stack)
Raster_TS <- ts(Raster-TS[[1]], start = 2004, frequency = 12)
```

```
BF <- bfast(Raster_TS, h = 0.006, season = c("harmonic"), max.iter = 10,
hpc = "none", level = 0.05, type= "OLS-MOSUM", breaks = 1)
TS_plot <- plot(BF,type="all")
Slope_TS <- sens.slope(TS_P, conf.level = 0.95)
bf2 <- bfast01(Raster_TS, test = c("BIC", "OLS-MOSUM", "supLM"), aggregate = any)
plot(bf2) bf2$test  bf2$breaks
plot(bf2, plot.type = "multiple", which = c("response", "season", "trend", "residuals"))
bfast01classify(bf3, alpha = 0.05, pct_stable = .53)
```

Appendix D: R Codes for Climate Variables analysis

```
###Rainfall analysis
Mon.RF <- read.csv("RF_data.csv", h=F) yr.RF
<- read.csv("RF_data.csv", h=F)

## Monthly rainfall series
fit.t <- tslm(ts(mon.RF, start= c(2004, 01), frequency = 12) ~ trend)
plot(ts(mon.RF, start= c(2004, 01), frequency = 12),
```

```
ylab="Total monthly Rainfall (mm)", xlab="Time")
lines(fitted(fit.t),col="blue", lwd=3) summary(fit.t)
trend.tm <- summary(fit.t)$coefficients[2,1]; #--extract trend and pValue pVal.tm
<- summary(fit.t)$coefficients[2,4]
legend("top", paste("Trend = ",round(trend.tm,3),"mm/month ; p-Value =",round(pVal.tm,
3)),
      adj = c(0, -1.49), bty="n", inset=.05, text.width = 10, text.col="red")
        #--use adj to set the position of the trend and pValue legend
Kendall(mon.RFDate, mon.RF)  #--Mann Kendall trend test


## Annual rainfall series
fit.ty <- tslm(ts(yr.RF, start= 2004, frequency = 1) ~ trend) plot(ts(yr.RF,
start= 2004, frequency = 1),
    ylab="Total Annual Rainfall (mm)", xlab="Time", main="Annual Rainfall")
lines(fitted(fit.ty),col="blue", lwd=3) summary(fit.ty)
trend.ty <- summary(fit.ty)$coefficients[2,1]; #--extract trend and pValue pVal.ty
<- summary(fit.ty)$coefficients[2,4]
legend("top", paste("Trend = ",round(trend.ty,3),"mm/year ; p-Value =",round(pVal.ty, 3)),
adj = c(0, -1.49), bty="n", inset=.05, text.width = 10, text.col="red") Kendall(yr.RFDate,
yr.RF)

###Temperature analysis
Temp <- read.csv(file = "temp_data.csv", head=TRUE,sep=",")
Tm <- tslm(ts(Temp, start= c(2004, 01), frequency = 12) ~ trend)
plot(ts(Tm, start= c(2004, 01), frequency = 12),      ylab="Mean
monthly Temperature (oC)", xlab="Time") plot.ts(TS, ylab =
"Mean Monthly Temperature") lines(fitted(Tm),col="blue",
lwd=3) summary(Tm)
trend.tp <- summary(Tm)$coefficients[2,1]; #--extract trend and pValue pVal.tp
<- summary(Tm)$coefficients[2,4]
legend("top", paste("Trend = ",round(trend.tp,3),"mm/month ; p-Value =",round(pVal.tp, 3)),
adj = c(0, -1.49), bty="n", inset=.05, text.width = 10, text.col="red")
```

```
Kendall(yr.TmDate, yr.Tm)
```


Appendix E: R Codes for Correlation between NDVI and Climate Variables

```
Required libraries (raster, spatialEco)

NDVI-TS <- brick("location of NDVI stack)
RainF-TS <- brick("location of rainfall stack)
Temp-TS <- brick("location of temperature stack)

#### NDVI and rainfall correlation
NDVI_RainFCor <- corLocal(NDVI-TS, RainF-TS,  method = c("kendall"), test = TRUE)
NDVI-RF_pValue <- raster.Zscore(NDVI_RainFCor, p.value = TRUE)   ## p-value
## masking p-value of < 0.05 (95% CI)
SigT_NDVI-RF <- mask(NDVI_RainFCor, NDVI-RF_pValue < 0.05, maskvalue = FALSE)

##### NDVI and temperature correlation
```

```
NDVI_tempCor <- corLocal(NDVI_TS, Temp-TS,  method = c("kendall"), test = TRUE)
NDVI-RF_pValue <- raster.Zscore(NDVI_RainFCor, p.value = TRUE)   ## p-value
## masking p-value of < 0.05 (95% CI)
SigT_NDVI-T <- mask(NDVI_tempCor, NDVI-RF_pValue < 0.05, maskvalue = FALSE)
```